Dicer interacts with the P-granule component GLH-1; both localize to *C. elegans* nuclear pores and to stress-induced oocyte RNP granules

---

A Dissertation

presented to

the Faculty of the Graduate School

University of Missouri – Columbia

In Partial Fulfillment

Of the Requirements for the Degree

Doctor of Philosophy

---

by

ERICA LEIGH BESHORE

Dr. Karen Bennett, Dissertation Supervisor

MAY 2010

The undersigned, appointed by the Dean of the Graduate Faculty, have examined the dissertation entitled

Dicer interacts with the P-granule component GLH-1; both localize to *C. elegans* nuclear pores and to stress-induced oocyte RNP granules

Presented by ERICA LEIGH BESHORE

a candidate for the degree of DOCTOR OF PHILOSOPHY

and hereby certify that in their opinion it is worthy of acceptance

---

Karen Bennett, PhD — Dissertation Supervisor

Anand Chandrasekhar, PhD

Chris Lorson, PhD

David Pintel, PhD

Change Tan, PhD

ACKNOWLEDGEMENTS

I would like to first and foremost thank my family, both Racen and Beshore, for all of their support and encouragement throughout the past 6 years. I would like to thank my husband, Brent Beshore, for being the best part of each and every day, and for never letting me give up. I would like to thank all of the undergraduate student helpers including Jordan Marshall and Adrienne Brigham who helped me a great deal in the laboratory. I would like to thank my committee members Dr. Karen Bennett, Dr. David Pintel, Dr. Chris Lorson, Dr. Anand Chandrasekhar, and Dr. Change Tan for all of their guidance and suggestions. I also would like to thank Dr. Timothy Morris, my college advisor, who taught me all I needed to know to endure graduate school and who encouraged me to go into research. I would like to thank past and current Bennett laboratory members Dr. April (Orsborn) Bauer, Dr. Ge Gao, Tamara McEwen, and Dr. Faten Deeb for their help and friendship. And finally I would like to thank my Lord and Savior Jesus Christ without whom I can do nothing.

I would like to first and foremost thank my family, both Racen and Beshore, for all of their support and encouragement throughout the past 6 years. I would like to thank my husband, Brent Beshore, for being the best part of each and every day, and for never letting me give up. I would like to thank all of the undergraduate student helpers including Jordan Marshall and Adrienne Brigham who helped me a great deal in the laboratory. I would like to thank my committee members Dr. Karen Bennett, Dr. David Pintel, Dr. Chris Lorson, Dr. Anand Chandrasekhar, and Dr. Change Tan for all of their guidance and suggestions. I also would like to thank Dr. Timothy Morris, my college advisor, who taught me all I needed to know to endure graduate school and who encouraged me to go into research. I would like to thank past and current Bennett laboratory members Dr. April (Orsborn) Bauer, Dr. Ge Gao, Tamara McEwen, and Dr. Faten Deeb for their help and friendship. And finally I would like to thank my Lord and Savior Jesus Christ without whom I can do nothing.

TABLE OF CONTENTS

List of Figures and Tables

LIST OF ABBREVIATIONS AND GLOSSARY

N2	wild type *Caenorhabditis elegans*
L1, L2, L3, or L4	first, second, third, or fourth larval stage
GLH	Germline RNA Helicase
DCR	Dicer
KGB	kinase that GLHs bind
FOG	feminization of the gonad
RNAi	RNA interference
P body	Processing body
GST	Glutatione-S-Transferase
6-His	Sequence tag of six consecutive histidine residues
RNP	Ribonucleoprotein
NPC	nuclear pore complex

Abstract

P granules are ribonucleoprotein complexes specific to the cytoplasmic side of the nuclear pores of *C. elegans* germ cells. While P granules are implicated in post-transcriptional control of maternally-transcribed mRNAs, their function remains elusive. Our laboratory is particularly interested in the P-granule component GLH-1 (Germline RNA Helicase-1). Through genetic studies our laboratory has shown that GLH-1 is essential for fertility; however, the biochemical function of the GLH complex is still unknown. With immunoprecipitations and GST-pulldowns, we report that GLH-1 and the riboendonuclease Dicer bind one another and their interaction is not RNA-dependent. Both GLH-1 protein and mRNA levels are reduced in the *dcr-1(ok247)* mutant background; conversely, a reduction of DCR-1 protein in the *glh-1(gk100)* deletion strain is also observed. Thus, in complex in the *C. elegans* germline, these two proteins seem interdependent. In addition, evidence indicates Dicer protein levels, like those of GLH-1, are regulated by proteosomal degradation and are much increased when the Jun N-terminal kinase KGB-1 is missing in the *kgb-1(um3)* null. In the adult *C. elegans* germline DCR-1 is located throughout the cytoplasm as well as at the inner nuclear pores of the germ cell nuclei, in close opposition to GLH-1. Under stress conditions in oocytes GLH-1 and DCR-1 both re-locate and recruit other components to large cytoplasmic RNP granules. We hypothesize the GLH-1/DCR-1 complex may function in the transport, deposition, or regulation of maternally-transcribed mRNAs perhaps with their associated miRNAs.

Chapter 1: Introduction

History of Developmental Biology

Perhaps one of the most fascinating areas of science is the study of developmental biology. The process of how a single cell develops into a differentiated, multi-functional organism has taught us much regarding how cells behave, diversify, and interact with each other. In fact, this process has long been of great intrigue to scientists. Aristotle (384-322 B.C.) was one of the first to describe the two prominent historical theories on embryonic development. The first of these theories, pre-formationism, suggested that an embryo or miniature individual preexists in either the mother's egg or the father's semen and begins to grow when properly stimulated. Pre-formationism was favored for many centuries as its core beliefs were centered in the idea that at the time of Creation, God preformed all creatures that were and were to come. The theory was strengthened in the seventeenth century with the invention of the microscope. Early microscopes had poor resolution and made it difficult to observe the details of the egg and sperm. For some, the sperm looked like a miniature adult with a tail, somewhat like a tadpole (Fig. 1.1). The second theory, favored by Aristotle, was known as epigenesis. Figure 1.2 depicts Aristotle's understanding of epigenesis. Epigenesis assumes that the embryo begins as an undifferentiated mass and that new parts are added during development. With advances in technology and microscopes it became evident that embryos were

Figure 1.1

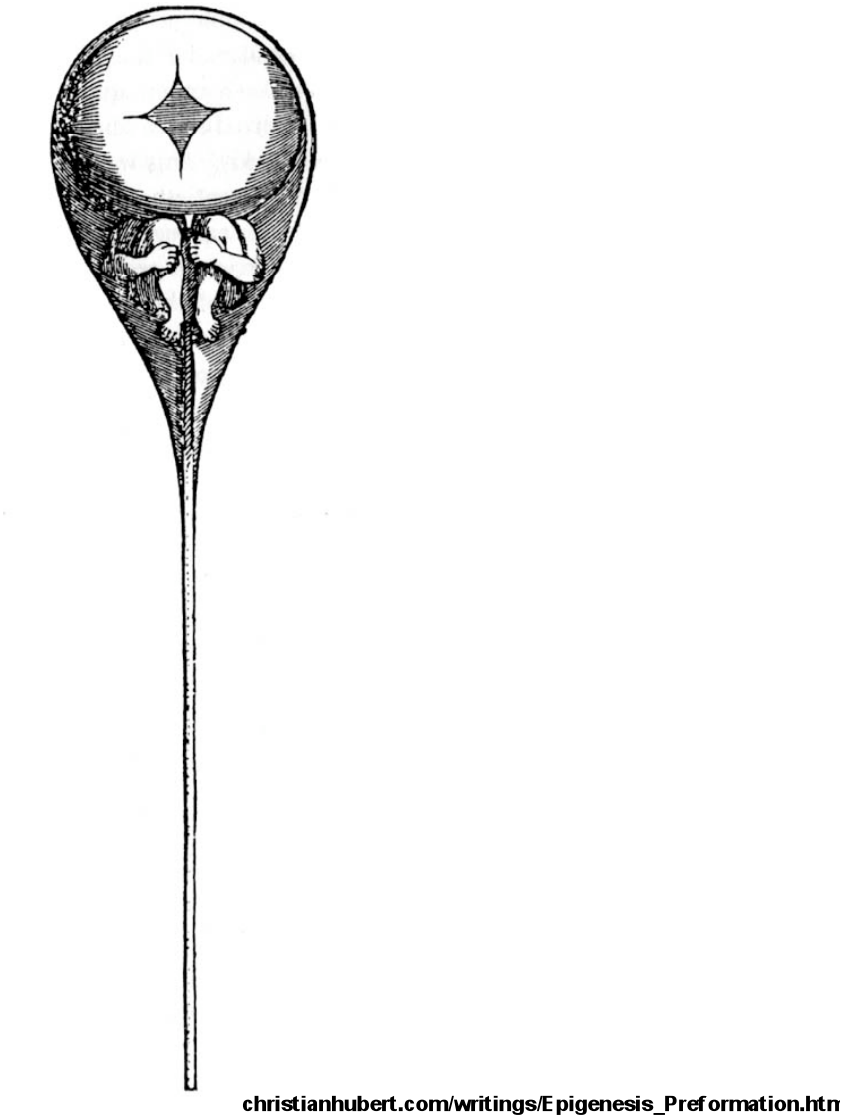

Figure 1.1. The Theory of Preformationism. Cartoon image of the preformed tiny human or "homunculus" housed in sperm. Preformationism theorized that all mankind was preformed at the Creation of the world and simply began to grow larger following fertilization. Figure adapted from www.christianhubert.com.

Figure 1.2

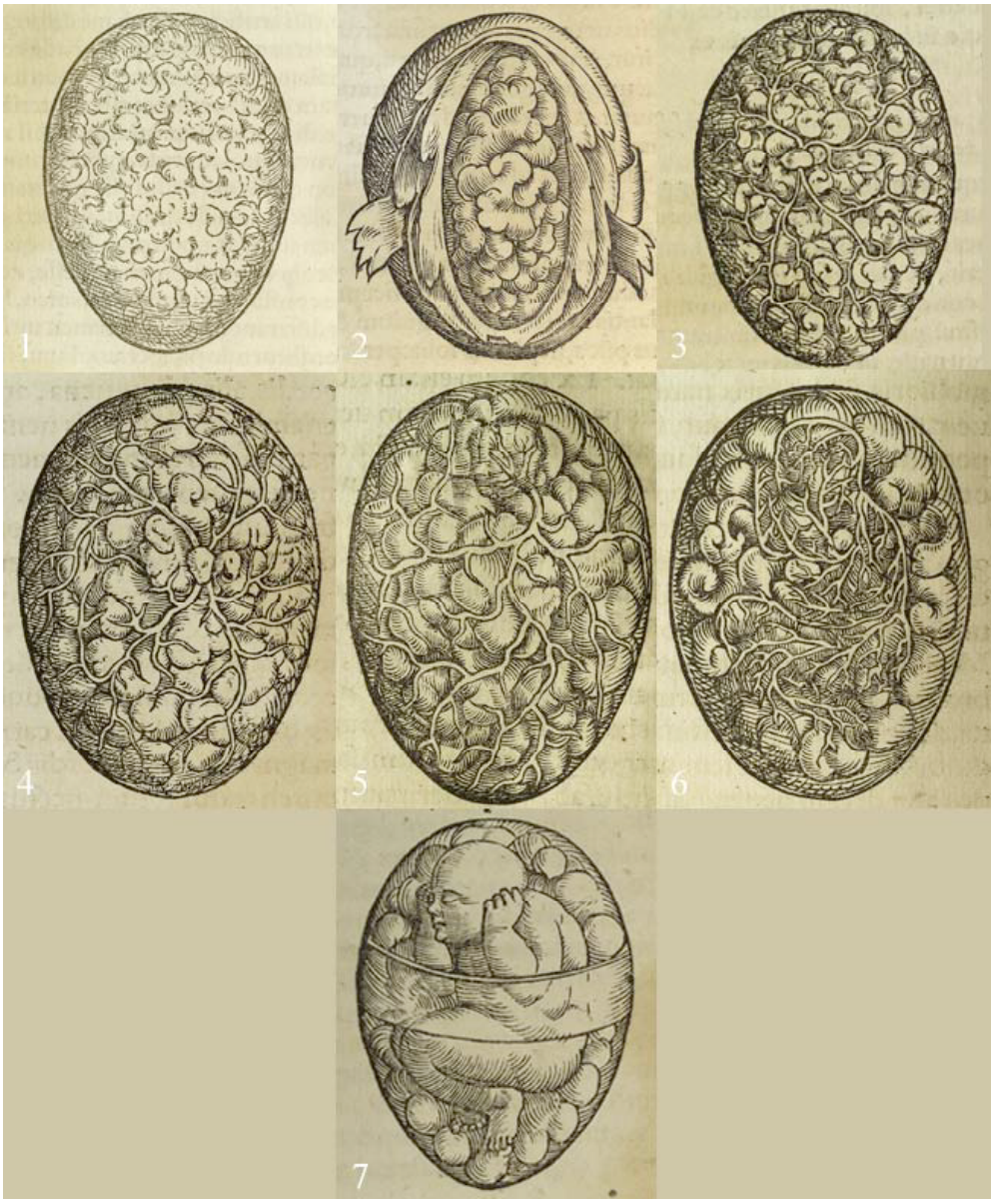

Figure 1.2. Aristotelian epigenesis. Depicted is a series of woodcuts from Rueff's textbook shows the gradual Aristotelian coagulation of male and female seeds into a child. The egg-shaped mass (1) covered with three membranes (2) gradually develops blood vessels and organs such as the liver and heart (3–5) that assume the form of a human being (6) and finally turn into a child (7). The

entire process supposedly took 45 days. By the end, the child would have ‘sense and feeling’, although enough strength for movement would not be acquired before the ninetieth day (twice 45). On the 270th day (three times 90), the infant would ‘hasten and come forth to the birth’ (quotes from the 1637 English edition, ff. 41–2). Figure adapted from www.hps.cam.ac.uk.

not preformed, but began as two haploid cells fusing together to create a single-celled diploid embryo. Following fertilization, human embryos undergo a number of cellular divisions and cell movement to set up the early patterning of the embryo (Wolpert, “Principles of Development”). It seems absurd to current minds, for we know today that epigenesis is how all animal organisms are formed. In fact, the development of the early embryo is a beautiful and well-orchestrated process that involves the coordination of appropriate cell signaling and gene expression, starting from an undifferentiated embryo.

If we jump forward to the 1950’s, after the helical structure of DNA was discovered, the world of molecular biology began to make its mark. Along with the study of DNA and the molecules it produces, came the study of developmental biology, which is the study of how genes influence the cell growth, differentiation, and morphogenesis. This field of developmental biology led into a search for organisms that would be suitable to study in the laboratory.

In 1963, researcher Sydney Brenner observed that much of what was known regarding molecular biology was made possible through the study of simple organisms, including bacteriophage. It was at this time that Dr. Brenner set out to develop an animal model organism that was simple to maintain and study in the laboratory. Brenner introduced and established *Caenorhabditis elegans* as a research model organism by producing methods for maintenance, genetic analysis, mutation balancing, and much more (Brenner, 1974; Herman et al.,

1976; Sulston and Brenner, 1974). Brenner's work has grown into a large community of scientists who study everything from behavior, immunity, neuronal development, apoptosis, gene regulation, RNA interference, to aging, and continues to grow.

Caenorhabditis elegans

Caenorhabditis elegans, is a free-living, hermaphroditic, non-parasitic soil nematode that can be easily grown and maintained in the laboratory. It is 1mm in length as an adult and has a transparent cuticle, which allows for visualization of organs and cellular division. Figure 1.3 depicts a schematic of the wild type adult *C. elegans* hermaphrodite. Note the large gonad (in dark and light blue), which makes up nearly half of the *C. elegans* body tissue. All wild type adult worms contain 959 somatic cells and each of these cells divides in a predictable and consistent manner. The entire cell-lineage has been mapped, making it possible to study the fate of a tissue starting at the first embryonic cell division. The worm has a quick 3-day life cycle from embryo to adult (Fig. 1.4) and each wild type worm can have on average 300 progeny. Additionally, *C. elegans* was the first higher eukaryotic organism, following yeast, to have its entire genome mapped and sequenced. The sequence was first published in 1998 (The C. elegans Sequencing Consortium, 1998), and completed in October of 2002 (www.wormbase.org).

Figure 1.3

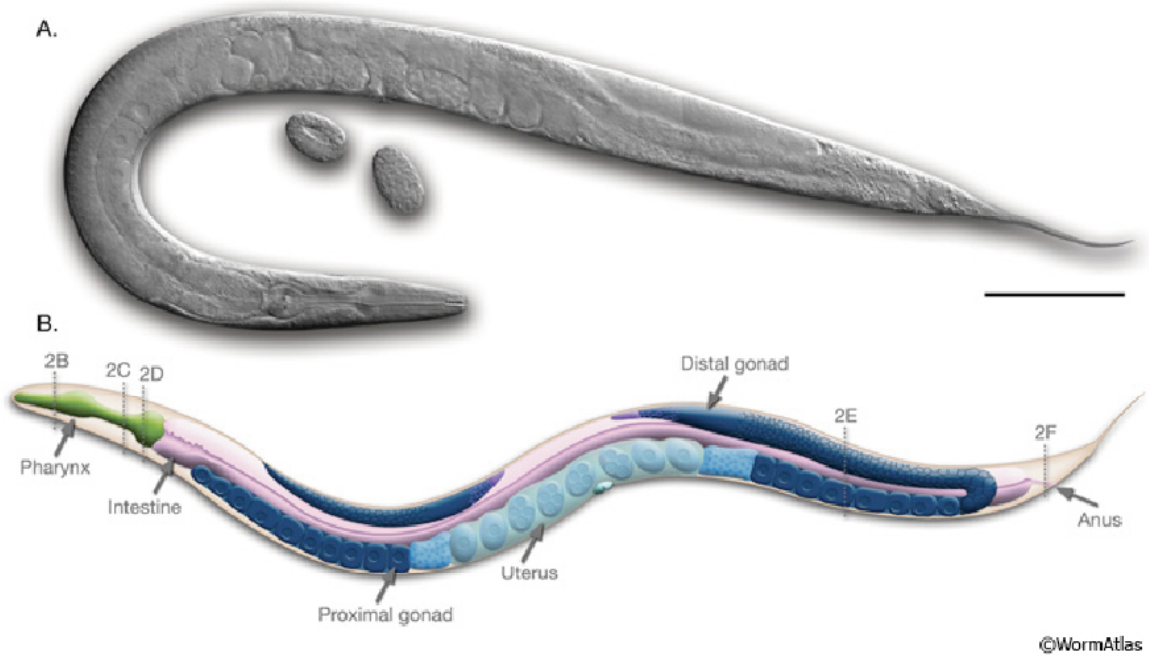

Figure 1.3. Anatomy of the adult *C. elegans* hermaphrodite. **A.** Nomarski optics of an adult hermaphrodite. Two embryos are seen below. Scale bar 0.1mm. **B.** Cartoon of the adult worm. The gonad is marked in dark and light blue. Figure adapted from www.wormatlas.org.

Figure 1.4

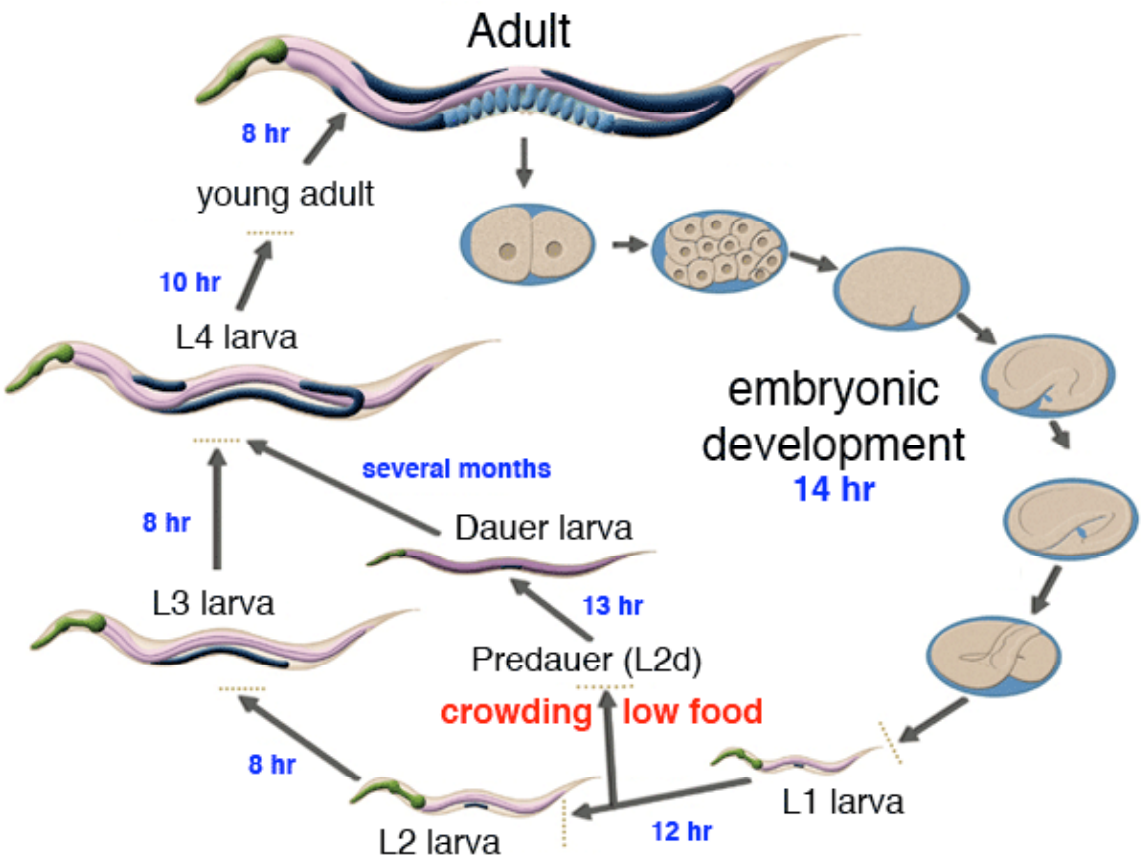

Figure 1.4. *C. elegans* life cycle. Schematic of the 3-day life cycle from fertilization to adult worm. Timing is based on a growth temperature of 22°C. The alternate pathway, dauer development, is shown in the case of starvation, overpopulation, or temperature stress following the L1 stage. Adapted from www.wormatlas.org.

While *C. elegans* are typically hermaphrodites, males, which have an XO genotype, do occur sporadically and can be generated in the laboratory. The male worm is smaller in size and has only a single gonad arm, compared to the two arms in the hermaphrodite. The male somatic tissues (sex organs) begin to develop at the L2 stage. The result of this development is a tail designed to hold open the female vulva and then release sperm (Fig. 1.5). In the laboratory, males are generated by heat shocking hermaphrodites to cause non-disjunction, resulting in the XO genotype. By this method males can be made for genetic crosses and mated with hermaphrodites. The male sperm is larger and faster than the sperm generated by the hermaphrodite, which allows for the sperm to be more competitive and the genetic cross possible and successful (LaMunyon and Ward, 1998).

Newly fertilized *C. elegans* embryos undergo a series of asymmetric divisions, allowing for the unequal distribution of cytoplasmic nutrients required for germline determination and positional patterning of the embryo (Fig. 1.6). The Bennett Laboratory is primarily interested in *C. elegans* germline development. The germline segregates with the posterior cell at the first cell division, the P1 cell. Germ cells continue to segregate with the P lineage, culminating with the P4 cell (Fig. 1.7). The P4 cell divides once more giving rise to Z2 and Z3 cells, which arrest until later larval stages of the worm. Z2 and Z3 begin to divide starting at the larval 2 (L2) stage and give rise to all the germ cells in the adult *C. elegans* gonad (Fig. 1.8). At the fourth larval stage (L4), mitotic germ cell nuclei enter

Figure 1.5

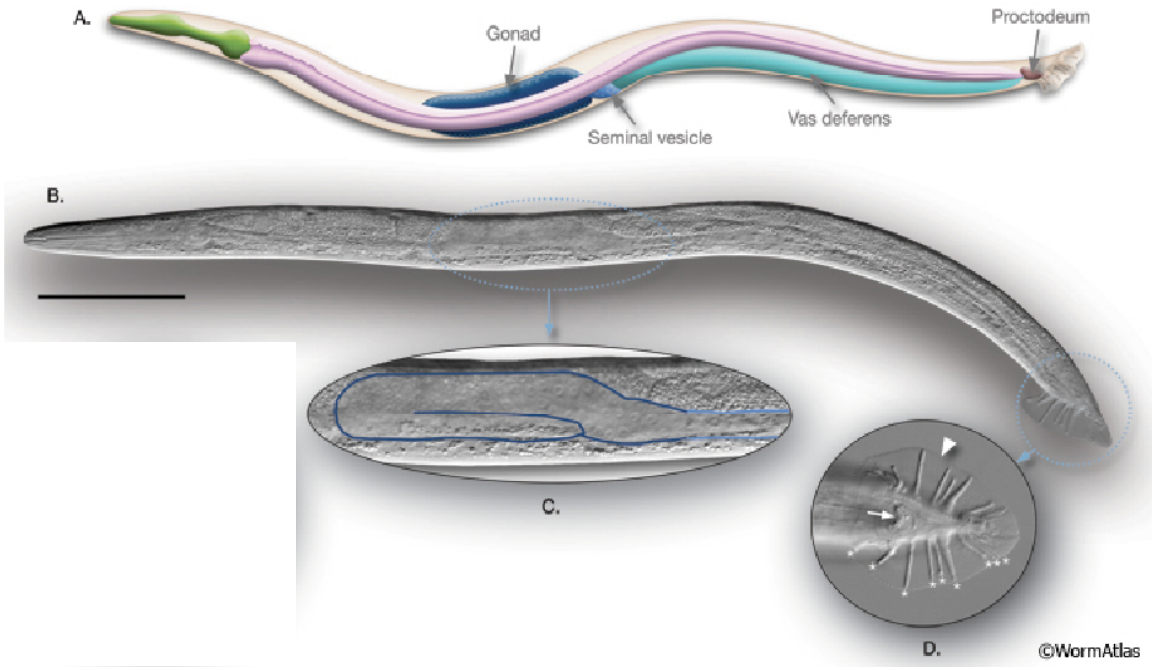

Figure 1.5. Anatomy of the adult *C. elegans* male. **A.** Cartoon of the adult male. **B.** Nomarski optics of an adult male. **C.** Enlargement of the male germline. Note the male has a single gonad arm. **D.** Enlargement and ventral view of the male tail. Arrow points to cloaca (anus), arrowhead point to the fan of the tail. Figures adapted from www.wormatlas.org.

Figure 1.6

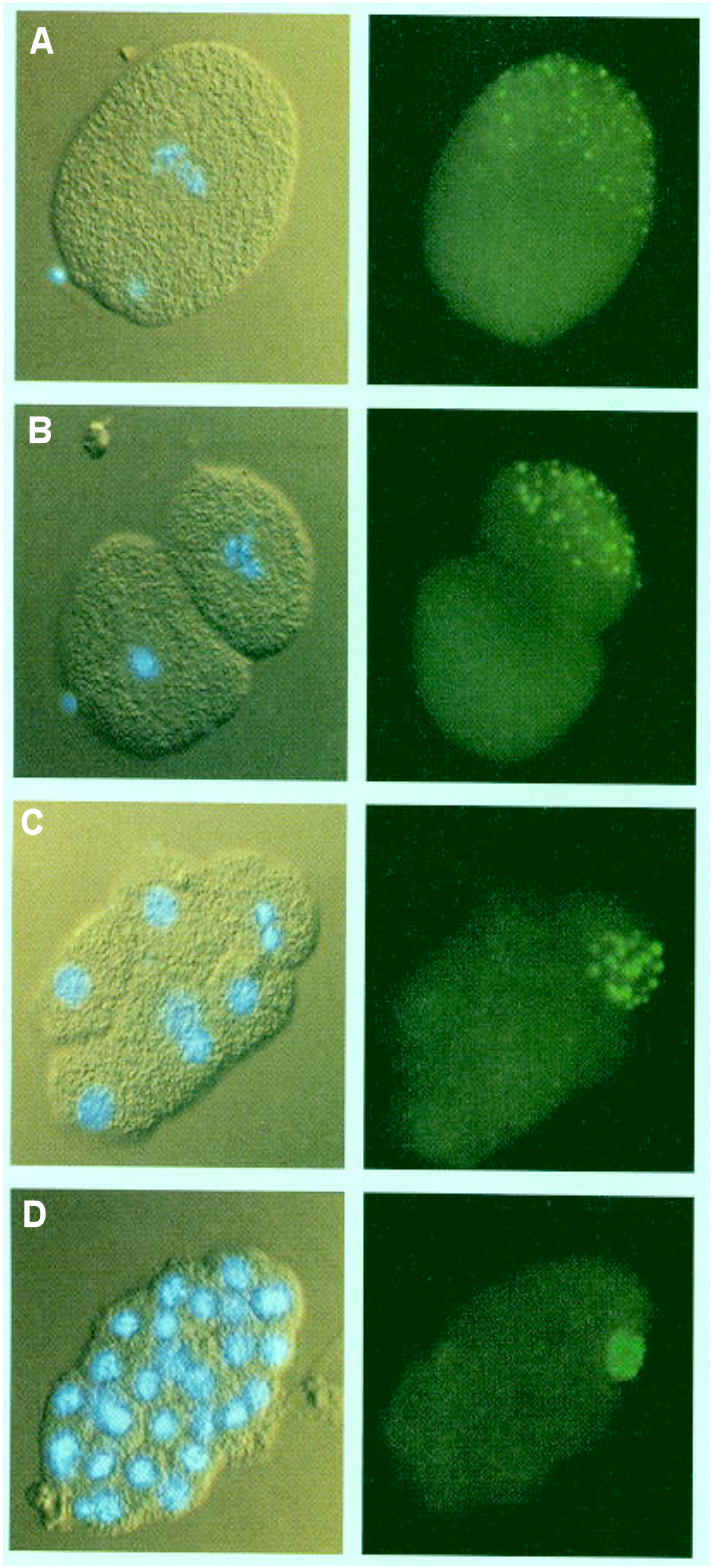

Figure 1.6. Segregation of P granules in *C. elegans* embryos. Left panels, Nomarski optics and DAPI staining. Right Panels, staining by immunofluorescence with the anti-PGL-1 antibody that marks P granules. **A.** A newly fertilized embryo about to divide. At this stage P granules have migrated toward the posterior of the embryo (upper right side). **B.** A two-cell embryo with P granules only in the P1 cell. **C.** An eight-cell embryo, P granules continue to localize with the P lineage in the P3 cell. **D.** A thirty-two-cell embryo, P granules found only in the germline progenitor cell. Adapted from www.8e.devbio.com.

Figure 1.7

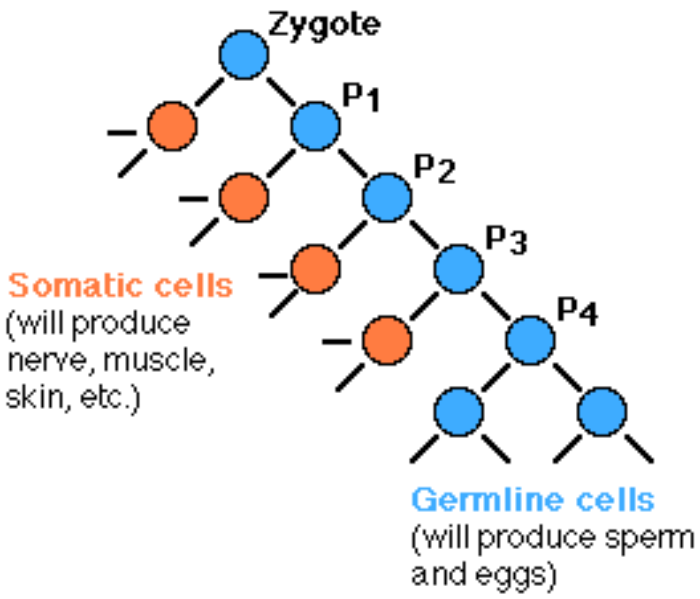

Figure. 1.7. Schematic of P lineage segregation in the first five cellular divisions of the *C. elegans* embryo. The germline segregates along the P lineage starting with the first embryonic division. Germline segregation culminates with the P4 cell, which divides once more giving rise to the Z2 and Z3 cells. These two cells will eventually produce all of the germ cells in *C. elegans* adult germline.

Figure 1.8

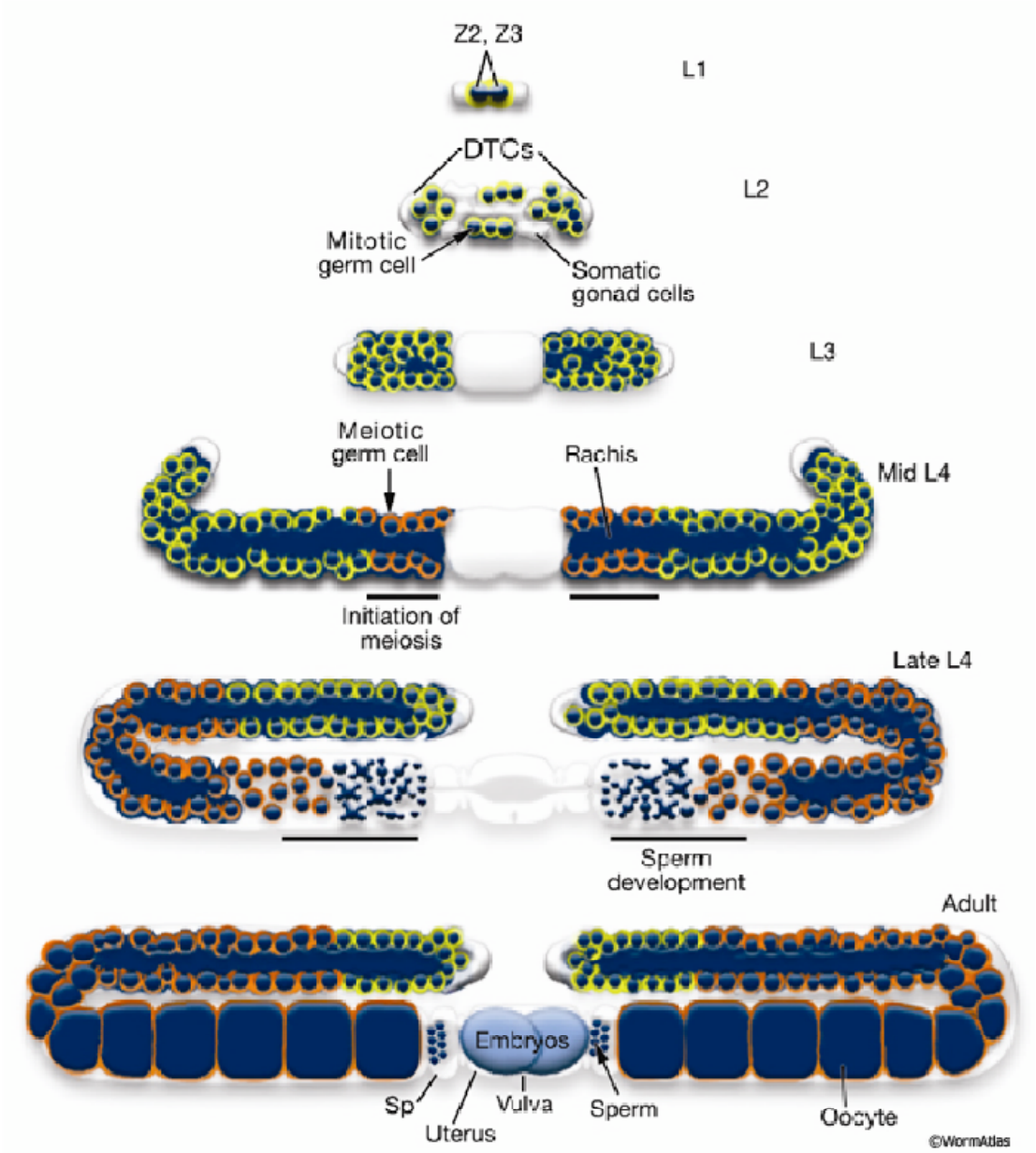

Figure 1.8. *C. elegans* germline development. The Z2 and Z3 cells give rise to the entire adult germline. Germ cells begin to divide mitotically in the L2 stage. By the L4 stage germ cells start to undergo meiotic divisions and differentiate into sperm. Once sperm development is completed germ cells switch to oocyte production. DTC = distal tip cell, sp = spermatheca. Adapted from www.wormatlas.org.

meiosis and begin sperm production. The sperm are then stored in the spermatheca. Following this stage no more sperm can be produced, making sperm the limiting factor in the production of progeny. After sperm production is completed, oocyte development commences. The worm contains two identical gonad arms. Each arm contains developing germ cells that go on to form oocytes. The fully developed oocytes are then ready for maturation and the most proximal oocyte is stimulated by major sperm protein (MSP) to then be pulled through the spermatheca where they are fertilized. The embryos begin early development, and are laid via the vulva at approximately the four-cell stage (www.wormbook.org).

The *C. elegans* two gonad arms are symmetrical, each containing hundreds of germ cells. At the distal tip of each gonad arm germ cells are signaled to undergo mitosis. As new mitotic cells are generated the older germ cells are pushed from the distal region, mitotic signals decrease and germ cells begin to undergo meiosis. At the bend of the gonad, germ cells are in the pachytene stage of meiosis and after diakinesis the oocytes begin to mature. In the distal gonad the germ cells surround a central anucleated core, called the rachis. Since germ cells lack cellular membranes on the interior, a syncytium is formed. This syncytial core (rachis) is where the nutrients produced by germ cells are transported and distributed to proximal oocyte. Figure 1.9 is a Normarski image of a single arm of the gonad. At the distal region near the distal tip cell (DTC) is where germ cells are actively in mitosis.

Figure 1.9

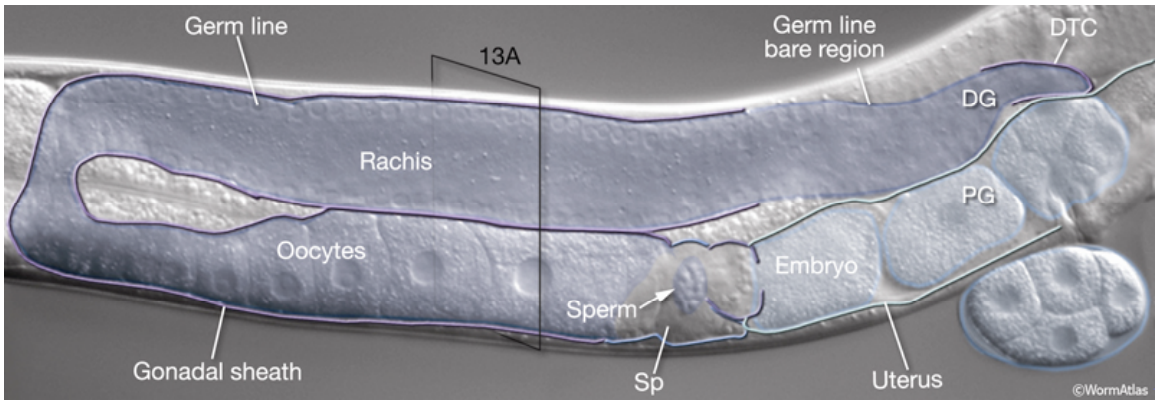

Figure 1.9. Nomarski image of an adult worm with one of the two gonad arms featured and highlighted in blue. At the distal region germ cells are undergoing mitosis, further down germ cells switch to meiosis and pachytene stages, and in the more proximal region oocytes are produced. The most proximal oocyte is stimulated by major sperm protein for ovulation and pulled through the spermatheca (Sp) where it is then fertilized, begins early embryonic development, and then laid via the vulva around the four-cell stage. Adapted from www.wormatlas.org.

Germ Granules

Germ granules are cytoplasmic ribonucleoprotein (RNP) aggregates found in most, if not all, studied organisms that contain a germline. These RNPs are germline determinants, required for germline development and differentiation. Germ granules are similar in function and composition among the studied species, but are referred to by different names in each organism. In *C. elegans* germ granules are referred to as P granules, polar granules and nuage (at various stages of development) in *Drosophila*, nuage in vertebrates, and chromatoid bodies in the sperm of mice. The *C. elegans* P granules are cytoplasmic, non-membrane bound, protein and RNA aggregates that segregate with the germline at the first cellular division and are found in all germ cells throughout the life of the worm (Strome and Wood, 1982; 1983). The location of P granules changes from a uniform cytoplasmic distribution in the newly fertilized zygote to a perinuclear localization in the primordial germ cell P4, which is born at the 14-cell stage of embryogenesis. Figure 1.10 is an image of a P granule in the P4 cell by electron microscopy, note at this stage the P granule is perinuclear. P granules remain perinuclear throughout subsequent larval stages and throughout development of the adult germline, until oocyte maturation occurs and P granules dissociate from the nuclear envelope (Strome and Wood, 1983). P granules are required for germline development and contain a number of proteins important for fertility. Although much is known regarding many of the P-granule components, the function of P granules remains elusive.

Figure 1.10

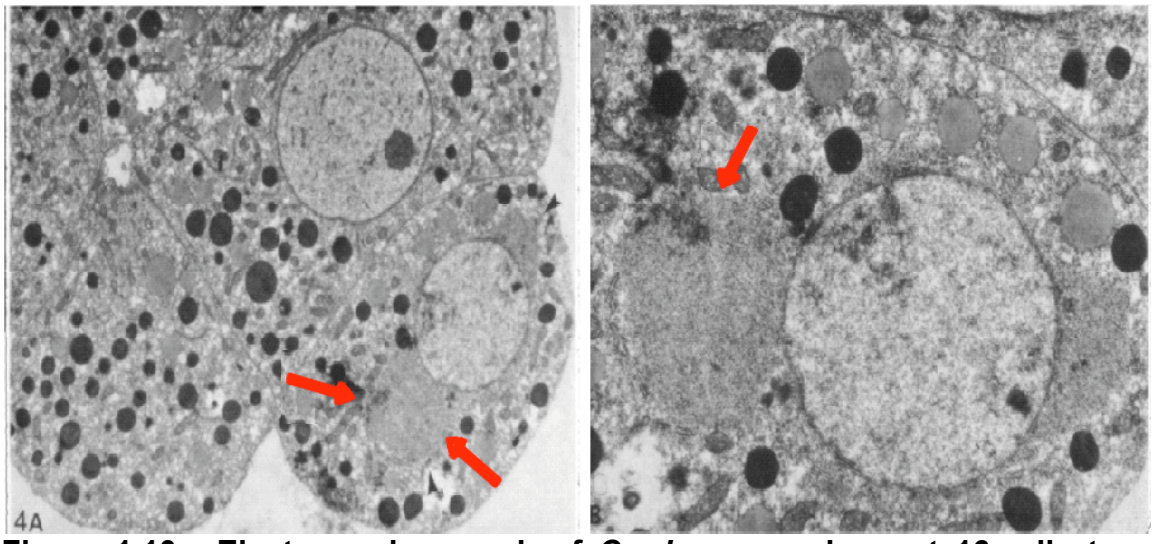

Figure 1.10. Electron micrograph of *C. elegans* embryo at 16-cell stage showing the electron dense P granules. Left panel: section through a *C. elegans* embryo, the P4 cell is in the bottom right corner, arrows point to the large electron dense granules that are perinuclear to the germ cell nuclei. Right panel: magnification of left panel showing only the P4 cell. The large P granule on the left is indicated by the red arrow. Adapted from (Wolf et al., 1983).

Hypotheses regarding the role of P granules predict that they are sites for translational control of maternally-transcribed mRNAs. Several mRNAs have been identified as P-granule components including *pos-1*, *mex-1*, *mex-3, pie-1* and *nos-2*, each of which are important for patterning the *C. elegans* embryo or for germline proliferation and differentiation, suggesting that P granules regulate maternally-transcribed mRNAs (Schisa et al., 2001). P granules also contain a large number of proteins involved in the binding and regulation of mRNA; including, PGL-1 a predicted RNA binding protein and the PGL family of proteins, the Vasa-related GLH family of proteins, CGH-1 a decapping enzyme involved in the degradation of mRNAs, and GLD-1, another P-granule component that has been shown to specifically regulate the translation of a subset of maternal mRNAs, supporting this hypothesis of translational control (Gruidl et al., 1996; Jones et al., 1996; Kawasaki et al., 1998; Kuznicki et al., 2000; Navarro et al., 2001). Many of the components identified to localize to *C. elegans* P granules are listed in Table 1.1, this list in incomplete as more and more proteins involved in mRNA regulation are being identified to transiently associate with P granules.

Vasa

One of the best-studied germ granule components is the *Drosophila* protein Vasa. Vasa is essential for fertility and formation of the pole cells, which are progenitor germ cells in the *Drosophila* embryo. It is known that Vasa is involved in regulating the translation of specific mRNAs when in complex with other protein binding partners (Hay et al., 1988; Lasko and Ashburner, 1988; Liu et al.,

Table 1.1

Table 1.1 Proteins present in P granules	
Proteins	Motifs/Functions
Embryos	Adults
PGL-1	RGG box
PGL-2	No recognizable motifs
PGL-3	RGG box
GLH-1	DEAD-box helicase motifs, 4 CCHC fingers
GLH-2	DEAD-box helicase motifs, 6 CCHC fingers
GLH-3	DEAD-box helicase motifs, 2 CCHC fingers
GLH-4	DEAD-box helicase motifs, 5 CCHC fingers
CGH-1	DEAD-box helicase motifs
PIE-1	2 CCCH fingers
MEX-1	2 CCCH fingers
POS-1	2 CCCH fingers
OMA-1	2 CCCH fingers
OMA-2	2 CCCH fingers
MEX-3	2 KH domains
GLD-1	KH domain; translational repressor
GLD-2	Cytoplasmic poly(A) polymerase (PAP)
GLD-3	KH-related domains; subunit of PAP
Sm proteins	Splicing factors
SPN-4	RNP motif
IFE-1	Translation initiation factor 4E

Table 1.1. List of proteins identified in C. elegans P granules and their relevant motifs. Figure adapted from www.wormbook.org.

2009; Styhler et al., 1998; Tomancak et al., 1998). Vasa is a DEAD-box RNA helicase protein, and while the helicase function is not necessary for its localization the helicase is required for the assembly of pole plasm (germ granules in flies) at pole cells. Vasa, in complex with the protein Oskar, is required for the posterior localization of *nanos* mRNA, another germline determinant (Liang et al., 1994). Additionally, Vasa is necessary for the translation of *nanos* mRNA by overcoming a repressive structure element in the 3' UTR of the mRNA (Gavis et al., 1996).

Vasa has been shown to bind eIF5B, a translation initiation factor that is involved in ribosomal subunit joining and this binding appears to have a functional role in the activation of translation. Translation of the *Drosophila* mRNA *grk* (Gurken) relies on Vasa and is disrupted in the *vas*-null oocytes (Styhler et al., 1998; Tomancak et al., 1998). Translation of *grk* is also disrupted in oocytes that express a form of Vasa (VasΔ617) protein that lacks the eIF5B-binding domain, suggesting that the disruption of *grk* mRNA translation is due to a defect in the recruitment of eIF5B to its target mRNAs (Johnstone and Lasko, 2004). Recent reports regarding the function of Vasa have shown that it specifically binds to a subset of mRNAs. One of these mRNA targets, *mei-P26*, is positively regulated for translation by Vasa. Vasa binds *mei-P26* at its (U)-rich 3' UTR, thereby activating its translation. The product of *mei-P26* is a protein that represses microRNA (miRNA) activity in germ cells and promotes germline stem cell differentiation (Liu et al., 2009). Thus, Vasa is a dynamic germline component

involved in the assembly of pole plasm in the developing oocyte, in the translational-regulation of a specific subset of germline mRNAs, and is indirectly involved in the regulation of the miRNA pathway.

Germline RNA Helicases

C. elegans has four Vasa homologues expressed in the germline, which were identified by the Bennett laboratory, these are the Germline RNA Helicase proteins 1-4 (GLH-1, -2, -3, and -4). Initially, searches by the Bennett laboratory identified a single *vasa* homologue, *glh-1* (Rousell and Bennett, 1993). However, with the sequencing of the *C. elegans* genome three more *glh* genes were identified, along with a pseudo-gene *glh-4b* (Gruidl et al., 1996; Kuznicki et al., 2000). All GLH proteins contain the eight conserved DEAD-box RNA helicase motifs in the C terminal region of the protein, multiple retroviral-like CCHC zinc fingers, and all but GLH-3 have regions of FGG repeats sequences in their N-termini. Figure 1.11 is a schematic depicting the GLH proteins and their motifs. Typically, in proteins containing conserved DEAD-box RNA helicase motifs, these motifs have little substrate specificity based on the helicase region alone. Therefore, it has been hypothesized that the non-helicase regions of the DEAD-box proteins are important for imparting substrate specificity. The Bennett laboratory has predicted that if the GLH proteins bind their substrates with specificity it may be due to either the CCHC zinc fingers or a combination of the zinc fingers and the FGG repeat regions (Roussell and Bennett, 1993).

Figure 1.11

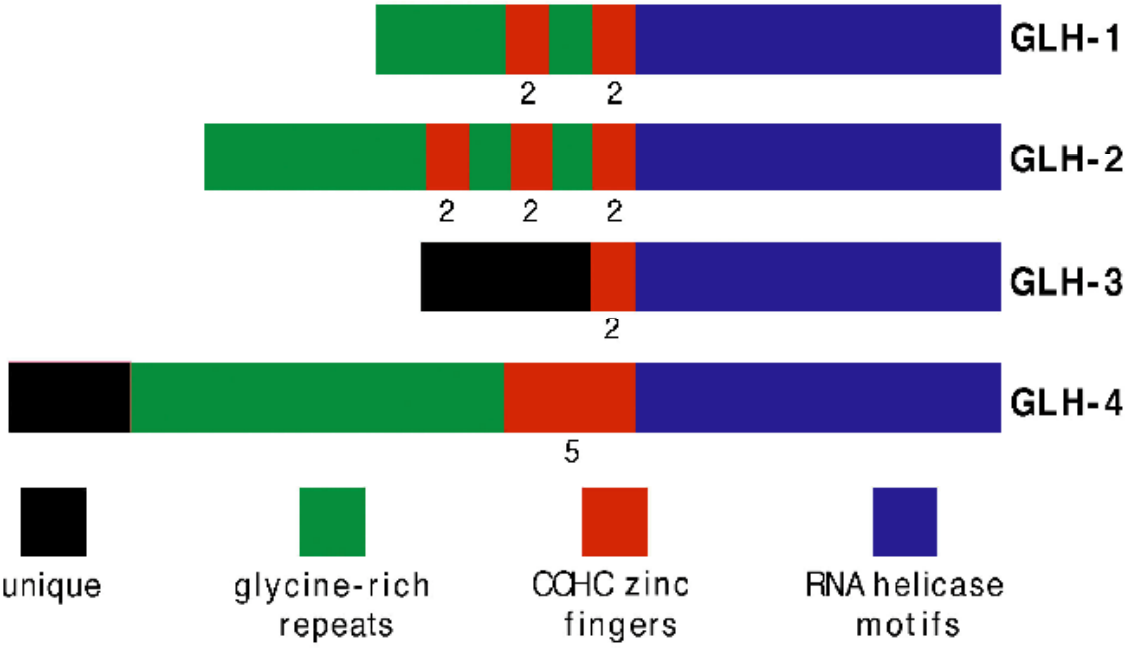

Figure 1.11. Schematic of the four Germline RNA Helicase proteins. All four of the GLH proteins contain the eight conserved DEAD-box RNA helicase motifs (blue) at the C-terminus of the protein. Additionally they all contain multiple retroviral-like CCHC zinc fingers (red) and all but GLH-3 contains glycine-rich (FGG) repeat regions in their N-terminus (green). Regions of unique sequence are indicated in black.

The GLH proteins are constitutively associated with the P granules and localize independently of one another (Fig. 1.12). The GLH proteins are also integral components of P granules. The Schisa et al., 2000 paper demonstrated that when *glh-1* and *glh-2* were knocked down in combination by RNAi the structure of P granules was lost. Normally by electron microscopy P granules appear as large electron dense regions that are perinuclear and associated with nuclear pores. In the *glh-1;glh-2* RNAi knockdown these large electron dense regions become condensed and loose their structure, suggesting that the GLHs are integral components of P granules (Fig. 1.13).

The GLH proteins are necessary for germline development. Studies of these proteins revealed that of the four family members, loss of GLH-1 is most critical (Gruidl, et al., 1996; Kuznicki, et al., 2000; Roussell and Bennett, 1993). GLH-1 is essential for proliferation of the germline; knockdown of *glh-1* by RNA interference (RNAi) affects P-granule structure (Kuznicki *et al*., 2000; Schisa *et al*., 2001). Worms injected with double-stranded RNA specific for *glh-1* and raised at the restrictive temperature of 26°C, produce F1 progeny that lack oocytes and that contain non-functional sperm (Kuznicki et al., 2000); *glh-1* deletion mutants are also temperature-sensitive sterile worms (Spike et al., 2008). When both GLH-1 and GLH-4 are knocked-down in combination by RNAi the resulting progeny are sterile, producing no oocytes and only non-functional sperm even when grown at the permissive temperature of 20°C (Fig. 1.14). In comparison, the *glh-1(gk100)* mutant has reduced fertility at the permissive

Figure 1.12

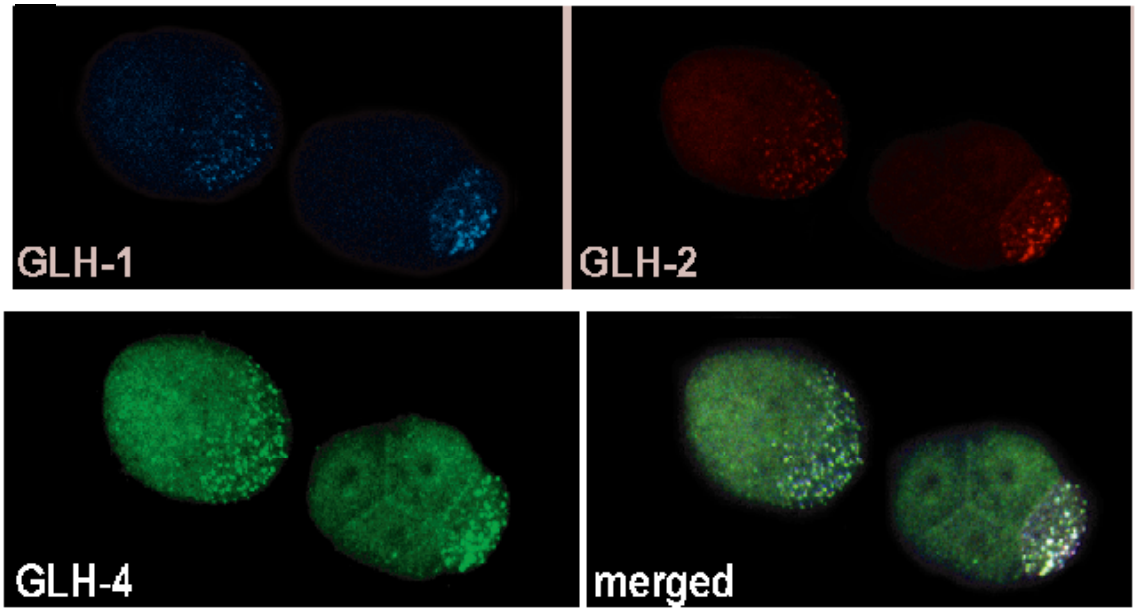

Figure 1.12. The GLH proteins localize to P granules in the absence of GLH-3. Immunolocalization of GLH-1 (top left panel, blue), GLH-2 (top right panel, red), and GLH-4 (bottom left panel, green) shows localization of all three proteins to P granules in two-cell and four-cell *glh-3(um1)* embryos. Merged image, bottom right panel.

Figure 1.13

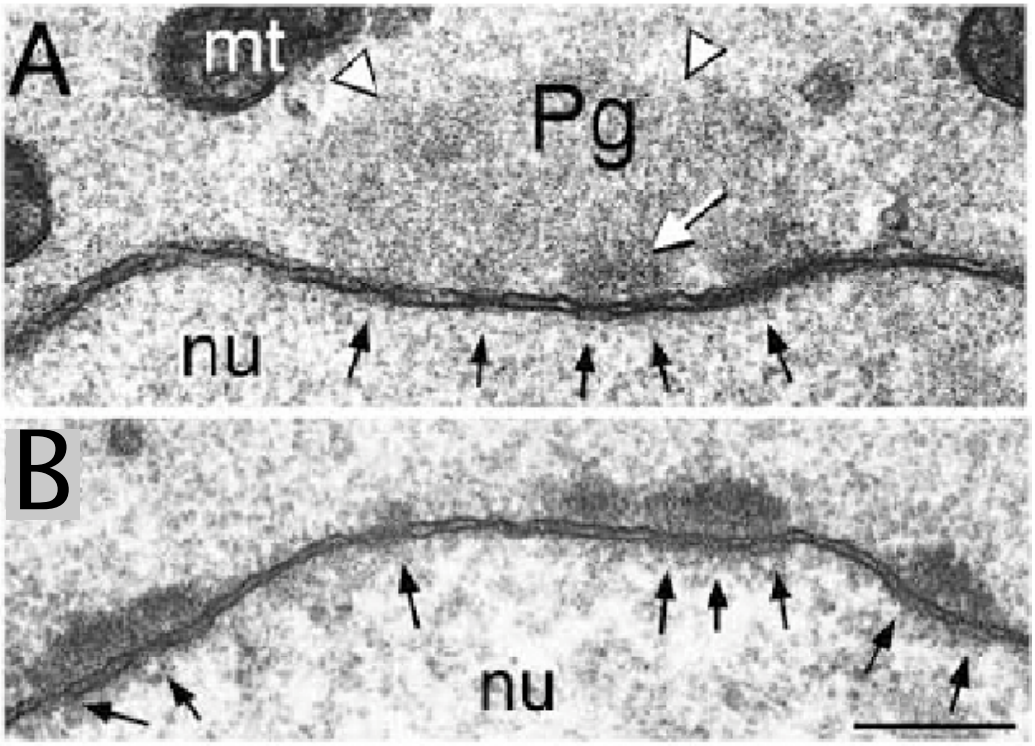

Figure 1.13. The structure of P granules is distorted by *glh-1/2* RNAi. A. A single P-granule at the nuclear membrane of a germ cell. **B.** Condensed P-granule structure around a germ cell nucleus following *glh-1/2* RNAi. White arrowheads point to fibular matrix of the P granule, white arrow points to electron dense region. Black arrows point to nuclear pores. mt = mitochondria, nu = nucleus, size bar is 0.2 μm. Adapted from (Schisa et al., 2001).

Figure 1.14

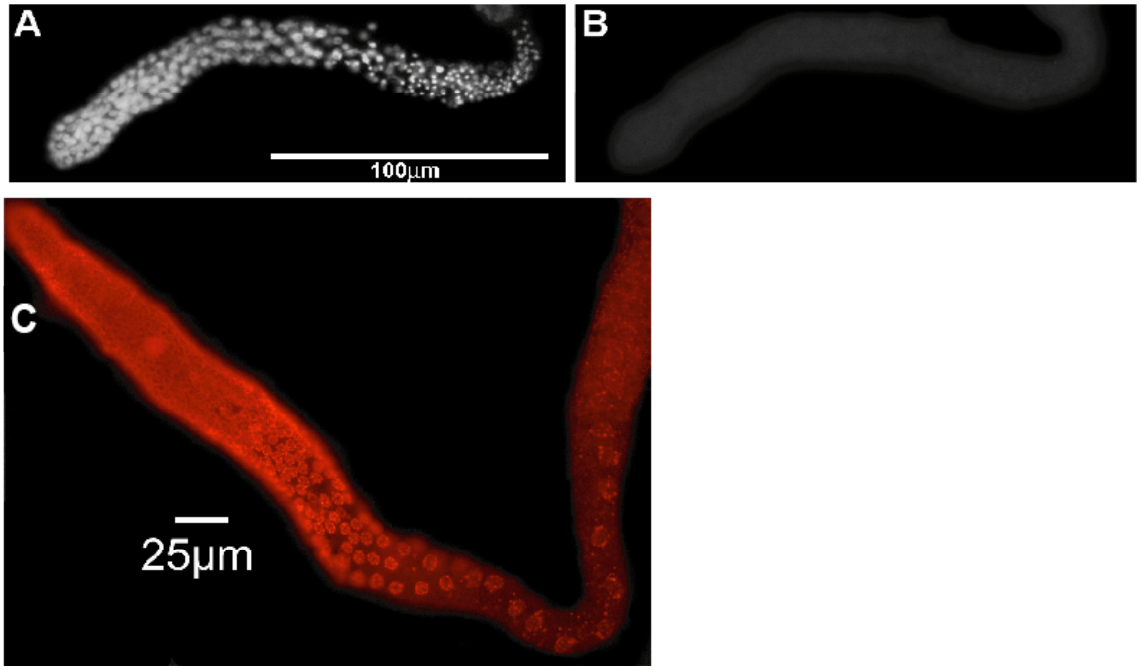

Figure 1.14. Loss of *glh-1* and *glh-4* in combination results in sterility and an underproliferated gonad. A. DAPI staining of an extruded gonad from a *glh-1/4* RNAi worm grown at 20°C. **B.** ICC of the same gonad reacted with anti-GLH-4 antibody to demonstrate knock-down of the protein. **C.** A wild type gonad extruded with the worm and reacted with antibodies to GLH-1 (red).

temperature of 20°C and is 100% sterile at the non-permissive temperature of 26°C.

Translational Regulation by the RNAi pathway

One of the most fascinating discoveries regarding mRNA regulation came with the discovery of RNA interference (RNAi). First identified in plants and later defined in *C. elegans*, RNAi is the process of specifically knocking-down the production of protein products through the exogenous administration of double-stranded RNA. The double-stranded RNA is taken up by the cells and associates with the protein Dicer, a riboendonuclease that processes the RNA into short, approximately 21 nucleotides, RNAs. These short interfering RNAs (siRNA) then associate with a complex of proteins referred to as the RNA-interfering silencing complex (RISC) machinery which dissociates the sense from the anti-sense strand and then matches the anti-sense strand to its target mRNA transcript. This process generally results in the degradation of the target mRNA and therefore inhibits the protein product from being produced. The exogenous small-interfering RNA (siRNA) pathway occurs when double-stranded RNA (dsRNA) is introduced in the cell. This dsRNA is then processed by Dicer in the cytoplasm into the short siRNAs (~21 nucleotides in length), the anti-sense strand is then loaded into the RISC complex which then targets the corresponding mRNA for degradation. In the endogenous RNAi pathway micro-RNAs (miRNAs) generated from the genome are utilized to regulate the timing of translation of target mRNAs. Within the genome there are coding sequences for

pre-miRNAs, which are small hairpin structured RNAs that are processed by Dicer into miRNAs. The miRNA pathway is a crucial aspect of gene regulation in maintaining the integrity of both the cell and the organism as a whole. miRNA-mediated translational repression often results in gene silencing through the imperfect base pairing of short anti-sense RNA molecules, which bind to the 3' UTR of their target transcripts. The interaction of miRNAs with their mRNA targets is facilitated by Argonaute proteins, which are members of RISC. In animals, imperfect base pairing of the miRNA to its mRNA target typically results in silencing of the mRNA, rather than degradation, which results in "knock-down" of the targeted mRNA in the exogenous siRNA pathway. While our knowledge regarding the widespread role of miRNAs in gene regulation is increasing, mechanisms by which miRNA-mediated translational repression occurs remain to be clarified (Ambros, 2004; Filipowicz et al., 2005; Grishok et al., 2005). A summary of both the endogenous miRNA and exogenous siRNA pathway is depicted in model form in Figure 1.15.

Transcripts that are targeted either for silencing or degradation have been shown to localize to discrete cytoplasmic RNP granules. These granules also contain a number of proteins involved in mRNA regulation, storage, and degradation. In the cytoplasm of somatic cells there are two of types of granules, Processing bodies (P bodies) and stress granules.

Figure 1.15

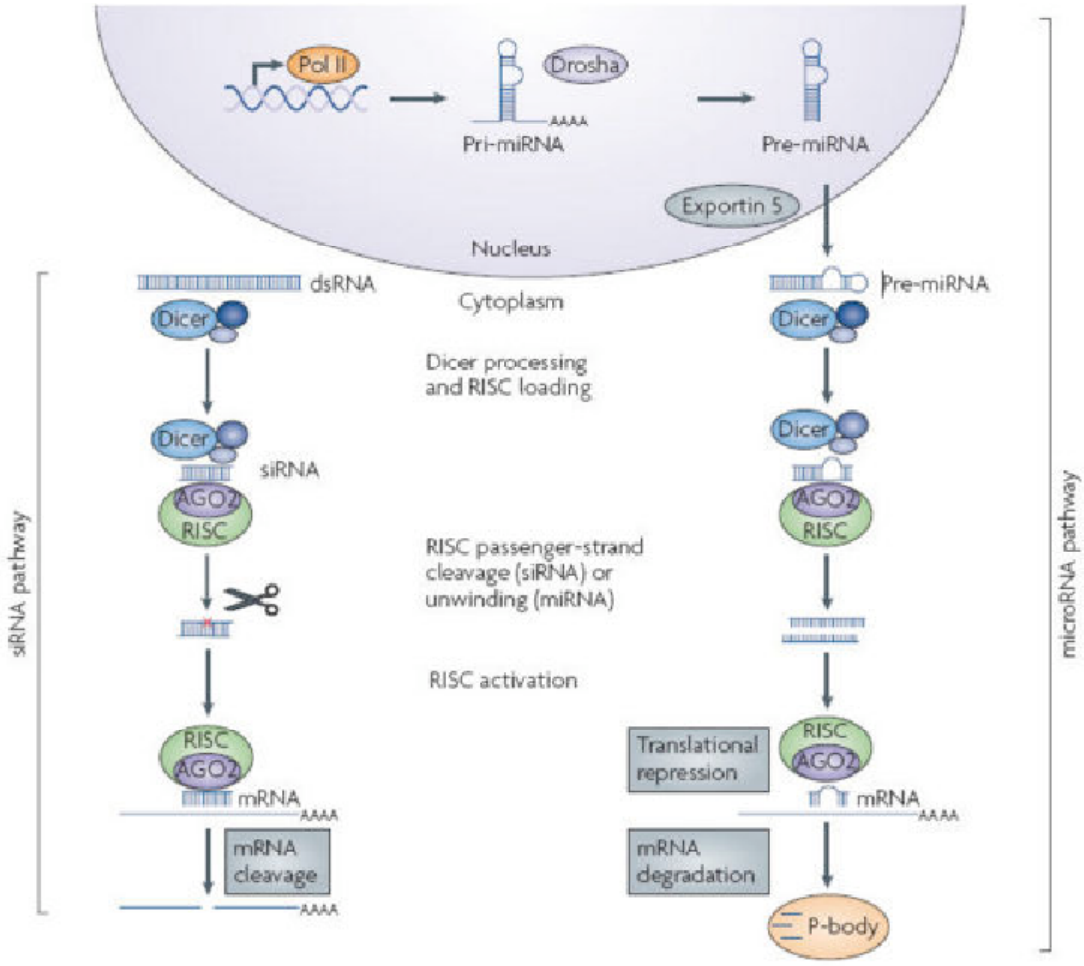

Figure 1.15. Schematic of the RNA interference pathway. The exogenous siRNA pathway is depicted on the left. The endogenous miRNA pathway is depicted on the right. Adapted from (de Fougerolles et al., 2007).

Processing bodies

The cytoplasmic foci termed Processing bodies (P bodies) are granular structures, composed of proteins and RNAs, which are dynamically involved in post-transcriptional gene regulation. Studies that inhibit the mRNA decay pathway result in the accumulation of poly(A)+ mRNA in P bodies (Sheth and Parker, 2003; Cougot et al., 2004; Anderson and Kedersha, 2006). Similarly, mammalian cells treated with siRNAs against the P-body component GW182, another P body component, are defective in the miRNA-dependent silencing of target mRNAs (Jakymiw et al., 2005; Liu et al., 2005). Together these data suggest that P bodies regulate expression of target mRNAs and thus play an important role in mRNA metabolism. Figure 1.16 lists the functions that have been associated with P bodies.

P bodies have been shown to contain a number of proteins essential for mRNA degradation. The 5'→3' exonuclease, XRN1, was the first of these proteins found associated with the structures (Bashkirov et al., 1997). Since this time, several other mRNA decay pathway protein members have been identified in P bodies. These include members of an mRNA decapping enzyme complex, of the non-sense mediated decay pathway, and of the RNA-induced silencing complex (RISC). The protein composition of P bodies appears to be dynamic, depending on cellular conditions. However, the mammalian proteins DCP1a, DCP2, and GW182 are restricted to P bodies. DCP1a/DCP2 are decapping enzymes and GW182 is an RNA-binding protein required for miRNA-dependent silencing

(Bashkirov et al., 1997; Lian et al., 2006; Liu et al., 2005). These proteins are thought to serve as the core around which the P body assembles (Anderson and Kedersha, 2006).

As depicted in Figure 1.16, P bodies are a diverse control center for mRNA processing. Transcripts targeted to P bodies may either be degraded or undergo translational silencing, depending on its interaction with various P body protein components. These functions appear to create equilibrium between actively translated mRNAs and those that are temporally regulated for silencing. From studies done in mammalian tissue culture and *S. cerevisiae,* it is known that P bodies accumulate in size and number in response to stress (Teixeira et al., 2005), are required for miRNA-mediated translational control (Liu et al., 2005), are motile structures that interact with the cytoplasmic stress granules (Kedersha et al., 2005), and that miRNA-silenced transcripts targeted to P bodies can be rescued for translation upon proper signaling (Bhattacharyya et al., 2006; Brengues et al., 2005). The current model for P-body gene regulation is that there is a finely tuned balance between translating and non-translating pools of mRNA associating with either polysomes or P bodies, respectively. This balance can be tipped and reversed in either direction depending on the state and needs of the cell. The interest in the translating versus non-translating balance stems from recent insights into the role of P bodies in miRNA-mediated translational silencing, the identification of the sub-cellular localization of the RISC machinery

Figure 1.16

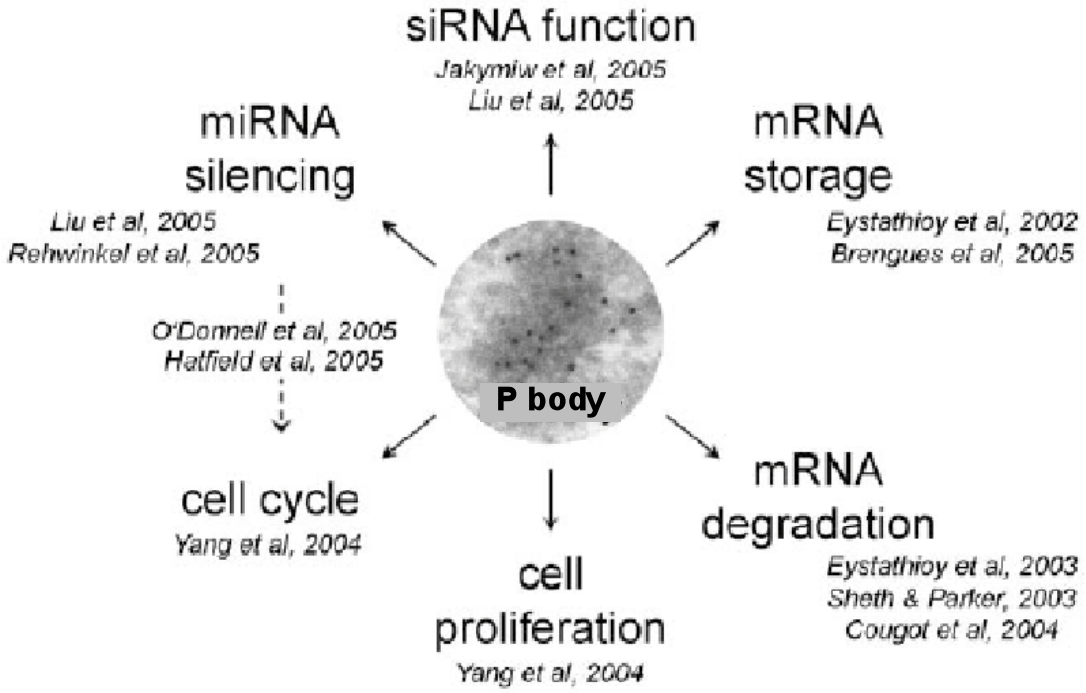

Figure 1.16. Summary of the multiple processes associated with the P-body. Adapted from (Lian et al., 2006).

to P bodies, and the explosion of knowledge regarding the role of miRNAs in gene regulation.

Germline RNP granules

Similar to the P bodies, and the related stress granules that form during stress or cell cycle arrest, are the germline-associated, cytoplasmic RNP granules. These large RNP granules form in the rachis, or germline core, and also in the downstream developing oocytes. RNP granules have been shown to form under several stress conditions, including heat shock, depletion of sperm, which are the limiting reagent in *C. elegans* fertilization, and hypoxia. The majority of the protein components identified thus far to localize to RNP granules are involved in mRNA regulation including CAR-1, CGH-1, DCP-2, and PAB-1 (Noble et al., 2008; Jud et al., 2008). Figure 1.17 is a representative image of the formation of PGL-1 and CAR-1 in RNP granules in the absence of sperm. It has been hypothesized that these granules may be similar to Processing bodies and stress granules as they contain many of the same components. Perhaps like their somatic counterparts, germline RNP granules form under stress and cell-cycle arrest to regulate maternal mRNAs for silencing or degradation. It is interesting to note that the formation of germline RNP granules is reversible. The *fog-2(q71)* strain is used in these studies as the mutant produces only oocytes and no sperm, thus RNP granules form in both the rachis and oocytes of *fog-2(q71)* female adults. When *fog-2(q71)* mutant females are mated with a male and provided with sperm, ovulation commences and the large granules disperse

Figure 1.17

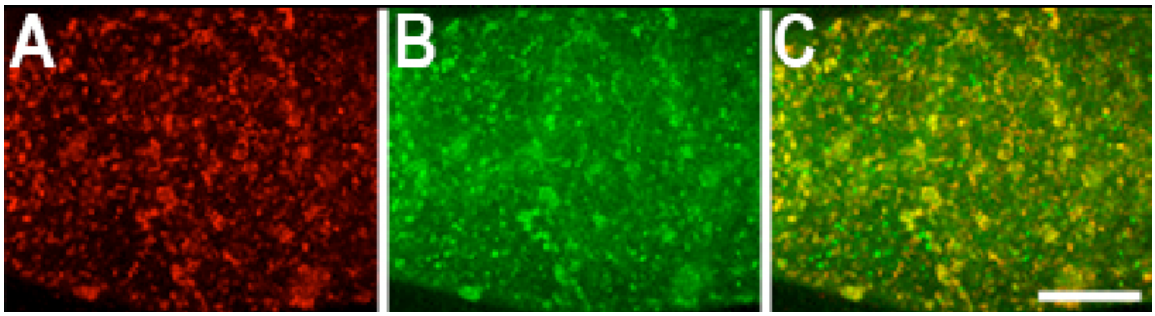

Figure 1.17. PGL-1 and CAR-1 localization to large RNP granules in arrested oocytes. Immunocytochemistry of arrested oocytes in *fog-2(q71)* unmated worms with anti-PGL-1 (red, A), anti-CAR-1 (green, B), and merged image (yellow, C). Adapted from Jud et al., 2008.

(Schisa et al., 2001). This indicates that even in the arrested state oocyte viability is maintained, perhaps due to the presence and function of the RNP granules.

Dicer

Following the discovery of the RNAi pathway in plants and worms came the introduction of the ribonuclease responsible for processing longer double-stranded RNAs into short, 21-23 nucleotide pieces, RNAs. This RNAse III ribo-endonuclease was given the appropriate name of Dicer, in reference to its "dicing" function (Bernstein et al., 2001). Dicer, like the GLH proteins, is a member of the DEAD-box RNA helicase family. It also contains a conserved Piwi Argonaute Zwille (PAZ) domain, which is commonly found in Argonaute and other RNA-induced silencing complex (RISC) associated proteins. PAZ domains are the protein regions responsible for binding small interfering RNAs of approximately 18 to 23 nucleotides in length. In Argonaute proteins this binding allows for the protein to complex with the target mRNA. In Dicer, the PAZ domain, along with the RNA binding domain, are responsible for Dicer binding to dsRNA and for determining the length of the siRNA or miRNA products. Additionally Dicer contains two RNAse III domains that are responsible for the cleavage of the miRNA and siRNA precursors.

In *C. elegans* Dicer has been shown to be important for a number of developmental properties, including the heterochronic pathway. Heterochronic

genes control the temporal dimension of development, meaning that they maintain the correct timing for expression and differentiation of stage-specific developmental events. A classic example of this in *C. elegans* is the regulation of LIN-14 and LIN-28 by *lin-4*. Both LIN-14 (a novel *C. elegans* protein) and LIN-28 (an RNA binding protein) are required during early larval stages, but at the L3 stage their protein levels begin to decrease. This decrease is the result of the binding of a small RNA *lin-4*, later defined as a miRNA, to the 3' UTR of *lin-14* and *lin-28* (Lee et al., 1993; Olsen and Ambros, 1999; Ambros, 2001). This binding resulted in the silencing of both *lin-14* and *lin-28* via the RISC machinery.

Dicer has also been found to play a significant role in germline development and female fertility. This role of Dicer will be discussed in more detail in the Introduction of Chapter 2 (Knight and Bass, 2001; Luense et al., 2009; Megosh et al., 2006; Murchison et al., 2007).

Nuclear pore proteins

The nuclear pore complex (NPC), found embedded in the nuclear membrane, serves as the gateway between the nucleus and the cytoplasm. This complex of proteins monitors every large molecule exiting and entering the nucleus, and thus serves an important role in gene regulation in part through the transport of mRNAs. NPCs contain a number of different proteins, including approximately 10 nucleoporin proteins, which make up the inner matrix of the pore structure. These nucleoporin proteins, like the GLHs, are FG rich and are thought to serve

as transport barriers by creating a meshwork through weak hydrophobic interactions. Transport proteins that shuttle in and out of the nucleus are able to overcome the barrier by interacting with the FG repeats to dissolve the barrier (Brohawn et al., 2009; D'Angelo and Hetzer, 2008).

Awaiting the exiting nutrients on the cytoplasmic side of *C. elegans* germ nuclei are the P granules. Intuitively, one might consider that these P granules are there for a distinct purpose, to exquisitely regulate the translation of the emerging mRNAs in a timely manner. Recent work published by the Priess laboratory has demonstrated that newly translated mRNAs are transported through nuclear pores into P granules. With the loss of P granule structure following *glh-1(RNAi)*, newly transcribed mRNAs no longer accumulate outside of the nucleus (Sheth et al., 2010). One hypothesis might be that the GLH proteins may directly bind with the nuclear pore FG meshwork through its own N-terminal FG-rich region to subsequently except mRNAs by its DEAD-box helicase and CCHC zing finger domains. Immunolocalization of GLH-1 and several nucleoporin proteins has demonstrated an incomplete co-localization between the two. GLH-1 protein is clearly external to the nuclear membrane but does show some overlap (Beshore et al., submitted for publication; Sheth et al., 2010). P granules that have dissociated from the nuclear membrane do contain fragments of nuclear pores indicating a strong association between the two. Initial attempts by myself, the Seydoux laboratory, and the Strome laboratory (UC Santacruz) at detecting a physical interaction between GLH-1 and members of the nucleoporin protein

family have failed. Exactly how P granules associate, bind, and function with nuclear pores is still of great interest.

Previous Findings

The Bennett Laboratory has done extensive work analyzing the protein GLH-1, both function and regulation. Pliny A. Smith, a previous graduate student in the laboratory, screened for protein interactors of GLH-1 by conducting yeast-two-hybrid experiments. The goal of his project was to identify other proteins that bind to GLH-1. This was done to determine the function or pathway for GLH-1. Pliny found multiple proteins that bind with GLH-1, including KGB-1 and CSN-5 (Smith et al., 2004). The role of KGB-1 and CSN-5 was later examined and described by a former graduate student in the Bennett Laboratory, April Orsborn Bauer. KGB-1 is a Jun N-terminal kinase that likely phosophorylates its protein targets, which subsequently targets them for degradation. KGB-1 was shown to be important for targeting GLH-1 for degradation via the proteosome. Loss of KGB-1 in the *kgb-1(um3)* mutant results in reduced fertility and elevated levels of GLH-1. The sterile worms produce endomitotically-replicating oocytes (EMO), which do not result in viable progeny. CSN-5 is a sub-unit of the COP9 signalosome and was found to protect GLH-1 from degradation. The *csn-5(ok1064)* homozygous mutant is sterile, resulting in a tiny gonad. Thus, KGB-1 and CSN-5 in *C. elegans* have competing functions in regulating GLH-1 and opposite phenotypes in the mutants. To test if loss of CSN-5 in the *kgb-1(um3)*

mutant could partially rescue the sterility resulting from an overabundance of GLH-1 protein, Dr. Bennett performed *csn-5(RNAi)* into *kgb-1(um3)* mutants. This experiment resulted in an increase in fertile worms, as compared to uninjected, and in lower levels of GLH-1. These data indicate that maintaining wild type levels of GLH-1 in the adult worm is important for fertility and that KGB-1 and CSN-5 have opposing functions in this role (Orsborn et al., 2007).

Aims of Dissertation

The aims of the work described in the following two chapters were to further define the role of GLH-1 in germline development by identifying other GLH-1 protein-binding partners. Because P granules localize at nuclear pore complexes, to likely regulate the translation of newly transcribed mRNAs, and because P granules contain proteins similar to the somatic P bodies, we set out to identify an interaction between GLH-1 and Dicer. It was and still is our goal to get a better understanding of how GLH-1 functions in the germline to regulate it's development and ultimately fertility of the worm. Because GLH-1 is a conserved protein found in flies (Vasa), mice (MVH), humans (DDX4), and in many other organisms, we find this work to be relevant to many fields of biology.

The second goal of this work was to describe the function of the GLH proteins based on results from the loss or decrease of the GLH proteins in the mutant strains. Because several different *glh-1* mutant strains were obtained that produce different truncated GLH-1 proteins we were able to begin to understand

how GLH-1 might function in P-granule assembly and function (Spike et al., 2008).

Chapter 2: Immunoprecipitation of the GLH-1 containing complex

Introduction

Previous work by our laboratory has demonstrated that GLH-1 interacts in complex with a number of proteins; including, the other GLH proteins, KGB-1, and CSN-5 (Orsborn et al., 2007; Smith et al., 2004). To further understand how GLH-1 might function in germline development we asked if GLH-1 interacts with components of the RNAi pathway, more specifically DCR-1.

Germ granules have been previously reported to contain several components involved in the miRNA pathway, including Argonaute proteins, Dicer, and miRNAs, it has been hypothesized that they may be similar in function to the somatic P bodies (Kotaja et al., 2006; Nagamori and Sassone-Corsi, 2008; Strome and Lehmann, 2007; Updike and Strome, 2009; Wickens and Goldstrohm, 2003). As described in Chapter 1, P bodies are cytoplasmic, ribonuclear protein (RNP) granules involved in mRNA degradation and storage that have been studied in a wide variety of organisms and cell types, from yeast to somatic mammalian cells (Ding et al., 2005; Jakymiw et al., 2005; Liu, et al., 2005a and 2005b; Sen and Blau, 2005; Anderson and Kedersha, 2006; Liu. and Gall, 2007; Balagopal and Parker, 2009; Zhao and Liu, 2009). P-body proteins are detected at high levels in the large cytoplasmic RNPs in *C. elegans* ooctyes, which form when ovulation arrests after hermaphrodites exhaust their limited

numbers of sperm, or after heat shock or other environmental assaults, including hypoxia (Gallo et al., 2008; Jud et al., 2007; Noble et al., 2008). One of the goals of this work was to further establish the relationship between these two classes of germline RNPs, the *C. elegans* P granules and the RNP granules in oocytes.

Dicer, the RNAse III ribo-endonuclease that processes non-coding RNAs in the RNAi and the microRNA pathways, was of particular interest to our laboratory due to its role in germline maintenance and oocyte development. In all organisms studied to date, loss of Dicer is lethal. Mice, fruit flies, and nematodes that are missing Dicer protein do not produce functional oocytes or offspring and thus, the gene is considered an embryonic lethal (Murchison et al., 2007: Megosh et al., 2006; Jin and Xie, 2007; Knight and Bass 2001). In *C. elegans* there is a single Dicer protein and homozygous *dcr-1(ok247)* null mutants of heterozygous *dcr-1* mothers develop to adults, with maternal rescue allowing germline development to proceed until the initiation of meiosis. During the pachytene stage of oogenesis in *dcr-1* null animals, although the gonad is of normal size, germline organization is lost and only irregularly-shaped, non-functional endo-replicating mitotic oocytes (EMO) are produced (Fig. 2.1) (Knight and Bass, 2001). In contrast, loss of Dicer either in mice or flies results in a much more severe phenotype. For example, in mice lacking Dicer the early embryos arrest due to a malfunction in chromatin segregation (Murchison et al., 2007) and neither in mouse nor fly do *dcr-1* homozygous mutants reach adulthood; therefore, it is difficult to study the role of Dicer in their germlines.

Figure 2.1

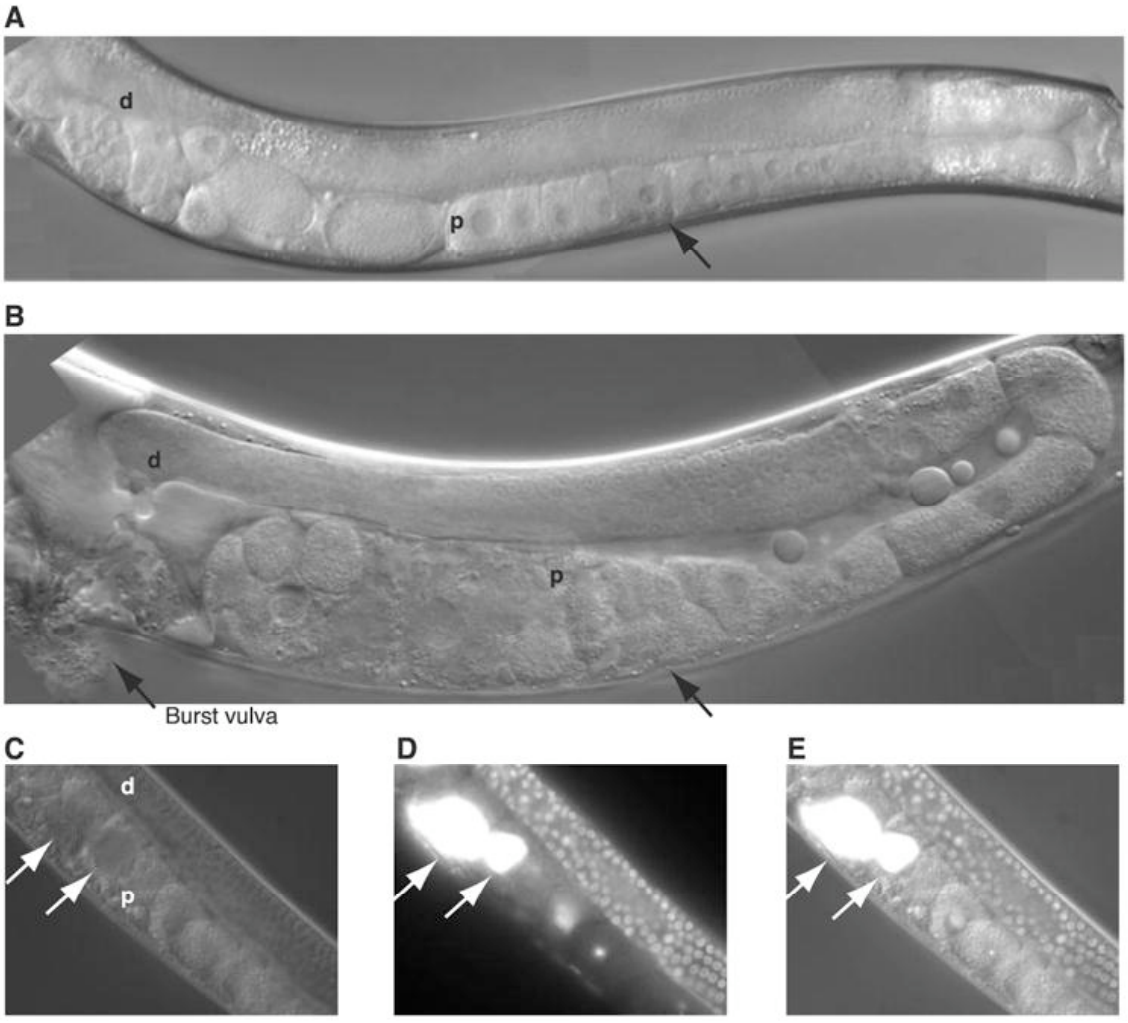

Figure 2.1. Germline development is abnormal in *dcr-1(ok247)* animals. (A through C) DIC micrographs. Distal (d) and proximal (p) orientation is indicated. (A) Wild-type adult hermaphrodite. The arrow points to a normal oocyte in the proximal gonad. (B) *dcr-1* adult hermaphrodite with a burst vulva. An abnormal misshapen oocyte is indicated by an arrow in the proximal gonad (arrow). (C) *dcr-1* adult hermaphrodite with enlarged oocyte nuclei (arrows). (D) Fluorescent micrograph of the DAPI-stained animal of (C). Areas of intense staining

colocalize to nuclei (arrows). (E) Merged micrograph of images in (C) and (D). Figure adapted from Knight and Bass, 2001.

Thus, *C. elegans* is a useful model to gain insight into the role of DCR-1 in the germline.

Previous studies in flies and mice have shown that Dicer protein interacts with the conserved germline RNA helicase protein Vasa or MVH (Mouse Vasa Homologue) (Megosh et al., 2006; Kotaja et al., 2006). In *Drosophila* there are two Dicer proteins and Vasa co-immunoprecipitates with Dicer-1. Depletion of Dicer-1 in fly embryos results in a dramatic decrease of Vasa, while no reduction of Vasa is seen in Dicer-2 depleted embryos. These results suggest that the loss of Vasa is associated with the Dicer-1-specific miRNA pathway (Megosh et al., 2006). In *Drosophila* ovaries Dicer-1 localizes diffusely throughout the cytoplasm of oocytes, but when the protein Maelstrom, a DNA binding protein and putative component of the miRNA pathway, is missing, Dicer-1 localizes to discrete perinuclear granules (Findley et al., 2003). And in mouse germ cells, Dicer co-immunoprecipitates with MVH, which is essential for development of the male germline. In this case the interaction with Dicer is dependent on the MVH C-terminus, and both Dicer and MVH localize in chromatoid bodies, the equivalent of germ granules in mouse spermatids. Other components of the miRNA pathway, including Argonaute proteins (Ago2 and Ago3) and miRNAs also localize to chromatoid bodies in male mice (Kotaja et al., 2006).

Here we build on the studies in flies and mice to show that the *C. elegans* DCR-1 binds GLH-1. With a newly-generated anti-Dicer antibody that is able to

recognize DCR-1 in worms, we report that DCR-1 localizes near GLH-1 and that DCR-1 spans the nuclear pore, is in P granules and in large RNP granules of arrested oocytes. Because deletion mutant strains are available for both DCR-1 and GLH-1, we determined that reduction of each has a dramatic effect on the other, including almost a 3-fold decrease in *glh-1* mRNA when DCR-1 is missing and a more than 2 fold loss of DCR-1 with the *glh-1(gk100)* deletion. In addition, with use of a *kgb-1* deletion strain these studies revealed DCR-1 and GLH-1 appear mutually regulated and both likely targeted for degradation by the kinase KGB-1. We also report that GLH-1 and DCR-1 dramatically re-localize within the cytoplasm of arrested oocytes, and are necessary for the formation of the oocyte cytoplasmic RNP granules.

Materials and Methods

Strains

Worm strains used in these experiments include: N2 (Bristol variety) as the wild type strain; PD8753 [*dcr-1(ok247)* III/hT2[bli-4(e937) let-?(q782) qIs48] (I;III)]; RB656 [*glh-1(ok439)* I]; VC178 [*glh-1(gk100)* I]; KB3 [*kgb-1(um3)* IV] and CB4108 [*fog-2(q71)* V]. The *dcr-1(ok247)* and *kgb-1(um3)* homozygous mutants will be referred to as *dcr-1* and *kgb-1* throughout this work. Nematodes were maintained on NGM plates at 20°C (Brenner, 1974). The *C. elegans* Knockout Consortium generated *glh-1(gk100), glh-1(ok439)* and *dcr-1(ok247)*, all of which are deletion strains. To maintain the strain *dcr-1(ok247)*, it is kept as a heterozygote over the ghT2 GFP-tagged balancer chromosome. Because *glh-1(gk100)* and *kgb-1(um3)* are both temperature-sensitive, they can be maintained without a balancer at the 20°C permissive temperature.

Western Blot Analysis

To compare protein levels of GLH-1 and DCR-1, equal numbers of adult worms, 50 per lane, were picked and prepared for western blot analysis. Lysates were loaded onto SDS-PAGE gels, 6% acrylamide for DCR-1 and 8% acrylamide for GLH-1, and transferred to nitrocellulose membranes. Some DCR-1 western blots were run on 7.5% Mini-PROTEAN® TGX™ precast gels (Bio-Rad) and transferred to Immobilon™-PSQ (Millipore) PVDF membranes; for these western blots 500 worms were loaded per lane. Rabbit antibodies against GLH-1 or DCR-1 were used to detect protein levels. The GLH-1 rabbit antibody raised against a GLH-1-specific peptide (Gruidl et al., 1996) was used at a dilution of

1:1000. A DCR-1 rabbit antibody (Duchaine et al., 2006), kindly provided by the Mello laboratory (U. Mass.), was used at a concentration of 1:750, while the DCR-1 rabbit antibody generated for this report was used at a concentration of 1:3000. For loading controls, rabbit anti-actin (Abcam) or rabbit anti-β-tubulin (Sigma) were diluted 1:5000. Goat anti-rabbit or goat anti-mouse secondary antibodies (Southern Biotech) conjugated to horseradish peroxidase were used at 1:10,000 – 1:20,000. A rabbit anti-PGL-1, kindly provided by the Strome laboratory (UC Santa Cruz), was diluted 1:10,000 for the GLH-1/PGL-1 pull-downs. Western blots were developed using Supersignal West Pico chemiluminescence (Pierce) and exposed to film. A LAS-4000 Fuji imager and MultiGauge software were used for quantification.

Immunoprecipitations

To prepare samples for immunoprecipitations (IPs), synchronized liquid cultures of adult worms were collected and frozen in liquid nitrogen (Epstein and Shakes, 1995). Samples were then thawed and diluted 1:1 in homogenization buffer plus protease inhibitor (recipe given below) on ice and then lysed by three passages through a French pressure-cell at 19000 psi. In addition, some lysates were prepared using the Bullet Blender™ according to manufacturer's directions (Next Advance). Lysates were centrifuged for 10 min at 10,000 *g*, removing insoluble materials. Protein concentrations of lysates were determined by Bradford assay (BioRad). For immunoprecipitations, 1 mg of worm lysate was first cleared with 100 μL of Protein G Resin (40–165 μm) (GenScript) for 20 min at 4°C. Following

pre-clearing, the worm lysate was incubated with 5 μL of rabbit anti-GLH-1 antibody for 1 hr at 4°C. The lysate/antibody mixture was then transferred to a fresh tube containing 25 μL of Protein G Plus/Protein A-Agarose beads (Calbiochem) for 1 hr at 4°C. The agarose beads were washed four times in 1 mL homogenization buffer, 15 mM Hepes pH 7.6, 10 mM KCl, 1.5 mM $MgCl_2$, 0.1 mM EDTA, 0.5 mM EGTA, 44 mM sucrose, with 1 mM DTT added immediately before adding the buffer to the worm pellet, along with one protease inhibitor cocktail tablet (Roche) per 10 mL homogenization buffer for a final concentration of 5X inhibitor. Proteins were eluted from the agarose beads with 25 μL of 4X protein loading dye (50 mM Tris-HCl; pH 6.8, 2% SDS, 10% glycerol, 5% β-mercaptoethanol, 12.5 mM EDTA, 0.02 % bromophenol blue), and analyzed by western blotting.

GST pull-down experiments

GST tagged constructs were expressed by baculovirus in HighFive insect cells (Invitrogen) as described (Smith et al., 2002). Proteins were tagged with GST- or 6-HIS and cloned into the pFastBac vector (Invitrogen). Protein samples and whole worm lysates were prepared as described for the IPs above. For pull-down analyses out of worm lysates, 200 μL of insect cell lysate was added to 750 μL of worm lysate and allowed to rotate on a spinning wheel for 1 hr at 4°C. The mixture was then transferred to a fresh tube containing 50 μL of Glutathione-Uniflow Resin (BD Biosciences Clontech) and spun for an additional 1 hr at 4°C.

Beads were washed four times in PBS containing 1% Triton-X 100, proteins were eluted with 4X protein loading dye, and were analyzed by western blotting.

Immunocytochemistry (ICC)

N2, *dcr-1(ok247)*, *glh-1(gk100)*, and *kgb-1(um3)* worms were grown at 20°C and adults were splayed to extrude their gonads as described (Kuznicki *et al*., 2000). For GLH-1 and PGL-1 localizations, adult gonads were fixed for 1 hr in 3% formaldehyde/0.1 M K_2HPO_4 pH 7.2 at room temperature, followed by 5 min in methanol at -20°C (Jones *et al*., 1996). For DCR-1, GLH-1, CGH-1, and nucleoporin protein (mAb414, AbCam) localizations, adult gonads were fixed for 1 min in methanol at -20°C, followed by 10 min in 3% formaldehyde at room temperature (Jud et al., 2008). For MEX-3 localizations, adult gonads were fixed for 5 min in -20°C MeOH, followed by 5 min in -20°C acetone (Draper et al., 1996). Chicken anti-GLH-1 antibody was used at 1:200, rabbit anti-PGL-1 antibody was used at 1:3000, rabbit anti-MEX-3 was used at 1:300, rabbit anti-CGH-1 was used at 1:200, and the nucleoporin antibody mAb414 was used at 1:5000. Since the existing antibodies against the *C. elegans* DCR-1 are effective for western blot analysis and IPs but ineffective for immuno-localization of the protein in worms, we generated new anti-DCR-1 antibodies and used them for western analysis and immunocytochemistry. These peptide antibodies were generated in rabbits with an N-terminal DCR-1-specific peptide, MVRVRADLQCFNPRDYQVEL, conjugated to KLH (keyhole limpet hemocyanin). Sera from two rabbits were affinity purified with high salt (2.5M KI) using the

SulfoLink Immobilization Kit for Peptides (Thermo Scientific); hyper-immune affinity-purified antibodies were diluted 1:10. Fluorescent secondary antibodies (Alexa Fluor, Molecular Probes) were diluted 1:3000 (MU) or at 1:400 (CMU). Some images were recorded with a Spot CCD camera on a Zeiss Axioplan microscope. Confocal images were taken on a Zeiss LSM 510 META NLO inverted confocal microscope at the University of Missouri Molecular Cytology Core. Confocal images taken at Central Michigan University were acquired on either an Olympus Fluoview FV300 laser scanning confocal microscope or (for the triple-stained images) a Nikon A1R laser scanning confocal microscope using a 60x (NA 1.4) objective lens. Images were analyzed using Adobe Photoshop. All confocal images shown in this report are single section images. When comparing images in a figure, the same laser levels and PMT voltages were used for each. For heat shock stress, worms were put at 34°C for 3 hrs prior to ICC (Jud et al., 2008). To assay the effect of oocyte arrest on DCR-1 and GLH-1, *fog-2(q71)* homozygous females were picked at the fourth larval stage (L4) and placed on a new plate for 1-2 days at the permissive temperature, 20°C; the unmated females were then fixed and stained. In order to isolate *glh-1(gk100)* and *dcr-1(ok247)* hermaphrodites depleted of sperm, L4-stage hermaphrodites were picked onto NGM plates and cultured at 15°C. The adults were moved onto fresh NGM plates every 2 days to separate them from their progeny. After 5 days, the uteri of the adults were examined for the presence of embryos. When embryos were no longer observed in the hermaphrodite uterus (at 5-7 days post-L4), and ovulated oocytes were present on the NGM plates, the hermaphrodites

were considered "purged" of sperm. RNAi depletion of *dcr-1* mRNA was performed using bacteria from the Ahringer library (K12H4.8, III-4C08) engineered to produce *dcr-1* dsRNA (Kamath and Ahringer, 2003) that were seeded on NGM agar plates containing 50 μg/ml carbenicillin and 1 mM IPTG. L1-stage, *fog-2* worms were fed this RNAi bacteria at 24°C for ~24 hours at which time males were removed, leaving L4-stage females. The females were fed an additional 12-24 hours at 24°C before fixation.

Quantitative real time RT-PCR

Wild type and *glh-1(gk100)* worm strains were collected by washing worms into M9 buffer (22mM KH_2HPO_4, 42mM Na_2HPO_4, 8.6mM NaCl, 1mM $MgSO_4$, pH 6.8). Worms from 20 plates were concentrated and frozen in 40 μl M9 and 10 μl 50x protease inhibitor (Roche). Approximately 3500 homozygous (non-green) *dcr-1(ok247)* worms were picked and frozen. RNA was extracted from N2, *dcr-1*, and *glh-1(gk100)* strains and analyzed, using TRIZOL and RNeasy® Mini Kit (Qiagen) according to the manufacturer's specifications. RNA concentrations were measured and equal amounts were reverse transcribed using the SuperScript® III RT kit (Invitrogen). 1.0 μl of the reverse transcription reactions was used for each quantitative real time PCR using the Maxima™ SYBR Green qPCR Master Mix (Fermentas) on a 7900HT Fast Real-Time PCR System (Applied Biosystems). Cycling conditions were: 1X [10 min 95°C] and 40X [15 s 95°C, 1 min 60°C]. Relative expression levels were determined according to

(Pfaffl, 2001), using the *eft-2* transcript as a standard. Experiments were performed in triplicate.

Quantitative real time RT-PCR primers

***glh-1* specific** Amplicon length 110 bp (nt 157–266)
Forward: 5' – TGCTAAGGCCAAAACTGGAT -3'
Reverse : 5'- TACT GGATTCGGTG GAGGAA -3'

***glh-2* specific** Amplicon length: 98bp (nt 643–740)
Forward: 5' – tagcggat tgaccaatggatt – 3'
Reverse: 5' – ttccaccagagttgcctcca – 3'

***glh-3* specific** Amplicon length: 86bp (nt 1875-1960)
Forward: 5' - AACGGTCGGCTGCTTTGAAA - 3'
Reverse: 5' - AATGTCAAGACCACGCTCAA - 3'

***glh-4* specific** Amplicon length: 94bp (nt 2830-2923)
Forward: 5' – aagttcgtcaaagagggtta - 3'
Reverse: 5' -TTCGAGGCACAGGAAGAAT - 3'

***kgb-1* specific** Amplicon length: 81bp (nt 877-957)
Forward: 5' - AATTGGGTCAGTCAGCTGCTA - 3'
Reverse: 5' - TATCAGGAACGATTTCACTGAA - 3'

***dcr-1* A** Amplicon length: 85bp (nt 381-465)
Forward: 5' - TTTGATTCGACATGCGTACT - 3'
Reverse: 5' - ATGTTGAGAACCGAGAGCAT - 3'

***dcr-1* B** Amplicon length: 101bp (nt 1705-1805)
Forward: 5' - ACTGCACAGATGGCAGTTGCA- 3'
Reverse: 5' - TTGGCAATCGACTCTCTTCCTT - 3'

***eft-2* N terminus** Amplicon length: 79bp (nt 816-894)
Forward: 5'-CAGTACTCAGACCGATGAGAGCAA-3'
Reverse: 5'-GACGGCGTCGAAGACCAT-3'

***eft-2* C terminus** Amplicon length: 80bp (nt 2080-2159)
Forward: 5'-GTTCGCTTCAACGTTCACGAT-3'
Reverse: 5'-CGGGCAGTTGGGATGATTT-3'

Proteosome and JNK Inhibitor experiments

Young N2 adults, 1 day beyond the L4 stage, were grown in liquid culture (7% χ1666), at 20°C with either 1 μM MG132 (Calbiochem) or 50 μM JNK inhibitor (SP600125, Calbiochem) or no inhibitor added. Inhibitor was added for the various times indicated and all worms were grown for a total of 5 hrs. Worms were collected and analyzed for DCR-1 by western blot analysis (50 worms/lane), using anti-actin (Abcam) as the loading control.

Results

DCR-1 and GLH-1 physically interact.

Initially, to determine if immunoprecipitation methods using the rabbit anti-GLH-1 antibody, generated in the Bennett laboratory, could be used to precipitate GLH-1 containing complexes we first tested for the presence of both GLH-1 and GLH-4 following immunoprecipitation by western blot analysis. We expected that GLH-4 should co-immunoprecipitate with GLH-1 as our laboratory had already tested for the interaction of the GLHs binding to each other (Pliny Smith, unpublished results). As expected, both GLH-1 and GLH-4 were found present in the lysates precipitated with anti-GLH-1 antibody (Fig. 2.2). Thus verifying that we were indeed able to immunoprecipitate GLH-1 and other proteins with which it forms a complex.

To identify components of GLH-1-containing complexes by methods other than two hybrid screens (Smith et al., 2004), we asked whether an interaction between GLH-1 and the constitutive P-granule component PGL-1 (P-Granule abnormality) could be detected by GST pull-downs. PGL-1, like all the GLH proteins, localizes to P granules throughout development and its P-granule localization has been shown dependent upon GLH-1 (Kawasaki et al., 1998; Spike et al., 2008). We conducted pull-downs using wild-type *C. elegans* lysates and several GST and HIS tagged GLH-1 constructs and analyzed the products by western blot. PGL-1 was pulled-down with full-length GLH-1 (Fig. 2.3B, lane 1) and the N-terminal GLH-1 construct (Fig. 2.3B, lane 2), but not with the control

Figure 2.2

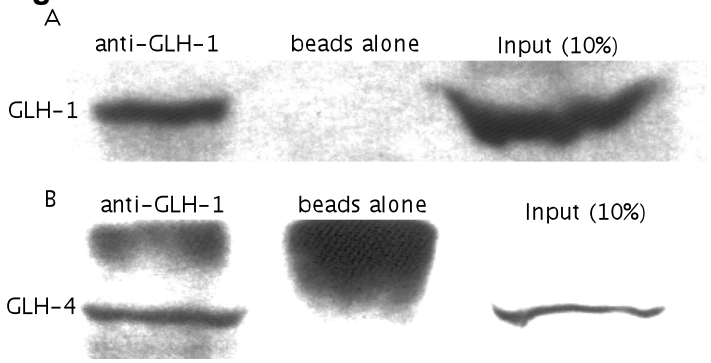

Figure 2.2. Immunoprecipitation of GLH-1 complexes out of wild type lysates. A. Immunoprecipitation out of wild type lysates using rabbit anti-GLH-1 antibody (lane 1) or beads alone (lane 2). Western blot reacted with mouse anti-GLH-1 antibody to demonstrate that GLH-1 can be immunoprecipitated. **B.** Immunoprecipitation out of wild type lysates using rabbit anti-GLH-1 antibody (lane 1) or beads alone (lane 2). Western blot reacted with rabbit anti-GLH-4 antibody.

Figure 2.3

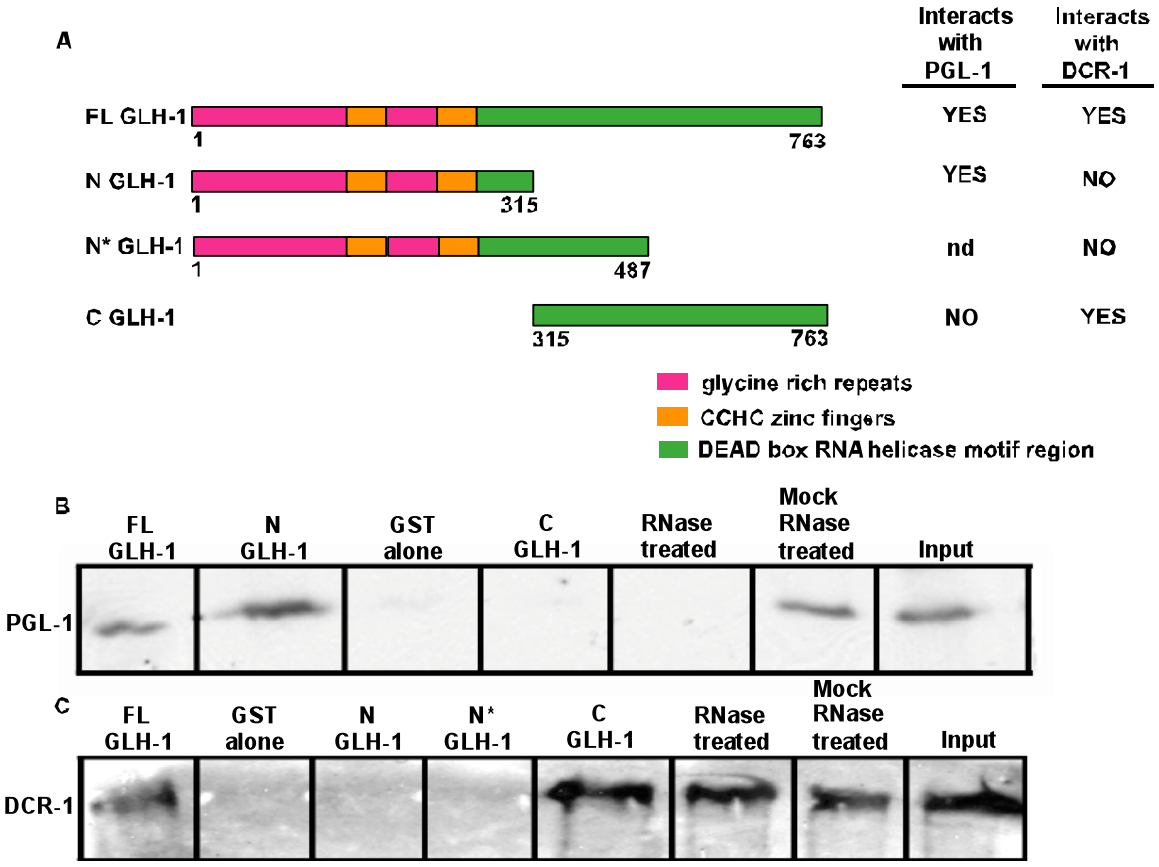

Figure 2.3. GLH-1 interacts in complex with PGL-1 and DCR-1. A. A cartoon summarizing the interactions seen in Figure 1B and 1C. **B**. Pull-downs out of wild type worm lysates with full length GST-GLH-1 (lane 1), N-GLH-1 (lane 2), GST alone (lane 3), HIS-tagged C-GLH-1 (lane 4), full-length GST-GLH-1 after adding RNase A (12 μg/μL) to the lysate prior to pull-down (lane 5), GST-GLH-1 without RNase A (lane 6), and 10% lysate input (lane 7). All lanes were tested by western blot analysis using α-PGL-1 antibodies. **C.** GST pull-downs out of wild type worm lysates with full length GST-tagged GLH-1 (lane 1), GST alone (lane 2), N-GLH-1 (lane 3), N*-GLH-1 (lane 4), HIS-C-GLH-1 (lane 5), full

length GST-GLH-1 with RNase A added to the lysate prior to pull-down (lane 6), GST-GLH-1 without RNase A (lane 7), and 10% lysate input (lane 8). Here the pull-downs were tested by western blot analysis using α-DCR-1 antibodies.

GST alone (Fig. 2.3B, lane 3) nor with the C-terminal GLH-1 construct (Fig. 2.3B, lane 4). The binding between full-length GLH-1 and PGL-1 indicated the efficiency of our assay. We hypothesized that the interaction between GLH-1 and PGL-1 might require an RNA intermediate. After adding RNase A to the lysates prior to immunoprecipitation, the interaction between GLH-1 and PGL-1 was lost (Fig. 2.3B, lane 5). These results indicate that GLH-1 and PGL-1 interact in complex, and this interaction is dependent on RNA. The GST input blots for the PGL-1 pull-down are shown Figure 2.4.

Several additional germline proteins reported in embryonic P granules were tested by western analysis for co-immunoprecipitation (co-IP) with GLH-1. These candidate proteins included: PAR-1, PAR-3, MEX-1, and GLD-1 (Etemad-Moghadam et al., 1995; Guedes and Priess, 1997; Guo and Kemphues, 1995; Jones et al., 1996). None of these candidates was detected in GLH-1 co-IPs (Fig. 2.5 and data not shown), indicating that our immunoprecipitations do not pull-down all P-granule components, but can detect physical associations, even when an RNA intermediate is required.

Based on work in *Drosophila and Mus* demonstrating interactions between VASA/MVH and Dicer, we next asked if the single Dicer protein in *Caenorhabditis*, DCR-1, interacts with GLH-1. We precipitated GLH-1-containing complexes and assayed for the presence of DCR-1 by western analysis. Indeed, incubation of a GST-GLH-1 protein with a *C. elegans* lysate recognized DCR-1

Figure 2.4

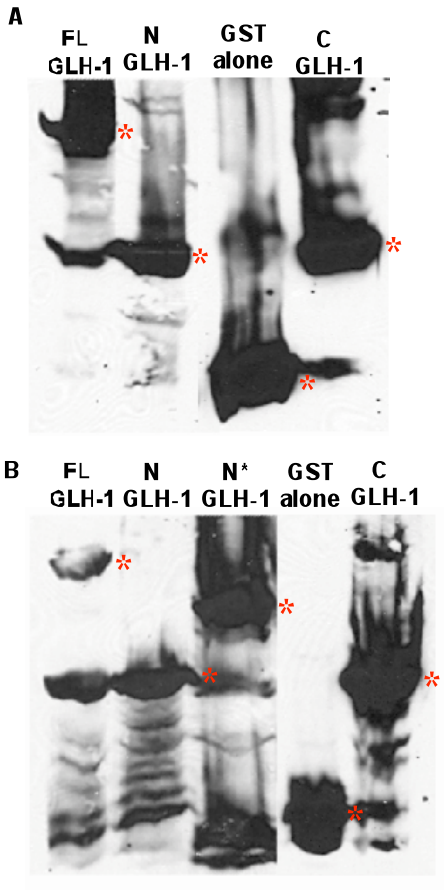

Figure 2.4. GST and His tagged proteins expressed in baculoviruse for each construct used in the pull-downs out of worm lysate. A. Antibody reactivity against GST (lanes 1-3) and HIS (lane 4) with insect cell lysates infected with the following baculoviral constructs; full-length GST-GLH-1 (lane 1), N-terminal GST-GLH-1 (lane 2), GST alone (lane 3), and C-terminal HIS-GLH-1 (lane 4). **B.** Antibody staining against GST (lanes 1-4) and HIS (lane 5) with insect cell lysates infected with the following baculoviral constructs; full-length GST-GLH-1 (lane 1), N-terminal GST-GLH-1 (lane 2), N*-terminal GST-GLH-1 (lane 3), GST alone (lane 4), and C-terminal HIS-GLH-1 (lane 5).

Figure 2.5

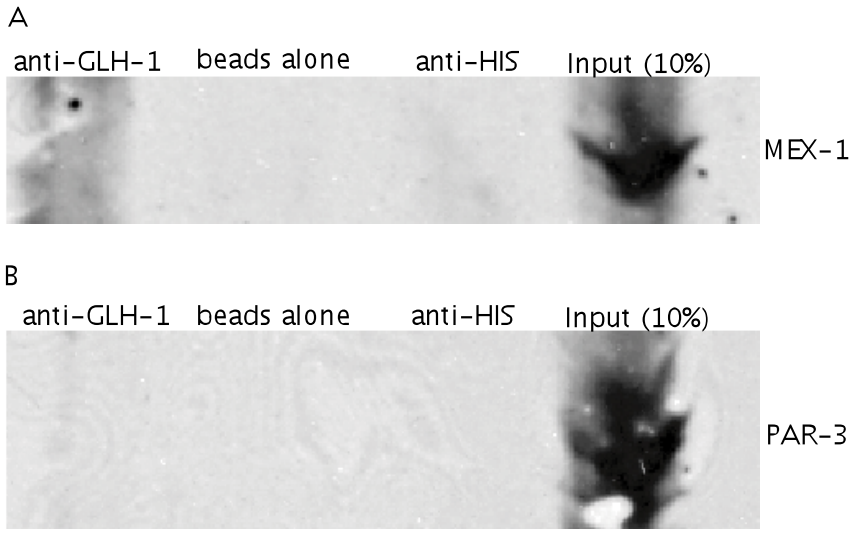

Figure 2.5. MEX-1 and PAR-3 do not co-immunoprecipitate with GLH-1. A. Immunoprecipitation out wild type lysates with anti-GLH-1 antibody (lane 1), beads alone (lane 2), an anti-HIS antibody (lane 3), and input (lane 4). Western blot analysis with anti-MEX-1 antibody. B. Immunoprecipitation out wild type lysates with anti-GLH-1 antibody (lane 1), beads alone (lane 2), an anti-HIS antibody (lane 3), and input (lane 4). Western blot analysis with anti-PAR-3 antibody.

protein, suggesting these proteins interact in complex (Fig. 2.3C, lane 1). To determine if this physical interaction is RNA dependent, we RNase A treated lysates and then pulled down GLH-1-containing complexes using the GST-GLH-1 protein. The interaction of GLH-1 with DCR-1 remained intact following RNase treatment, indicating the interaction is not RNA-dependent (Fig. 2.3C, lane 6). To verify the GST pull-down results, we conducted immunoprecipitations out of wild type worm lysates using an anti-GLH-1 antibody to pull-down GLH-1 containing complexes. Here too, GLH-1 co-immunoprecipitated with DCR-1 (Fig. 2.6C, lane 1).

The C-terminus of GLH-1 is necessary for an interaction with DCR-1.

To identify the regions of GLH-1 required to interact with DCR-1, truncated GST and His-tagged GLH-1 constructs were tested (Fig. 2.3A). The first of these, N-GLH-1, contains the first 315 amino acids of GLH-1, thereby removing most of the helicase region but leaving the four CCHC zinc fingers intact. When this protein was incubated in wild-type worm lysate, it did not pull down DCR-1 (Fig. 2.3C, lane 3). A second, longer, N-terminal construct, N*-GLH-1, that contains 487 amino acids also did not interact with DCR-1 (Fig. 2.3C, lane 4). To determine if the C-terminus of GLH-1 is sufficient for the DCR-1 interaction, a 6-His-tagged GLH-1 construct lacking the first 315 amino acids of the N-terminus of the 763 amino acid protein was tested. This construct included the entire helicase region but none of the FGG, glycine-rich repeats, nor the four CCHC zinc fingers, and it successfully pulled down DCR-1 (Fig. 2.3C, lane 5). Thus, the

Figure 2.6

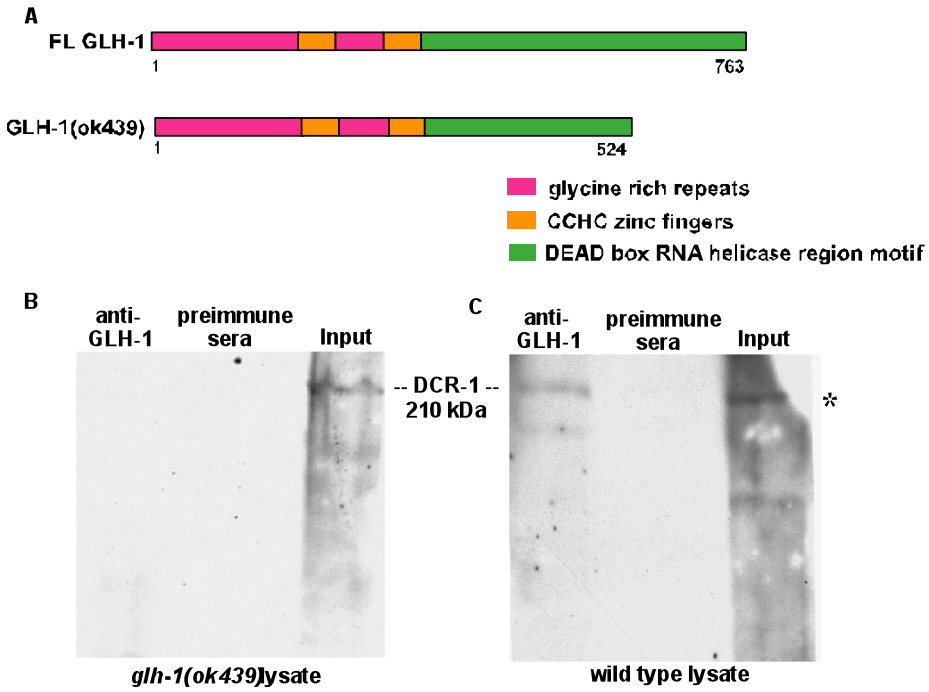

Figure 2.6. *glh-1(ok439)* mutant lysates do not co-immunoprecipitate DCR-1 using α- GLH-1 antibodies; wild type lysates IP DCR-1. A. Schematic of full-length GLH-1 and the predicted protein made in the *glh-1(ok439)* mutant. **B.** Immunoprecipitation out of *glh-1(ok439)* mutant lysates using anti-GLH-1 antibody (lane 1), rabbit pre-immune sera (lane 2), and 10% input lysate (lane 3). The western blot was reacted with anti-DCR-1 antibody and showed no evidence of DCR-1 binding. **C.** Immunoprecipitation out of wild type lysates using anti-GLH-1 antibody (lane 1), rabbit pre-immune sera (lane 2), and 10% input lysate (lane 3). The western blot was reacted with anti-DCR-1 antibody and DCR-1 was seen in the immuoprecipitations.

C-terminal construct containing only the DEAD-box helicase region is sufficient for interacting with DCR-1.

DCR-1 localizes to the germline cytoplasm and at nuclear pores.

Because GLH-1 and DCR-1 are binding partners in a GLH-1/DCR-1 complex (Fig. 2.3), we next wanted to determine if the two proteins co-localize *in vivo*. To date no localization studies of DCR-1 have been reported in *C. elegans*. To produce an antibody that recognizes DCR-1 in immunocytochemistry experiments, we generated both rabbit and mouse polyclonal antibody against DCR-1 specific peptides corresponding to the first and last 20 amino acids of DCR-1 (for peptide sequence, see Materials and Methods this Chapter), which is specific to *C. elegans* DCR-1. Five mice were immunized, three with the N-terminal peptide and two with a C-terminal peptide specific to DCR-1. Two of the three mice immunized with the N-terminal peptide resulted in the most useful antibodies for immunocytochemistry (Fig. 2.7). Therefore, we decided to immunize two rabbits, the first with the N-terminal peptide alone and the second with both the N-terminal and C-terminal peptides. Both rabbits generated good antibodies that worked well by ICC. Rabbit 2 was chosen for the following experiments, as it was useful both for ICC and western blot analysis. The anti-DCR-1 antibody was tested for specificity in recognizing the *C. elegans* DCR-1. Immunocytochemistry (ICC) using anti-DCR-1 with the *dcr-1* mutant showed no staining in either germline or somatic tissue, while the anti-DCR-1 antibodies

recognized both germline and somatic tissues in the adult wild type worm (Fig. 2.8B); these results imply the

Figure 2.7

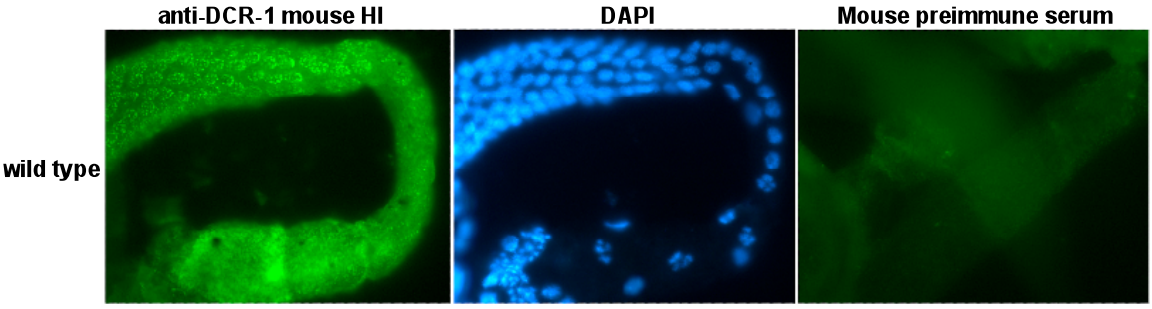

Figure 2.7. Wild type gonad reacted with anti-DCR-1 mouse antibody (left panel, green) and DAPI stained (middle panel, blue). Preimmune sera from mouse prior to antibody production shows no staining (right panel).

Figure 2.8

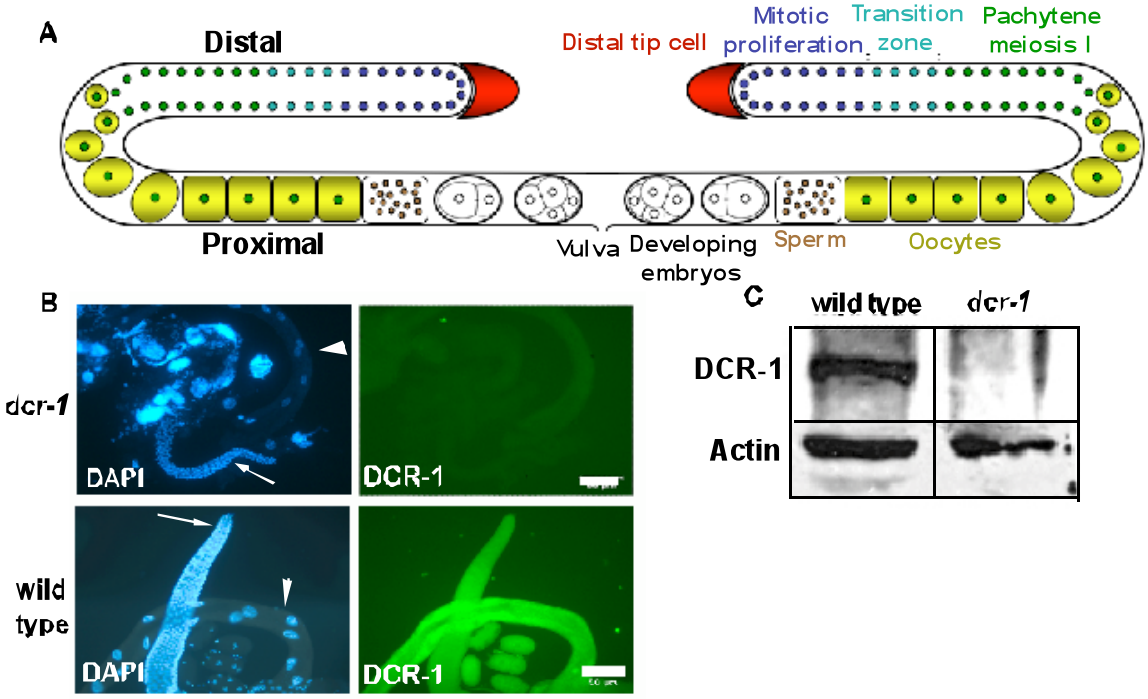

Figure 2.8. The new DCR-1 antibody is specific and is found both in the germline and in the soma. A. A schematic of the *C. elegans* gonad from an adult hermaphrodite, containing the adult germline adapted from Minasaki et al., 2009. In the distal gonad, the somatic distal tip cell directs mitotic germ cell proliferation and then the germ cells transition into meiosis and enter the pachytene stage. The distal region refers to the syncytial gonad, while the proximal gonad, after the bend, refers to the area in which, oocytes cellularize and mature before passing through the spermatheca, where they are fertilized by the stored sperm that were produced by the hermaphrodite during the L4 stage. Embryos are stored in the uterus until laid through the vulva. **B.** Immunocytochemisty (ICC) using α-DCR-1 antibodies (green, right panels) in the *dcr-1* null mutant (top) and in wild type animals (bottom). Shown is the adult

gonad (arrow); gut (arrowhead); and DAPI staining of each, the left panels. **C.** Western blot analysis using the α-DCR-1 antibody reveals a band at the predicted DCR-1 size, 210 kDa, in wild type worms, with no band in the *dcr-1* mutants.

antibody is specific. By western analyses the anti-DCR-1 antibodies recognized a protein of 210 kDa, the expected size for DCR-1 (Fig. 2.8C, lane 1) and no protein was detected in homogenates for *dcr-1* mutants, again indicating antibody specificity (Fig. 2.8C, lane 2). Initial images taken by our laboratory's Spot CCD camera on the Zeiss Auxioplan microscope of wild type worms reacted by ICC with the anti-DCR-1 antibody, we generated, and the anti-GLH-1 antibody revealed that two proteins were indeed in close proximity. At this magnification, DCR-1 appeared to be both cytoplasmic and in P granules with GLH-1 (Fig. 2.9). This co-localization appeared to be more robust in the pachytene region of the gonad.

To more closely examine DCR-1 in worms, confocal images were used and DCR-1 was detected in the pachytene region of the germline in wild type worms (see schematic Fig. 2.8A; Fig. 2.10A). While DCR-1 was uniformly distributed in small granules throughout the cytoplasm of all germ cells, DCR-1 was concentrated at the pachytene region in distinct perinuclear granules that were internal and adjacent to puncta stained by mAb414, an antibody that recognizes several nucleoporin proteins (Fig. 2.10A). To further examine the perinuclear DCR-1 granules, wild type adults were triple-labeled with DCR-1, GLH-1, and mAb414, (Fig. 2.10B). As seen in Fig. 2.10A, DCR-1 was perinuclear within the germ cell nuclei, and was concentrated at the nuclear pores, while GLH-1 was perinuclear on the cytoplasmic side of the nucleus. These triple labeled images were taken by our collaborator Dr. Jennifer Schisa at Central Michigan University

Figure 2.9

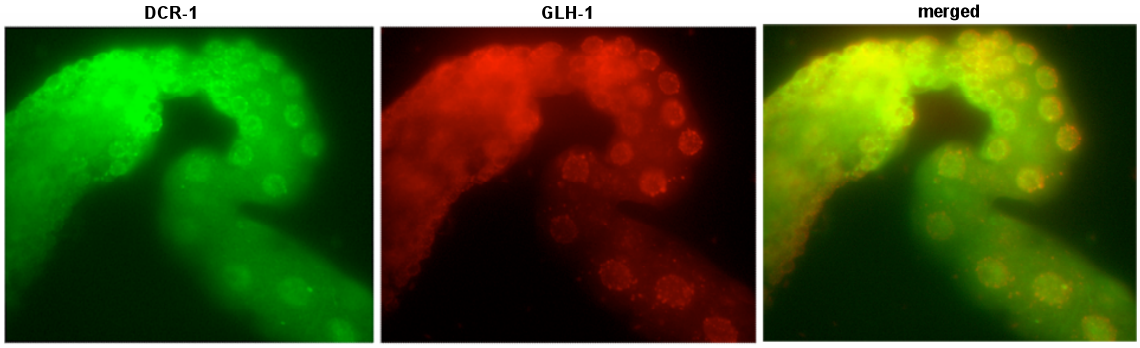

Figure 2.9 Immunolocalization of DCR-1 and GLH-1 in a wild type gonad. Immunocytochemistry analysis in a splayed wild type gonad reacted with antibodies against DCR-1 (green), GLH-1 (red), and merged image (yellow).

Figure 2.10

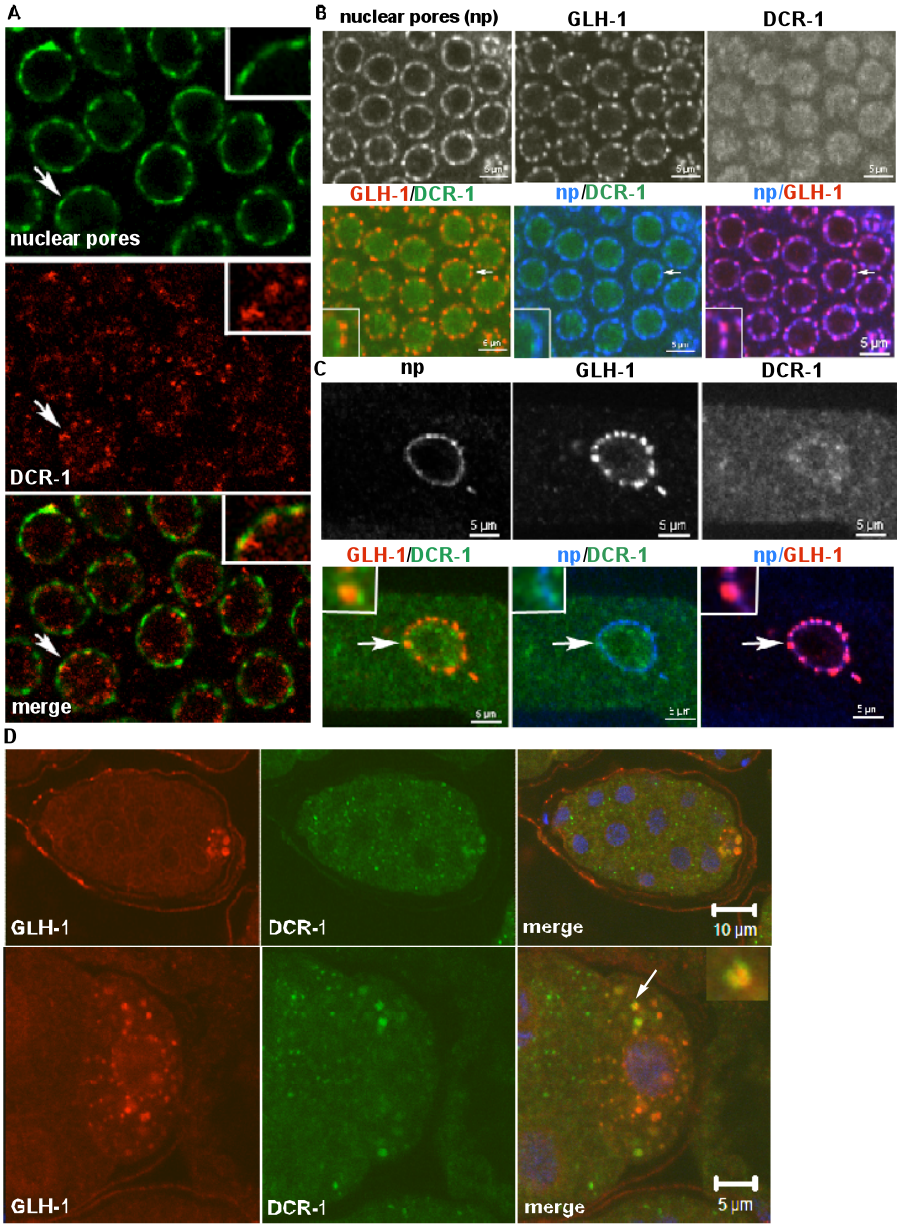

Figure 2.10 DCR-1 localizes to nuclear pore regions within the germ cell nuclei. **A.** ICC in a wild type adult gonad using mAb414 nuclear pore antibody (green), which is reported to recognize the FG repeats of several nucleoporins (Davis and Blobel, 1986), α-DCR-1 antibody, red, and merged image, lower panel. The arrow points to the region shown enlarged in the inset. **B.** ICC in the

pachytene region of a wild type adult hermaphrodite gonad showing nuclear pores (mAb414 antibody) (blue), P granules (α-GLH-1 antibody) (red), and α-DCR-1 antibody (green). Arrow denotes enlarged inset image. **C.** ICC in a wild type oocyte showing nuclear pores (mAb414 antibody) (blue), P granules (α-GLH-1 antibody) (red), and α-DCR-1 antibody (green). **D.** ICC in wild type embryos with α-GLH-1 antibody (red), α-DCR-1 antibody (green); merged image, right panel; and DAPI staining (blue), left panel. The images in the top row are of a 16-cell stage embryo and the bottom row focuses in on the P2 cell, the germline precursor, in a 4-cell embryo. The eggshell of the 16-cell embryo has captured anti-chicken red secondary antibody; this staining is not specific or reproducible. Arrow points to a GLH-1/DCR-1-containing granule. Images from A-C taken by Jennifer Schisa, Ph.D.

with antibodies we provided. Thus, DCR-1 and GLH-1 appeared connected through the nuclear pore complex as internal and external components, respectively. In the most proximal wild type oocyte (schematic in Fig. 2.8A), DCR-1 was detected in the cytoplasm and nucleus, slightly enriched at the plasma membrane, and was less evident at nuclear pores (Fig. 2.10C). In early embryos DCR-1 staining was uniformly granular in all embryonic blastomeres including the somatic blastomeres and the germline progenitor cell, marked by GLH-1. DCR-1 was also localized to a few, but not all, of the embryonic P granules at both the 6 cell and 16 cell stages (Fig. 2.10D). In dividing blastomeres, DCR-1 was enriched at the positions of centrosomes (Fig. 2.11).

Dicer and GLH-1 interact *in vivo* and are interdependent.

Since GLH-1 and DCR-1 biochemically interact and localize in close proximity to one another at the germ cell nuclear membrane, we investigated the fate of GLH-1 and DCR-1 when the other protein is depleted. We took advantage of deletion mutants for each of these genes. Schematics for the *dcr-1(ok247)* and *glh-1(gk100)* mutations are depicted in Fig. 2.12. While the *dcr-1* mutant is a protein null, whose sterile EMO phenotype was briefly described in the Introduction to this chapter, *glh-1(gk100)* worms, with a 581 nt internal deletion in the *glh-1* gene that removes three of the four GLH-1 CCHC zinc fingers, produce a truncated GLH-1 protein at 10% or less of wild type levels. These animals are generally fertile, but have reduced brood sizes at the permissive temperature of 20°C and are 100% sterile at 26°C (Spike et al., 2008). The germline defects seen with the

Figure 2.11

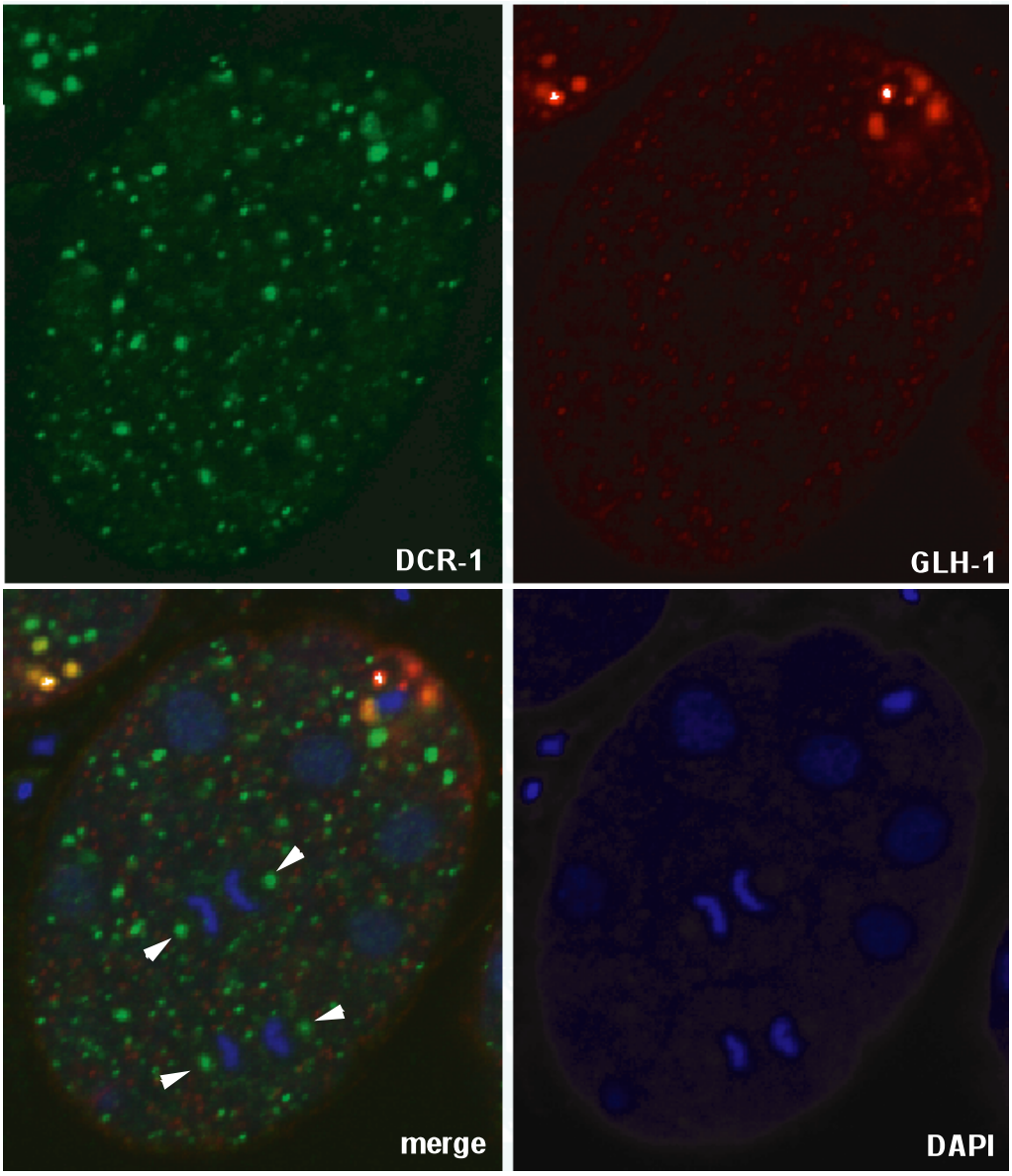

Figure 2.11. DCR-1 is enriched at the centrosomes in the two dividing blastomeres. Immunocytochemistry of a mated *fog-2(q71)* embryo with antibodies against DCR-1 (green), GLH-1 (red), DAPI (blue), and merged image. Arrowheads indicate centrosomes. Images taken by Jennifer Schisa, Ph.D.

Figure 2.12

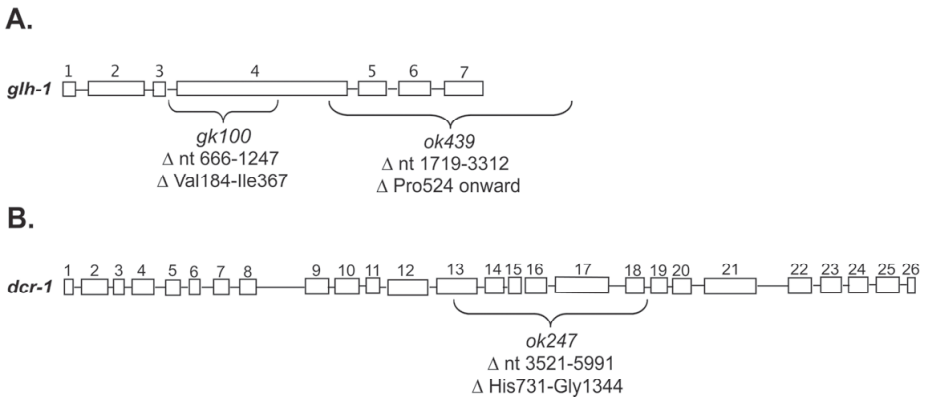

Figure 2.12. Schematic of the *glh-1* and *dcr-1* mutant strains used in these studies. The deletions in the *glh-1(gk100)* and *dcr-1(ok247)* genes are shown schematically (Spike et al., 2008; Welker et al., 2007). The genes are not to scale as the *dcr-1* gene at 8359 nts is almost 3 times longer than the 2850 nt *glh-1* gene.

glh-1(gk100) mutant are variable at 20°C, ranging from the germline being essentially absent, to animals with a small germline and tiny gonad arms, to worms with relatively normal germlines (Spike et al., 2008). To begin to test for a possible interdependence, wild type and *dcr-1* protein lysates were analyzed by western analysis to assess GLH-1 levels. In the *dcr-1* mutant a dramatic loss of GLH-1 protein was seen (Fig. 2.13A, lane 2). Conversely, DCR-1 protein levels were assayed in the *glh-1(gk100)* mutant, revealing DCR-1 reduced by 2.5 fold when compared to wild type worms (Fig. 2.13B, lanes 1 vs. 2). Thus, GLH-1 and DCR-1 appear to be dependent on each other to maintain wild type levels of both proteins.

Assaying for GLH-1 by immunocytochemistry in *dcr-1* mutant worms confirmed the decreased levels of GLH-1 seen by western analysis (Fig. 2.13A). In wild type animals, GLH-1 protein localized to P granules; however, in the majority of homozygous *dcr-1* mutants GLH-1 was not detectable (Figs. 2.13C, comparing right and left images). However, in about 10% of the *dcr-1* animals, moderate levels of GLH-1 staining were detected in the more proximal regions of the gonad (Fig. 2.14). We next analyzed the effect of loss of DCR-1 on the P-granule protein PGL-1 to determine if other P-granule components were also disrupted. By immunocytochemistry the localization of PGL-1 was mildly disrupted in the *dcr-1* mutants. PGL-1 localized to P granules in most of the proximal germline, but was more diffuse throughout the cytoplasm in more distal regions (Fig. 2.14D). This observation is consistent with previous reports indicating the

Figure 2.13

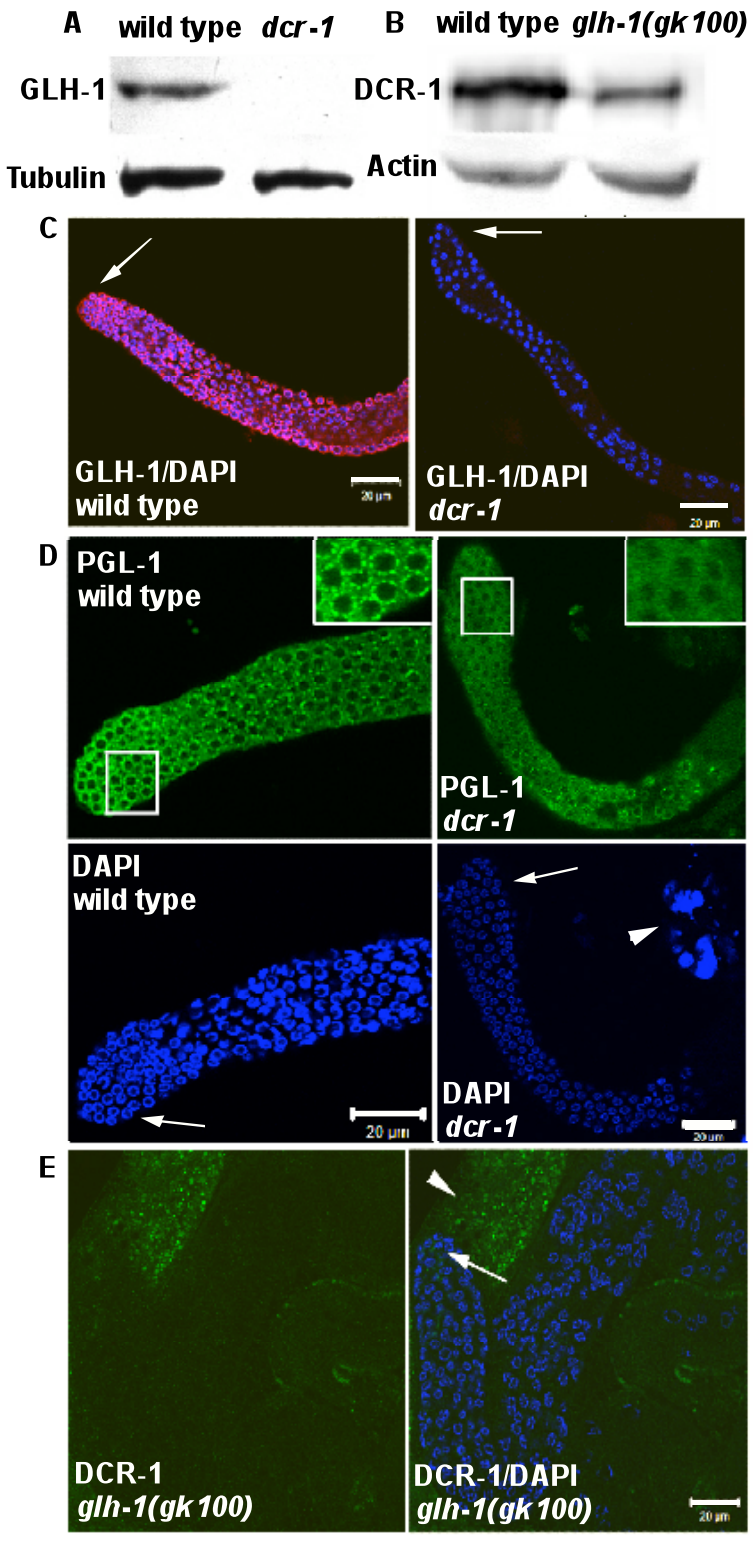
A
wild type
dcr-1
GLH-1
Tubulin
B
wild type
glh-1(gk100)
DCR-1
Actin
C
GLH-1/DAPI
wild type
GLH-1/DAPI
dcr-1
D
PGL-1
wild type
PGL-1
dcr-1
DAPI
wild type
DAPI
dcr-1
E
DCR-1
glh-1(gk100)
DCR-1/DAPI
glh-1(gk100)

Figure 2.13. GLH-1 in *dcr-1(ok247)* and DCR-1 in *glh-1(gk100)* worms are each reduced, while PGL-1 remains in P granules in *dcr-1* worms. A. Western blot analysis of N2 versus *dcr-1* protein lysates with α-GLH-1 antibody, with α-Tubulin as a loading control. **B.** Western blot analysis of N2 (wild type) versus *glh-1(gk100)* protein lysates with α-DCR-1 antibody. Actin is the loading control. Because of the large size of DCR-1, the loading controls for 4B were loaded on separate, higher percentage gels with identical amounts of worm lysate. The western blot in 4A used 50 worms per lane, while those in 4B used 500 worms per lane. **C.** GLH-1 is seen localizing to P granules in a wild type gonad extruded from the worm, while no GLH-1 is detected in a *dcr-1* mutant gonad using α-GLH-1 antibodies for ICC (red), and DAPI-stained nuclei (blue). **D.** ICC of a wild type and a *dcr-1* mutant gonad using α-PGL-1 antibody (green), and DAPI-stained nuclei (blue). The arrowhead in D points to two endo-replicating mitotic oocytes (EMO) in the germline, a characteristic of the *dcr-1* mutant. Insets in D emphasize the diffuse nature of PGL-1 in the *dcr-1* mutant when compared to wild type. **E.** A *glh-1(gk100)* extruded gonad and gut stained with DAPI (blue) and reacted with α-DCR-1 (green). Arrows in each figure point to the distal tip of the gonad. The arrowhead in E points to a small section of *the C. elegans* gut.

Figure 2.14

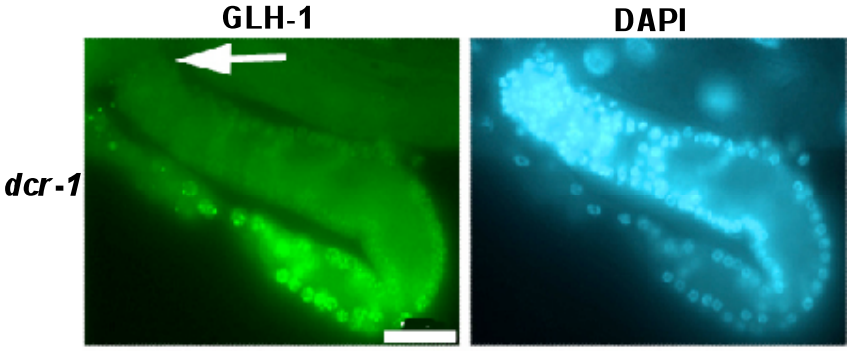

Figure 2.14. GLH-1 is occasionally present in a *dcr-1* mutant gonad. ICC in a *dcr-1* mutant gonad reacted with an anti-GLH-1 antibody (green, right panel) and DAPI stained (blue, left panel). Arrow points to the distal region of the gonad. GLH-1 staining is infrequently seen in the proximal gonad.

localization of PGL-1 to P granules depends upon GLH-1 (Kawasaki et al., 1998; Spike et al., 2008). To determine if other GLH family members were reduced in the *dcr-1* mutant, we tested GLH-4 by western analysis. Unlike GLH-1, but similar to PGL-1, GLH-4 protein levels were only slightly changed as compared to wild type (not shown and Fig. 2.15). The results with PGL-1 and GLH-4 reveal that loss of DCR-1 does not dramatically affect every P-granule component.

Analysis of DCR-1 in the *glh-1(gk100)* mutants by ICC, also revealed a marked reduction but not a total loss of DCR-1 staining, similar to results by western analysis (Fig. 2.13E; Fig. 2.13B). Notable differences in DCR-1 localization were observed in the germlines of *glh-1(gk100)* mutants. In the germlines of the majority of *glh-1(gk100)* animals, DCR-1 was detected at much lower levels than in wild type and yet was still present in the somatic, gut tissue (arrowhead), which underlies the germline in Fig. 2.13E. The presence of DCR-1 in somatic tissue probably accounts for the remaining DCR-1 proteins seen by western analysis in Fig. 2.13B. In summary, we find that in the *dcr-1* null mutant, GLH-1 levels are missing or very reduced in worms, while levels of the P-granule proteins PGL-1 and GLH-4 levels are essentially unchanged. Similarly, the 90% or more reduction of GLH-1 in the *glh-1(gk100*) deletion mutant results in a dramatic reduction of DCR-1 from the germline.

Figure 2.15

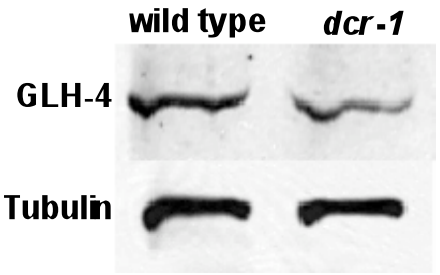

Figure 2. 15. GLH-4 protein levels are not reduced in the *dcr-1* mutant as compared to wild type. Western blot analysis of GLH-4 protein in wild type (top band, lane 1) and *dcr-1* worms (top band, lane 2). Tubulin serves as the loading control.

***glh-1* mRNA levels are reduced in *dcr-1* mutants.**

To determine whether the reduction of GLH-1 protein in the *dcr-1* mutants reflects regulation of GLH-1 at the protein or mRNA level, graduate student Tamara McEwen performed quantitative real-time PCR (qRT-PCR) on *glh-1* mRNA in both wild type and *dcr-1* worms. *glh-1* mRNA levels were reduced almost 3-fold in the *dcr-1* mutant compared to wild type (Fig. 2.16, Table 2.1). In addition, mRNA levels for *glh-2*, *glh-3*, and *glh-4* were tested in *dcr-1* worms using primers specific for each gene. *glh-2* levels were also reduced almost 4-fold, while *glh-3* and *glh-4* levels were not significantly different than wild type (Table 2.1). Because KGB-1 is the Jun N-terminal kinase that targets GLH-1 for degradation via the proteosome (Orsborn et al., 2007), we asked if *kgb-1* mRNA levels were affected by the loss of *dcr-1*. Interestingly, when compared to wild type worms, *kgb-1* mRNA levels were increased more than 3-fold in the *dcr-1* mutants.

Since a reduction in the DCR-1 protein level was observed in the *glh-1(gk100)* worms (Fig. 2.13B), Ms. McEwen conducted qRT-PCR to compare *dcr-1* mRNA levels in *glh-1(gk100)* and wild type worms and found *dcr-1* mRNA was not reduced in the *glh-1(gk100)* mutant background (Table 2.1), indicating the regulation of DCR-1 by GLH-1 is at the protein level, in contrast to the regulation *of glh-1* mRNA by DCR-1 seen by qRT-PCR.

Figure 2.16

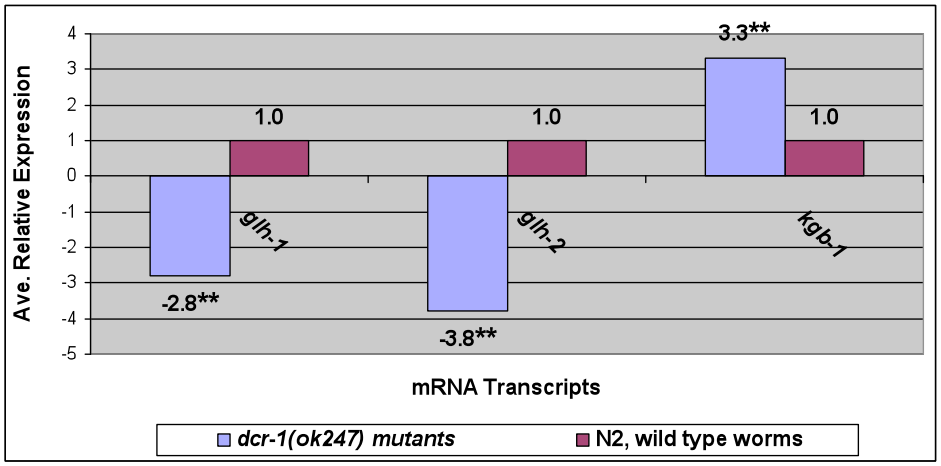

Figure 2.16. Relative transcript levels in *dcr-1(ok247)* mutants as compared to wild type worms. Transcript levels of *glh-1, glh-2,* and *kgb-1* were assayed in triplicate by qRT-PCR in *dcr-1* mutants as compared to wild type worms (**p value<0.001). The statistical significance of differences in relative expression levels was determined using the Relative Expression Software Tool (REST), software version REST 2009 (www.gene-quantification.de/rest.html). The data are also shown in Table S1. Quantitative RT-PCR performed by Tamara McEwen.

Table 2.1

Gene	Expression	Range	Std. Error	Result
glh-1	**0.354**	**0.11-0.42**	**0.175-0.819**	**2.8-fold DOWN**
glh-2	**0.264**	**0.13-0.61**	**0.137-0.551**	**3.8-fold DOWN**
glh-3	**0.875**	**0.55-1.83**	**0.458-1.685**	**No change**
glh-4	**1.024**	**0.60-1.80**	**0.638-1.828**	**No change**
kgb-1	**3.282**	**2.38-4.85**	**1.698-6.849**	**3.3-fold UP**

Gene	Expression	Range	Std. Error	Result
dcr-1*	**1.015**	**0.81-1.69**	**0.808-1.342**	**No change**
dcr-1+	**0.996**	**0.73-2.28**	**0.689-1.578**	**No change**

Table 2.1 Relative transcript levels in *dcr-1(ok247)* and *glh-1(gk100)* mutants as compared to wild type worms. Transcript levels for *glh-1, glh-2,* and *kgb-1* differ in *dcr-1* mutants when compared to wild type worms. Quantitative real-time PCR was utilized to assay transcript levels of *glh-1, glh-2, glh-3, glh-4*, and *kgb-1* in *dcr-1* mutants and of *dcr-1* in *glh-1(gk100)* mutants. There are two separate entries for *dcr*-1 as two different primer sets were used (see Materials and methods). The statistical significance of differences in relative expression levels was determined using the Relative Expression Software Tool (REST), software version REST 2009. * **a** primer set +**b** primer set. Quantitative RT-PCR performed by Tamara McEwen.

DCR-1 is likely targeted for degradation by KGB-1.

Previous studies in our laboratory have reported a role for the Jun N-terminal kinase KGB-1 in regulating GLH-1 (Orsborn et al., 2007). In light of the relationship between DCR-1 and GLH-1, undergraduate Jordan Marshall and I asked if DCR-1 might be similarly targeted for degradation by KGB-1. When wild type worms grown in liquid culture were treated with the proteosomal inhibitor, MG132 or with the JNK inhibitor, SP600125, and examined at several time points after addition of the inhibitor, DCR-1 protein increased (Fig. 2.17A). The level of DCR-1 accumulated with an approximate 3.5 fold increase with the proteosomal inhibitor and 2.7 fold increase with the JNK inhibitor from the 0 hour to the 5 hour time point (Fig. 2.17B). These results suggest that DCR-1 is regulated and targeted for degradation via the proteosome by a JNK, which may be KGB-1. Only three Jun N-terminal kinases are found in the *C. elegans* genome; KGB-1 and KGB-2 are expressed in the soma and the germline, and loss of *kgb-1* results in sterility at non-permissive temperatures, while loss of *kgb-2* has no observable phenotype (Smith et al., 2004; Orsborn et al., 2007). The third family member, JNK-1, plays important roles in the nervous system and has no observable germline effects (Villanueva et al., 2001). Therefore, it seems likely that KGB-1 is the JNK that regulates DCR-1.

To determine if loss of KGB-1 affects levels of DCR-1 protein, *kgb-1(um3)* lysates were compared to wild type worm lysates. Because loss of KGB-1 has both age-related and temperature-sensitive effects on GLH-1 levels (Osborn et

Figure 2.17

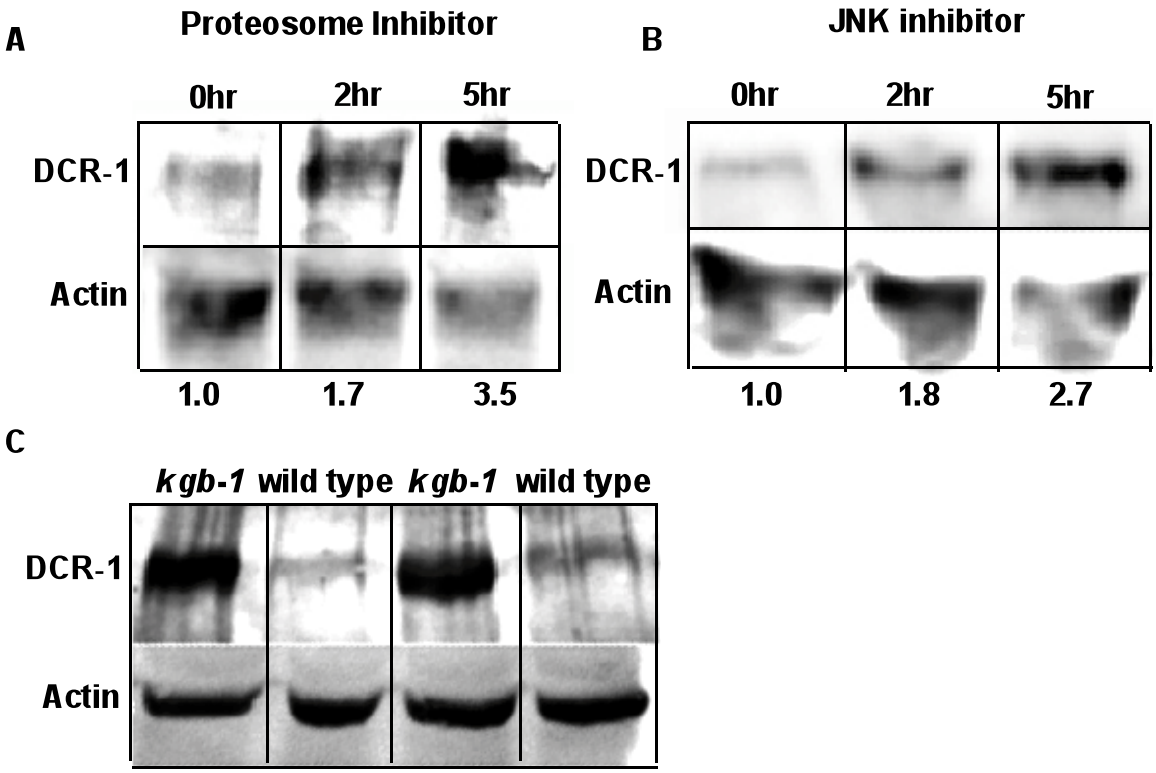

Figure 2.17. DCR-1 accumulates when the proteosome and JNK pathway are inhibited; DCR-1 levels are elevated in *kgb-1* worms. A. Wild type worms were treated with 1 μM of the proteosomal inhibitor, MG132, for 0, 2, and 5 hrs. Fifty worms per time treatment were collected at the end of 5 hrs and analyzed by western blot for DCR-1 protein levels. **B**. Wild type worms were treated with 50 μM of the JNK inhibitor, SP600125, for 0, 2, and 5 hrs. Fifty worms per time treatment were collected at the end of 5 hrs and analyzed by western analysis for DCR-1 protein levels. Actin was used as a loading control. Experiments performed by Jordan Marshall, undergraduate researcher, and Erica Beshore.

al., 2007), age-matched *kgb-1* and N2 animals (two days past the L4 stage), grown at the non-permissive temperature of 26°C, were tested. We found DCR-1 levels were elevated 4.3 fold in the *kgb-1* mutant worms when compared to wild type (Fig. 2.17C, lanes 1 and 3 compared to lanes 2 and 4). Additionally, *kgb-1* worms were analyzed by ICC for increased levels of DCR-1 and GLH-1 compared to wild type. To visualize if there were differences in DCR-1 between *kgb-1* and wild type, confocal images were taken at the same laser levels and PMT voltages. The signal from DCR-1 in the *kgb-1(um3)* gonads was so intense that only very low laser levels and voltages could be used to collect the image of the pachytene region seen in Fig. 2.18A. Using the same settings for wild type worms, only faint signals were detected for DCR-1 and GLH-1 (Fig. 2.18E). Similarly, in *kgb-1* embryos DCR-1 was found at much higher levels than in wild type, both in the germline and in somatic cells when compared to a wild type embryo (Figs. 2.18C vs. 2.18G). These combined data suggest that DCR-1, similar to GLH-1, is targeted for degradation by KGB-1 and that when KGB-1 is missing, both GLH-1 and DCR-1 levels increase.

GLH-1 and DCR-1 regulate the assembly of cytoplasmic RNP granules in stressed *C. elegans* oocytes.

Large, cytoplasmic RNP granules form in the *Caenorhabditis* germline under a variety of conditions, including heat shock or other environmental stresses, or with the arrest of oocytes that occurs when the *C. elegans* hermaphrodite becomes depleted of sperm (Schisa et al., 2001; Jud et al., 2007; Jud et al.,

Figure 2.18

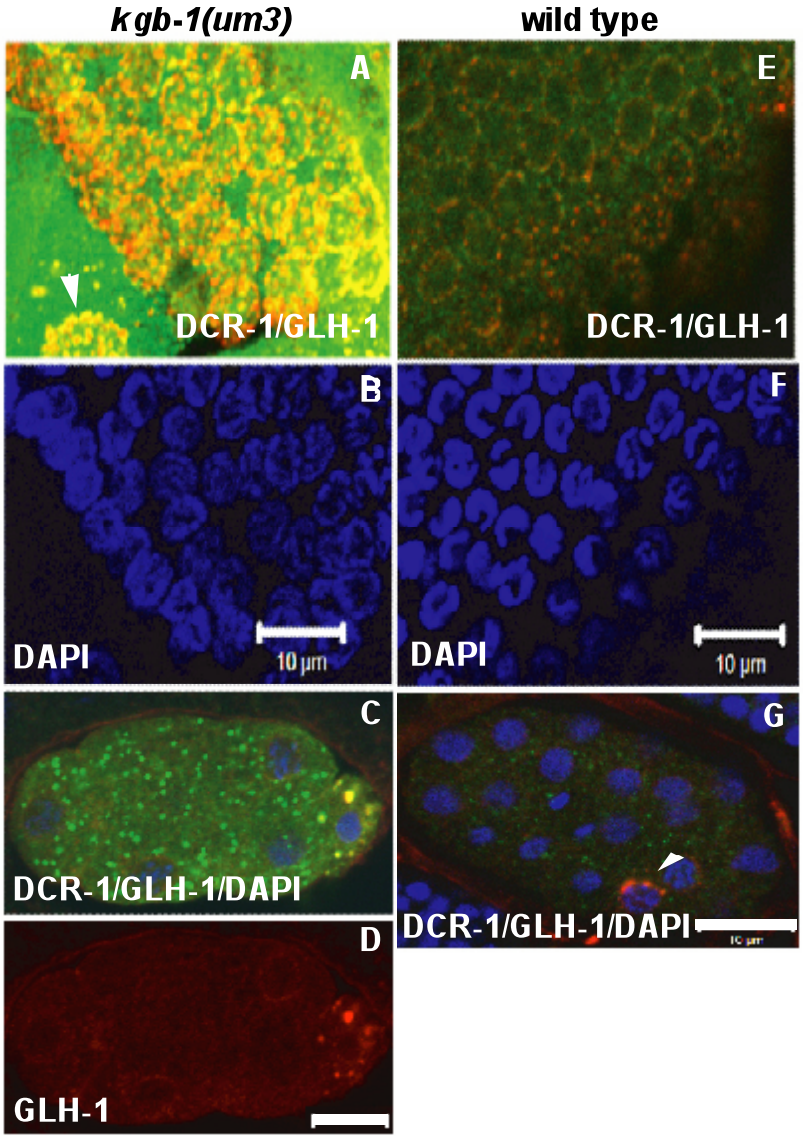

Figure 2.18. DCR-1 and GLH-1 are more abundant in *kgb-1(um3)* than in wild type worms. A. A *kgb-1(um3)* mutant gonad reacted with antibodies against DCR-1 (green), and GLH-1 (red), merged; the pachytene region and a single oocyte are seen in this image. The oocyte nucleus, completely surrounded by large P granules, is indicated with an arrowhead. Similar engorged P granules were reported for GLH-1 alone in *kgb-1* worms (Smith et al., 2004). **B.** DAPI of the same *kgb-1(um3)* gonad in A (blue). **C.** A single *kgb-*

1(um3) embryo reacted with antibodies again DCR-1 (green), GLH-1 (red) and DAPI stained (merged). **D.** The same *kgb-1(um3)* embryo as in C, seen here with GLH-1 (red) alone. **E**. The pachytene region in a wild type gonad reacted with α-DCR-1 (green), and α-GLH-1 (red), merged. **F.** DAPI staining of wild type gonad in E (blue). **G.** Wild type embryo reacted with antibodies against DCR-1 (green), GLH-1 (red), and DAPI-stained nuclei, blue (merged). GLH-1 marks the Z2, germ cell progenitor (arrow), in the older embryo in G. Size markers indicate 10 μm. Confocal images A-G, taken with the same laser levels and PMT voltages and in a single focal plane, show both DCR-1 and GLH-1 are greatly enriched in *kgb-1* when compared to wild type worms.

2008). These large RNP granules share characteristics with P bodies and have been proposed to assemble to protect maternally-transcribed mRNAs from being degraded or being precociously translated before oocyte development and fertilization can continue.

Components of the germline RNP granules include MEX-3, a predicted RNA binding protein, CGH-1, a DExD/H box helicase (as are the GLH proteins) and the P-granule proteins GLH-1 and PGL-1 (Navarro and Blackwell, 2005; Jud et al., 2008; Noble et al., 2008; Schisa et al., 2001). To determine if DCR-1 localizes to these large RNP granules, I first did a co-staining experiment to detect DCR-1 and MEX-3. Transgenic GFP::MEX-3 worms were heat shocked and stained with the anti-DCR-1 antibody. I found DCR-1 co-localized with GFP::MEX-3 in many distinct granules in the oocytes of heat-stressed worms (Fig. 2.19).

The *fog-2(q71)* mutant worm produces oocytes but lacks sperm, such that ovulation is essentially quiescent and oocytes are in an “arrested” state even when the *fog-2* animals are young adults (Schedl and Kimble, 1988). The distribution of GLH-1 in arrested oocytes differs from the small, dispersed P granules seen in actively ovulated oocytes to enrichment in much larger RNP granules that are cortically localized (Schisa et al., 2001; Fig. 2.20A). Our collaborator, Dr. Jennifer Schisa at Central Michigan University conducted staining with our DCR-1 antibody, Dicer was also detected at high levels in the

Figure 2.19

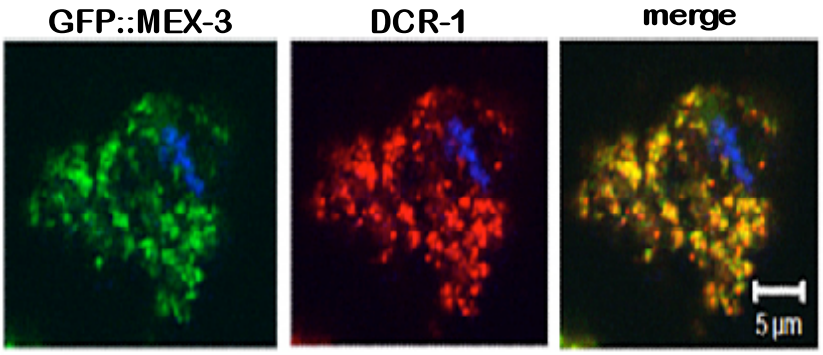

Figure 2.19 Dicer co-localizes with MEX-3 in heat stressed oocytes. Fluorescence imaging of GFP::MEX-3 (green) and ICC with α-DCR-1 antibody (red), shown here in a single, heat-stressed oocyte. The last panel is the merged image (yellow). DNA is seen with DAPI (blue).

Figure 2.20

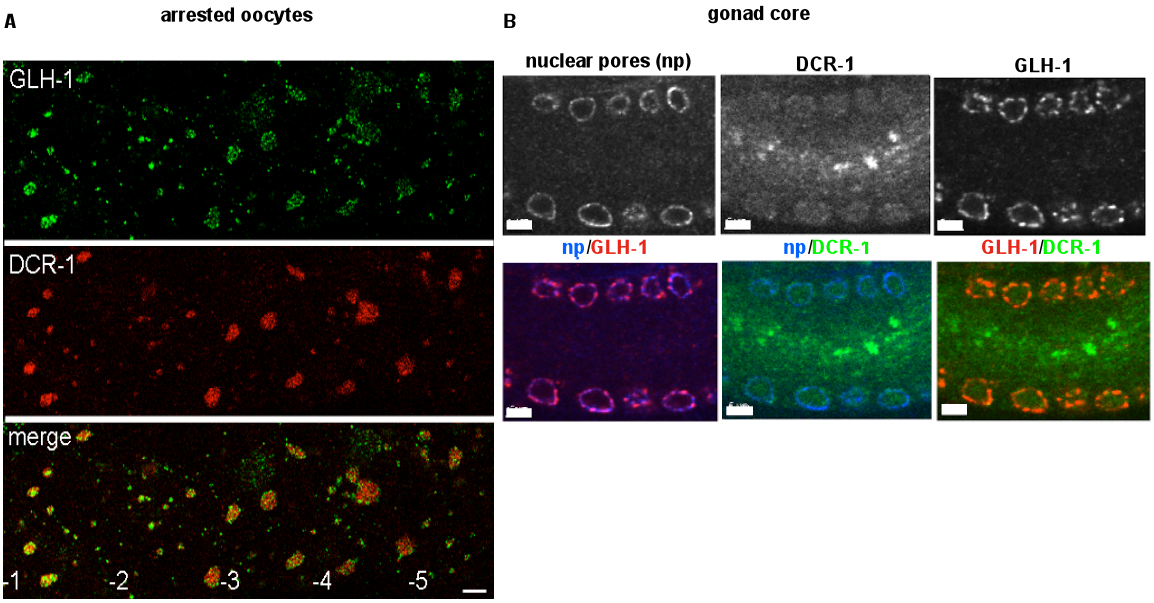

Figure 2.20. DCR-1 localizes to RNP granules both in arrested oocytes and in the central rachis of the distal gonad in *fog-2* mutants; GLH-1 localizes to RNP granules in *fog-2* arrested oocytes. A. Confocal single plane images of the five most proximal *fog-2* arrested oocytes in the gonad reacted with antibodies against GLH-1 (green), and DCR-1 (red), and merged. Size bars in A and B indicate 5 μm. **B.** ICC in the gonad core of a *fog-2* adult gonad against nuclear pores (first panel, top row), DCR-1 (second panel top row), and GLH-1 (third panel top row). Combined localizations are shown in the merged images (bottom row). Images by Jennifer Schisa, Ph.D.

large RNP granules of arrested oocytes (Fig. 2.20A). In oocytes of GLH-1/DCR-1 co-stained worms, granules of GLH-1 appeared to be “docked” on the larger DCR-1 granules, occupying a subdomain of the RNP granules (merged image, Fig. 2.20A); this was reminiscent of the granules of the P body protein DCAP-2 that appear “docked” on granules of the stress granule protein PAB-1 (Jud et al., 2008). Co-staining of GLH-1 with the RNP marker CGH-1 revealed a similar distribution of GLH-1 granules localized on the surface of CGH-1 granules in *fog-2* arrested oocytes (Schisa, Fig. 2.21A). In addition, CGH-1, but not GLH-1 localized to large granules in the rachis, where the center of the gonad arm is surrounded by syncytial germ nuclei; (Schisa, Fig. 2.21B) and, in contrast to DCR-1, GLH-1 was not observed in large granules in oocytes of heat stressed worms (Fig. 2.22).

In *fog-2(q71)* germlines, DCR-1 was also detected at high levels in large granules in the central rachis of *fog-2* worms, again, in contrast, GLH-1 was not detected in large granules in the gonad core of *fog-1* worms (Fig. 2.20B). Like GLH-1, PGL-1 also localizes to large cytoplasmic granules in arrested but not in heat stressed oocytes and not to granules in the gonad core (Jud et al., 2008; Schisa et al., 2001). In summary, GLH-1, DCR-1, along with the previously characterized components MEX-3 and CGH-1, localize to RNP granules in *fog-2* arrested oocytes, but while CGH-1 and DCR-1 also assemble into distinct RNP granules in the rachis of *fog-2* gonads, GLH-1 does not.

Figure 2.21

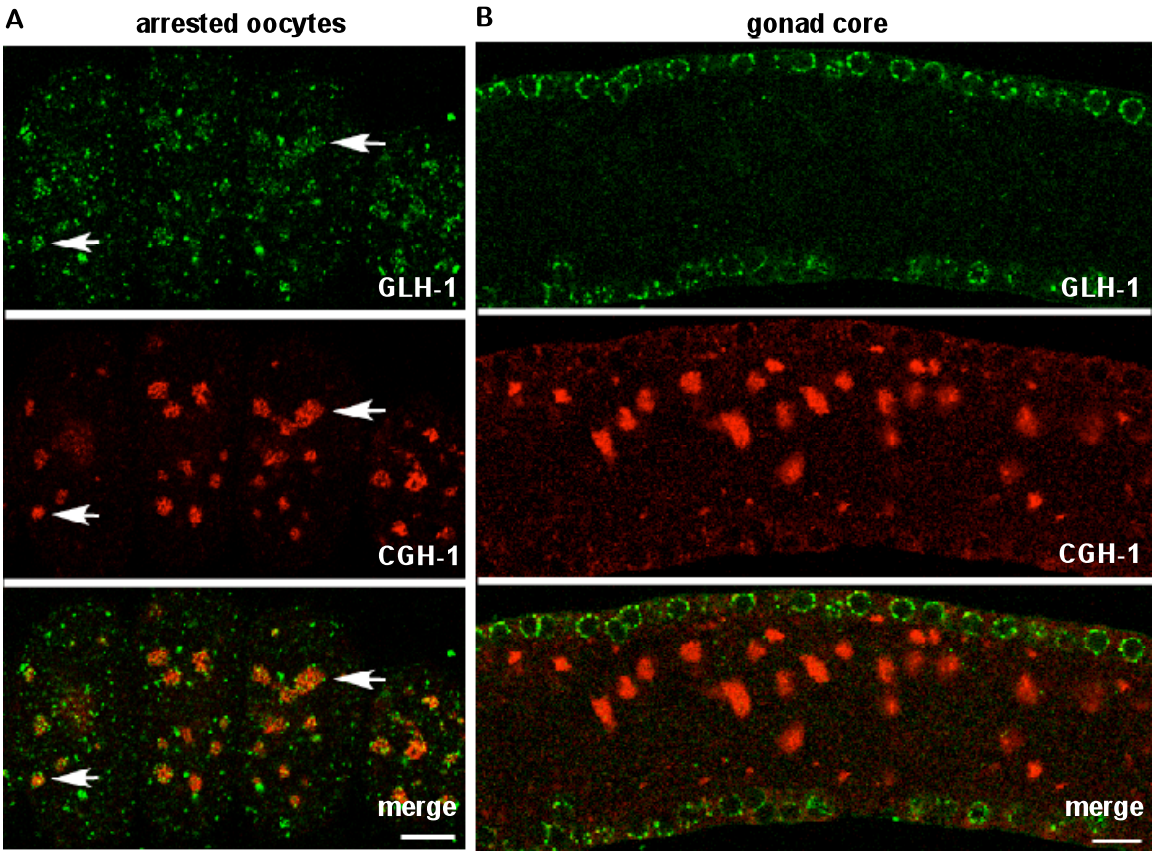

Figure 2.21. Only CGH-1 localizes to RNP granules in the gonad core but both GLH-1 and CGH-1 both localize to RNP granules in arrested oocytes. **A.** ICC staining in the arrested oocytes of a *fog-2* mutant adult with α-GLH-1 antibody (green), and α-CGH-1 antibody, (red). Arrows in A. point out two RNP granules containing both DCR-1 and GLH-1. **B.** ICC staining in the core of a *fog-2* adult gonad with α-GLH-1 antibody (green), and α-CGH-1 antibody, (red). Images by Jennifer Schisa, Ph.D.

Figure 2.22

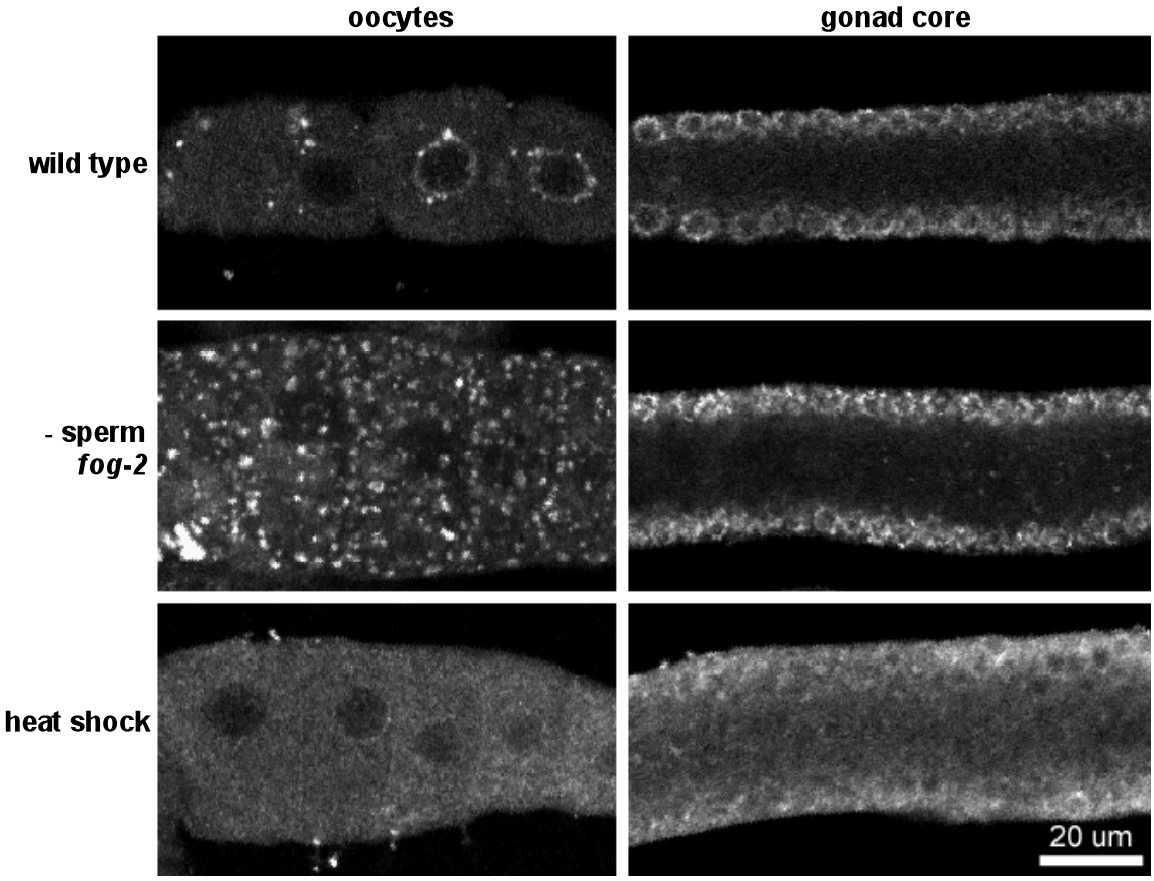

Figure 2.22. GLH-1 localizes to large RNP granules in arrested oocytes but not in heat stressed oocytes or to RNP granules in the rachis. A. Immunolocalization of GLH-1 in wild type oocytes (top panel), unmated *fog-2* mutant oocytes (middle panel), and heat shocked worms (bottom panel). **B.** Immunolocalization of GLH-1 in a wild type gonad core (top panel), unmated *fog-2* mutant core (middle panel), and heat shocked gonad core (bottom panel). Images by collaborator Molly Jud.

To determine whether GLH-1 and DCR-1 are necessary for the assembly of these large germline RNP granules, the distribution of three of the RNP granule components, MEX-3, CGH-1, and PGL-1 was assessed by our collaborator Ms. Molly Jud Central Michigan University in the *glh-1(gk100)* strain, in the *dcr-1* mutants or by *dcr-1(RNAi)*. We found that MEX-3 did not localize to RNP granules in *glh-1(gk100)* arrested oocytes (-sperm, Fig. 2.23, row 2), and fewer MEX-3 granules were seen in *dcr-1(RNAi)* oocytes (Fig. 2.23, row 4). RNAi of *dcr-1* was performed to avoid analysis of the irregular and EMO oocytes in *dcr-1(ok247)* worms. Interestingly, MEX-3 granules formed normally in *glh-1(gk100)* oocytes after heat shock (Fig. 2.24, row 3). CGH-1 failed to localize to RNP granules in approximately 33% of purged *glh-1(gk100)* oocytes, and was not detectable at any discernable levels after heat shock stress (Fig. 2.23, row 3). In the syncytial core of the *glh-1(gk100)* gonads, CGH-1 was much reduced under both the conditions of heat shock and oocyte arrest (not shown). PGL-1 was not detected in large granules in *glh-1(gk100)* oocytes when ovulation was arrested nor after heat shock (Fig. 2.23, row 2 and 3).

CGH-1 and CAR-1 are commonly found in complex together and this interaction is RNA dependent (Boag et al., 2005). Because of this CGH-1/CAR-1 relationship we next asked if CAR-1 co-localizes with DCR-1 and whether the localization of CAR-1 is affected in the *dcr-1* and *glh-1(gk100)* strains. To determine if DCR-1 co-localizes with CAR-1 in heat stressed or oocyte arrested worms we co-stained against DCR-1 and CAR-1. DCR-1 and CAR-1 co-localize

Figure 2.23

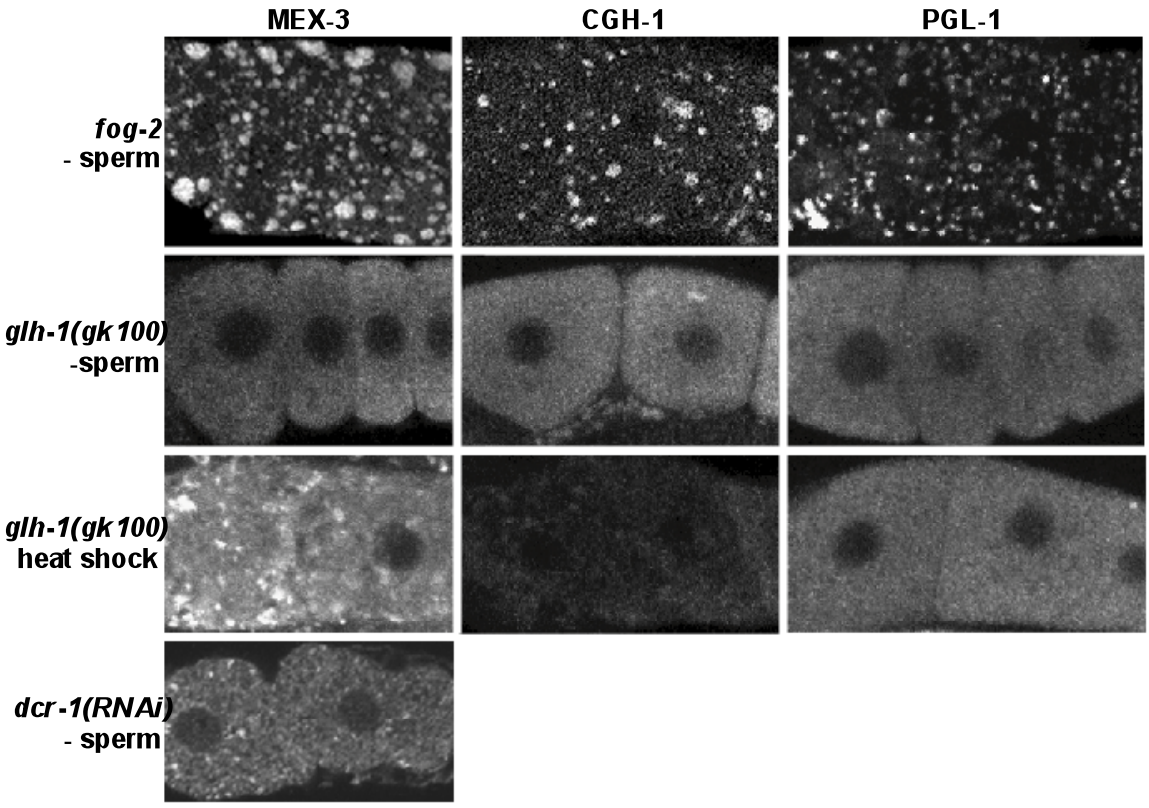

Figure 2.23. Reduction of GLH-1 or DCR-1 disrupts the distribution of MEX-3, CGH-1, and PGL-1 in cytoplasmic RNP granules. The top row shows unmated *fog-2* mutants as a control for normal RNP granule assembly. -sperm in rows 1, 2, and 4 indicate arrested oocytes in purged *glh-1(gk100)* worms or *dcr-1(RNAi);fog-2* worms that lack sperm. Heat shock of the *glh-1(gk100)* worms was carried out at 34°C for 3 hrs (panels in row 3). DCR-1 was knocked down by RNAi. MEX-3, CGH-1 and PGL-1 were visualized with their respective antibodies. Images by our collaborator Molly Jud.

Figure 2.24

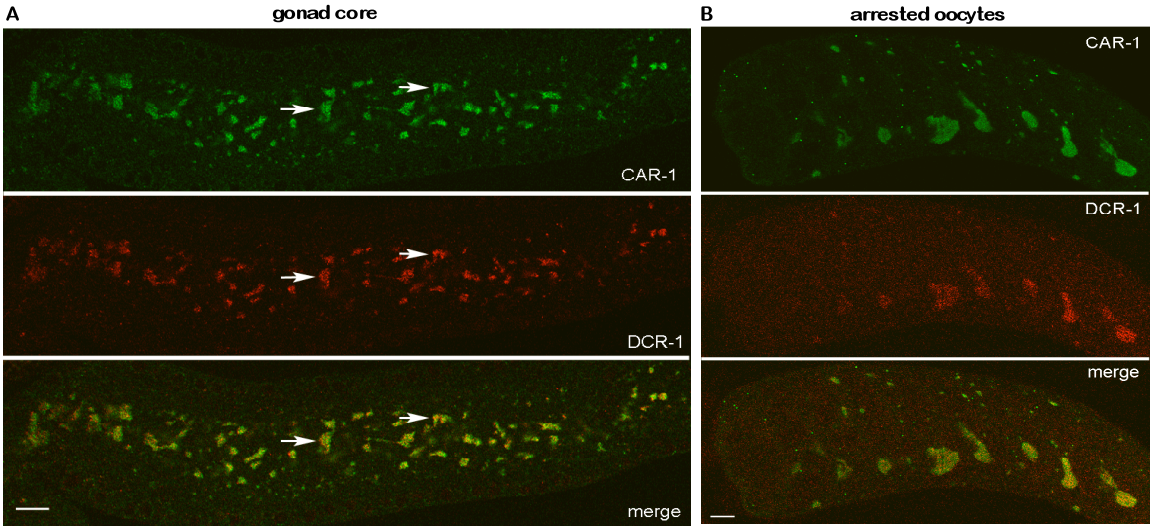

Figure 2.24. Both CAR-1 and DCR-1 co-localizes to RNP granules in the gonad core and to RNP granules in arrested oocytes. A. ICC staining in the gonad core of a *fog-2* mutant adult with α-CAR-1 antibody (green), and α-DCR-1 antibody, (red). Arrows in A. point out two RNP granules containing both CAR-1 and DCR-1. **B.** ICC staining in the core of a *fog-2* adult gonad with α-CAR-1 antibody (green), and α-DCR-1 antibody, (red). Images by Jennifer Schisa, Ph.D.

in distinct germline granules (Fig. 2.24). However, surprisingly CAR-1 was not affected by loss of GLH-1 in the oocytes and continued to localize to RNP granules, despite the fact that GLH-1 and CGH-1 are not at high levels in these heat shocked oocytes (Fig. 2.25) and, in contrast to it being unaffected in oocytes, CAR-1 was absent in the core of the *glh-1(gk100)* gonads with heat shock and oocyte arrest (Fig. 2.25). And in *dcr-1* worms CAR-1 is also dramatically reduced under both conditions. Overall, these data suggest GLH-1 and DCR-1 play an upstream role in the assembly of germline RNP granules and that decreased levels of DCR-1 or GLH-1 prevent their complete assembly.

Discussion

We have uncovered a complex relationship between GLH-1, a *C. elegans* P-granule component, and DCR-1 the RNA-processing ribonuclease required for both the RNAi and microRNA pathways. This interaction, likely occurring across nuclear pores or in cytoplasmic P granules, may function to transport, deposit or regulate germline mRNAs and miRNAs. This work has shown that loss of DCR-1 results in decreased levels of GLH-1 protein and *glh-1* mRNA. Similarly, the *glh-1(gk100)* mutant results in decreased levels of DCR-1 protein; however, levels of *dcr-1* mRNA do not appear to be affected. Our results indicate DCR-1 and GLH-1 are targeted for degradation via the proteosome, likely through the activity of the Jun N-terminal kinase KGB-1. Additionally, both proteins localize to large germline RNP granules in arrested oocytes, where they regulate the assembly of a subset of the RNP granule components.

Figure 2.25

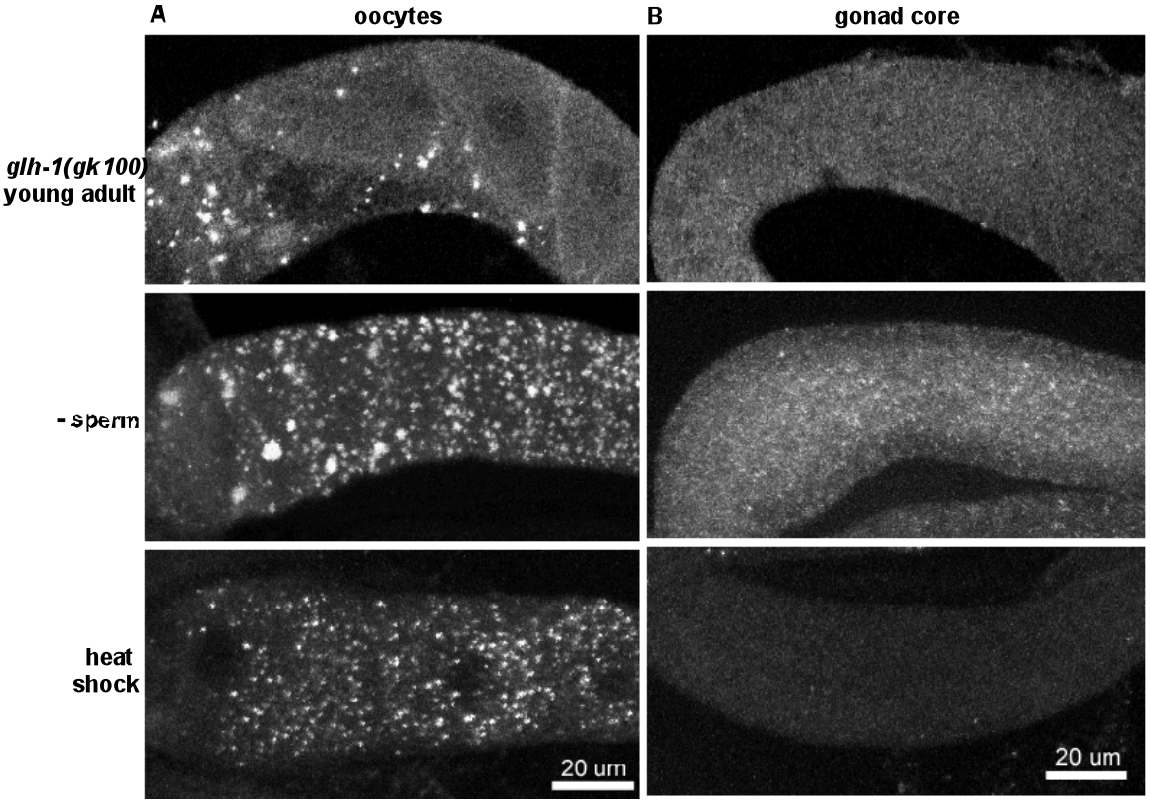

Figure 2.25. CAR-1 localizes to RNP granules in *glh-1(gk100)* in arrested and heat stressed oocytes, but not in the core of the same gonads. A. *glh-1(gk100)* adult oocytes reacted with anti-CAR-1 antibody. Images of an unstressed young adult (top panel), older purged of sperm *glh-1(gk100)* oocytes (middle panel), and heat shocked *glh-1(gk100)* oocytes (bottom panel). **B.** *glh-1(gk100)* adult rachis reacted with anti-CAR-1 antibody. Images of an unstressed young adult (top panel), older purged of sperm *glh-1(gk100)* core (middle panel), and heat shocked *glh-1(gk100)* core (bottom panel). Images by Molly Jud.

Why are GLH-1 levels lower in *dcr-1* mutants?

Published microarray studies have compared the RNA levels from *dcr-1* mutants to those in wild type worms (Welker et al., 2007). Among the 1537 genes differentially regulated in *dcr-1(ok247)* mutants, 488 genes are down-regulated and of these 488 genes, 38% are germline specific. In contrast, only 1% of the up-regulated genes are germline specific (Welker et al., 2007). One of the germline-specific genes reported down-regulated in *dcr-1* worms was *glh-1* and in this report we quantified the reduction of *glh-1* mRNA in *dcr-1* mutants as a 2.8 fold decline (Fig. 2.16; Table 2.1). Thus, perhaps *glh-1* mRNA, and many of the other down-regulated germline transcripts, are normally subjected to global, germline-specific miRNA activation; that is, germline miRNAs may act as decoys, along with RNA binding proteins, resulting in protection of their mRNA targets and translational inhibition, as found in recent work with mi-328 and leukemic blasts (Eiring et al., 2010). However, a role for DCR-1 in processing a class of activating miRNAs that regulate *glh-1* and other germline mRNAs is only speculative. Alternatively, the down-regulation of *glh-1* mRNA in the *dcr-1* mutant may be an indirect effect; an unidentified transcriptional activator of *glh-1* mRNA, and of many germline mRNAs, could be among the *dcr-1* up-regulated genes.

The dramatic reduction of GLH-1 protein in the *dcr-1* mutant, Fig. 2.13A, may only partially be accounted for by the approximately three-fold decrease at the mRNA level (Table 2.1). One of the functions of KGB-1 is to target GLH-1 for

degradation (Orsborn et al., 2007), which could be triggered by the loss of DCR-1 from the DCR-1/GLH-1 complex. This targeted degradation would likely add to or be synergistic with the loss of *glh-1* mRNA. Interestingly, in the *dcr-1* mutant, *kgb-1* mRNA levels are elevated almost four-fold. This finding and the *glh-1* and *dcr-1* relationships discussed above suggest regulatory feedback loops operate among these three proteins.

Reduction of DCR-1 in *glh-1(gk100)* mutants

The finding that DCR-1 protein is reduced in the *glh-1(gk100)* mutant was unexpected. One explanation for this is that DCR-1 is somehow stabilized by GLH-1 and when GLH-1 is reduced, DCR-1 is readily targeted for degradation. We did not directly test by IPs if the GLH-1 protein made by the *glh-1(gk100)* strain interacts with DCR-1 due to the low levels of both GLH-1 and DCR-1 detected in this mutant. However, since DCR-1 protein levels were not reduced in the *glh-1(ok439)* strain that produces ~40% of a C-terminally truncated GLH-1 protein and lysates from *glh-1(ok439)* do not co-precipitate with DCR-1 in IPs (Fig. 2.6), these findings may indicate that only when DCR-1 is in complex with GLH-1 is DCR-1 subjected to degradation. An alternative explanation for how GLH-1 regulates DCR-1 might be that GLH-1 regulates the translation of *dcr-1* mRNA or of the mRNA of another, unidentified protein that interacts to stabilize DCR-1. Another factor that could contribute to the dramatic loss of DCR-1 (Fig. 2.13B, E) is the variable phenotype of the *glh-1(gk100)* strain (Spike et al., 2008). Since some *glh-1(gk100)* adults have small gonads, even at 20°C, the

permissive temperature at which all our experiments were carried out, a portion of the reduction in DCR-1 protein levels may reflect the reduced *gk100* germlines.

DCR-1 is targeted for degradation via the proteosome.

In this work, inhibition of the JNK pathway and of the proteosome resulted in an accumulation of DCR-1 (Figs. 2.17A-B), implying that DCR-1 is targeted for proteosomal degradation by a Jun N-terminal kinase. Supporting this idea, DCR-1 protein levels are higher in *kgb-1(um3)* worms both by western blot analysis (Fig. 2.17C) and by ICC (Fig. 2.18). It is plausible that DCR-1 is targeted for degradation by KGB-1 as it contains a consensus MAP kinase D (docking) site, RLGKKLGI (Jacobs et al., 1999) (reviewed by Sharrocks et al., 2000), and a putative phosphodegron motif, which is consensus except in the second position, IDTPT (Orlicky et al., 2003; Ye et al., 2004). It is also possible that KGB-1 does not directly target DCR-1 for degradation, but rather GLH-1 could be the only pertinent KGB-1 target, and the higher levels of GLH-1 in *kgb-1(um3)* animals could serve to recruit and stabilize DCR-1 in the *kgb-1* worm, accounting for the higher levels seen by western and ICC (Figs. 2.17C and 2.18).

Our previous results indicated that either over-expression or under-expression of GLH-1 results in sterility, with homeostasis achieved through opposing actions of KGB-1 and CSN-5, a COP9 signalosome subunit (Orsborn et al., 2007; Spike et al., 2008). Perhaps not surprisingly, maintaining appropriate DCR-1 levels also

appears critical to the germline; sterility occurs either when too much or too little DCR-1 is present. While the absence of DCR in the *dcr-1* null worms or excess DCR-1 in the *kgb-1* mutant each results in a similar EMO phenotype, the causes of endoreplication may be unrelated, since DCR-1 processes many small RNAs and KGB-1 may phosphorylate multiple targets. However, it seems likely that careful titration of both GLH-1 and DCR-1 is necessary for normal oocyte development.

Dicer Localization in the Germline

The anti-DCR-1 antibody generated for this work has allowed visualization of DCR-1 in whole-mount *C. elegans*. Triple-labeling experiments demonstrate that GLH-1 and DCR-1 are perinuclear and concentrated at the nuclear pores of germ nuclei, with DCR-1 detected on both the nuclear and cytoplasmic faces of the germ cell nuclear pores (inset, Fig. 2.10A). DCR-1 localizes not only to germ cell nuclei, but also throughout the cytoplasm of both germline and somatic tissues. Thus, *C. elegans* DCR-1 is detected both in the nucleus and in the cytoplasm, a pattern similar to what was recently reported in fission yeast (Emmerth et al., 2010). In *S. pombe* it was reported that Dicer (Dcr1) acts as a shuttling protein between the nucleus and the cytoplasm, perhaps functioning in the nucleus to regulate mRNA transcription and the maintenance of heterochromatin. We predict that in the *C. elegans* germline, DCR-1 regulates pre- or processed miRNAs, shuttling processed miRNAs out of the nuclei via the nuclear pores, handing them off to GLH-1 where they may find their mRNA targets and be

transported to the rachis or stored in cytoplasmic RNP particles, rather than seeing a standard RISC complex. Previously affinity purified DCR-1 out of adults pulled down both ALG-1 and 2, the best-studied of the ~27 Argonaute-like proteins in *C. elegans*, along with GLH-1 (Duchaine et al., 2006; D. Conte, U Mass, personal comm.). It will be of interest to determine whether Ago-like proteins are in the GLH-1/DCR-1 complex along with identifying the mRNAs and miRNAs bound.

GLH-1 and DCR-1 in Germline RNP Granules

In analyzing the germline RNP granules that form under certain conditions in developing oocytes we observed a failure of MEX-3, PGL-1, CGH-1, and CAR-1 to assemble into large RNPs in *glh-1(gk100)* and *dcr-1(RNAi)* worms. It was previously reported that knockdown *of glh-1 and glh-4* by RNAi results in a dramatic reduction of CGH-1, with ~30% of the *glh-1/4(RNAi)* worms showing no CGH-1 staining in the gonad; in contrast, knockdown of *pgl-1* by RNAi did not affect CGH-1 levels or localization (Navarro and Blackwell, 2005). Our analyses confirm this previous finding and indicate that GLH-1 and DCR-1 regulate the assembly of germline RNP granules. It seems likely that under certain stressful conditions, during which mRNA translation of many transcripts halts, GLH-1 and DCR-1 may be critical structural components of RNP granules and may also bring maternal mRNAs and their companion miRNAs to these granules for storage. Interestingly, the regulation of RNP components is complex and varies depending on the trigger inducing their assembly; for example, GLH-1 is not

required for MEX-3 to assemble into large RNP granules after heat shock, while GLH-1 and DCR-1 differ with regard to their presence in the central rachis due to arrested oogenesis. We know from previous work that the components of RNP granules vary depending on the stimulus inducing their assembly (Jud et al., 2008); therefore, these findings may not be surprising.

Dead-box RNA helicases have roles in the miRNA pathway.

To date several DEAD-box RNA helicases have been identified that interact with and modify the miRNA pathway. One such protein is Dead end (Dnd), a vertebrate germ granule component involved in the de-repression of mRNAs targeted by miRNAs (Kedde et al., 2007; Slanchev et al., 2009). CGH-1 is a *C. elegans* DEAD-box RNA helicase whose localization to large RNP granules is regulated by *glh-1* and *dcr-1* (Fig. 2.23 and not shown). In somatic cells CGH-1 functions, along with the TRIM domain protein NHL-2 to enhance the repression of several miRNA targets. The authors proposed the interaction between CGH-1 and NHL-2 modulates the efficiency of binding of miRNAs to their mRNA targets in this novel somatic miRISC (Hammell et al., 2009). Because GLH-1 localizes to RNA granules, interacts in complex with Dicer, and regulates the assembly of germline RNP granules, we propose GLH-1 may also function as a component of a germline-specific miRISC.

While evidence points to a relationship of GLH-1 with the microRNA pathway, GLH-1 does not appear to play a role in the exogenous siRNA pathway. When

glh-1(gk100) worms were injected with several different dsRNAs, the genes targeted for RNAi were efficiently knocked down (Spike et al., 2008). Therefore, it seems likely this new-found relationship of GLH-1 with DCR-1 may specifically relate to DCR-1's miRNA functions.

Relationship of P granules to the nuclear pore complexes

Three recent analyses relate to findings presented here. The Strome laboratory identified proteins affecting the integrity of P granules, uncovering interesting links between P granules, RNAi pathway components and nuclear pores. Using an RNAi screen with a PGL-1::GFP transgene, they assayed changes in P granule morphology and identified 173 genes whose knock-down affects P granules. In particular, they report that knockdown of CSR-1; a germline Argonaute protein associated with the siRNA pathway results in the accumulation of PGL-1, GLH-1, and RNA into much larger perinuclear P-granules (Updike and Strome, 2009). A second study from the Seydoux laboratory took a similar experimental approach and found that knockdown of the mRNA encoding the nuclear pore protein NPP-10 (the *C. elegans* Nup98 protein) results in the disruption of P-granule stability and the mis-expression of the P-granule associated mRNA *nos-2* (Voronina and Seydoux, 2010, in press). Their findings strengthen the view that P granules are involved in regulating the translational regulation of maternally-transcribed mRNAs. Additional work from the Priess group also examined the relationship of P granules to nuclear pore complexes and found that the perinuclear P granules accumulate newly transcribed and

exported mRNAs in wild type worms. They found that knockdown of GLH-1 by *glh-1(RNAi)* results in smaller P granules with reduced accumulations of mRNA at the nuclear pore (Sheth et al., 2010). While PGL-1, nuclear pores, and GLH-1 were all integral to these studies, the finding that DCR-1 is also a binding partner of GLH-1 adds exciting new possibilities to mechanisms of P granule action.

Figure 2.26 presents a model to visualize aspects of the GLH-1/DCR-1 interaction discovered during these studies. Our results indicate that GLH-1 and DCR-1 physically interact, and that this interaction likely takes place in or near P granules and the nuclear pores. We hypothesize that the DCR-1/GLH-1 interaction is important for an as yet unknown process occurring with miRNAs and maternal mRNAs at nuclear pores and in P granules. A storage function in cytoplasmic RNP granules that are induced by arrested ovulation or stress, may also be carried out by the DCR-1/GLH-1 complex, since DCR-1 and GLH-1 are required for the complete assembly of these cytoplasmic granules.

A physical interaction between Dicer and GLH-1, Vasa or MVH, is now known to occur in flies and mice and worms; thus, we expect that many of the additional, new findings presented here, including the nuclear pore location of DCR-1, the roles of both GLH-1 and DCR-1 in the formation of stress-induced RNPs, the targeting of each protein for degradation by JNKs, and the interdependence of each protein on the other, may be conserved “from hydra to man” (Eddy, 1976) as are the germ granules themselves.

Figure 2.26

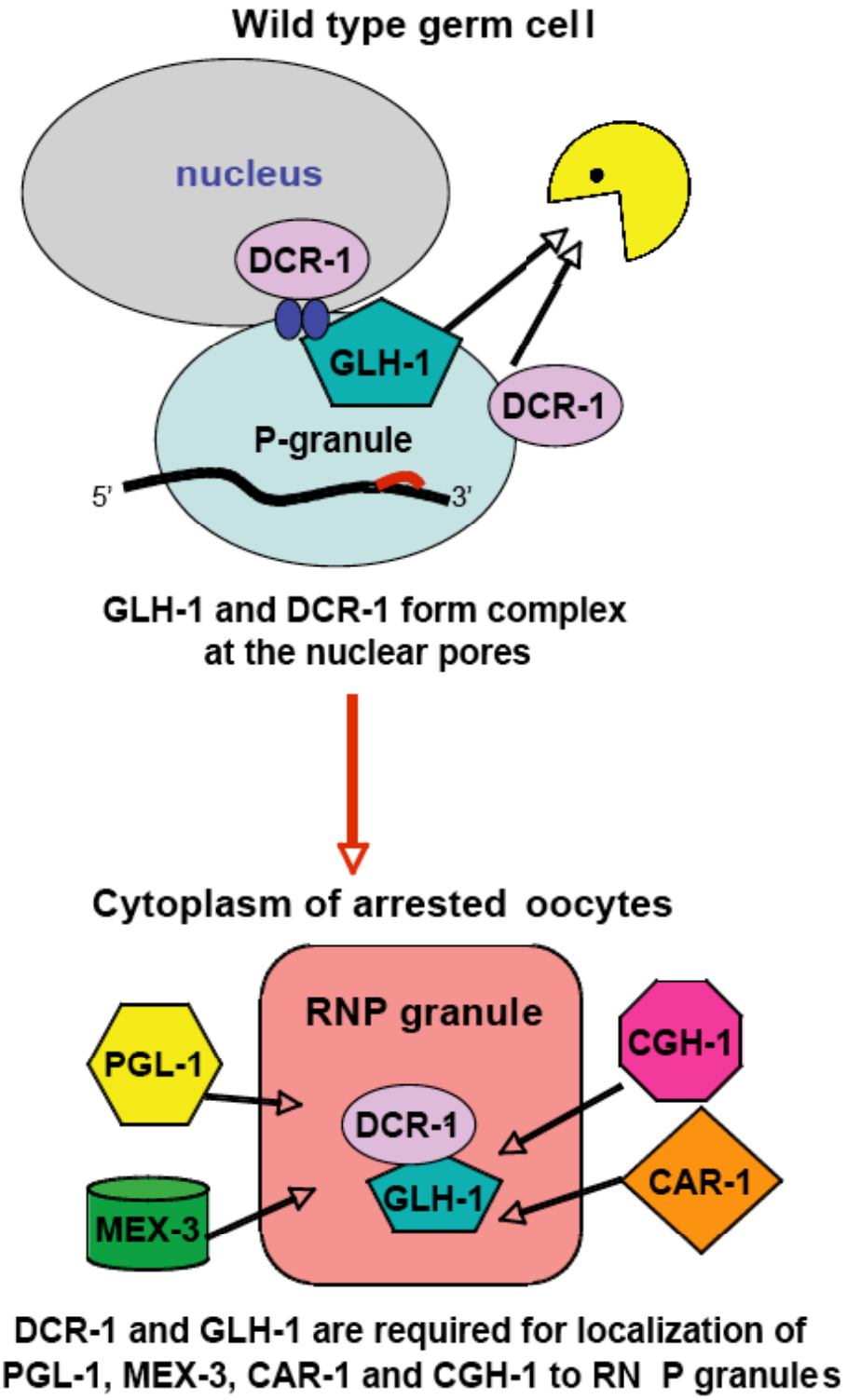
Wild type germ cell
nucleus
DCR-1
GLH-1
DCR-1
P-granule
5'
3'
GLH-1 and DCR-1 form complex
at the nuclear pores
Cytoplasm of arrested oocytes
RNP granule
PGL-1
CGH-1
DCR-1
GLH-1
CAR-1
MEX-3
DCR-1 and GLH-1 are required for localization of
PGL-1, MEX-3, CAR-1 and CGH-1 to RN P granules

Figure 2.26. Model for the role of GLH-1 and DCR-1 in P granules and RNP granules. In wild type worms both GLH-1 and DCR-1 localize to P granules, possibly to regulate the fate of maternal mRNAs and their associated miRNAs in P granules. Under conditions of arrested ovulation both GLH-1 and DCR-1 re-localize to large RNP granules in the oocytes and are important for the recruitment MEX-3, PGL-1, CAR-1, and CGH-1, where they may regulate maternal mRNAs during delays in fertilization. The blue dots indicate the nuclear pores; the red line indicates a miRNA bound to the 3'UTR of its target mRNA.

Chapter 3: Genetic Analysis of the *Caenorhabditis elegans* GLH Family of P-Granule Proteins

Introduction

The GLH proteins were first discovered in the Bennett laboratory and were previously described as being germline specific helicase proteins associated with P granules (Gruidl et al., 1996; Kuznicki et al., 2000; Roussell and Bennett, 1993). Analyses of the GLHs using RNAi to deplete the proteins individually revealed a hierarchy of GLH function, with GLH-1 being the most important for germline development, followed by GLH-4. By RNAi, both GLH-2 and GLH-3 appeared to have little importance for fertility. However, RNAi does not typically result in a total knock-down of the target protein. Therefore, to better understand the roles of the GLH proteins individually it was necessary to analyze mutant alleles. To this end, several mutant strains in the four genes were generated to analyze the loss of gene phenotype. Four *glh-1* mutant strains were obtained both by the *C. elegans* Knock-Out Consortium (*glh-1(gk100)* and *glh-1(ok439)*) and the Strome laboratory (UC Santa Cruz) (*glh-1(bn103)* and *glh-1(bn125)*), for alleles see Fig. 3.1. Kathleen Kuznicki, a former member of the Bennett laboratory (University of Missouri), isolated mutations for both *glh-2* and *glh-3* (*glh-2(um2)* and *glh-3(um1)*), for alleles see Fig. 3.2. The *C. elegans* Knock-Out Consortium also isolated a deletion in *glh-4* (*glh-4(gk225)*). These strains were then analyzed for sterility, brood size, embryonic lethality, number of germ cells, and gonad morphology. The outcome of this work was published in *Genetics* in

Figure 3.1

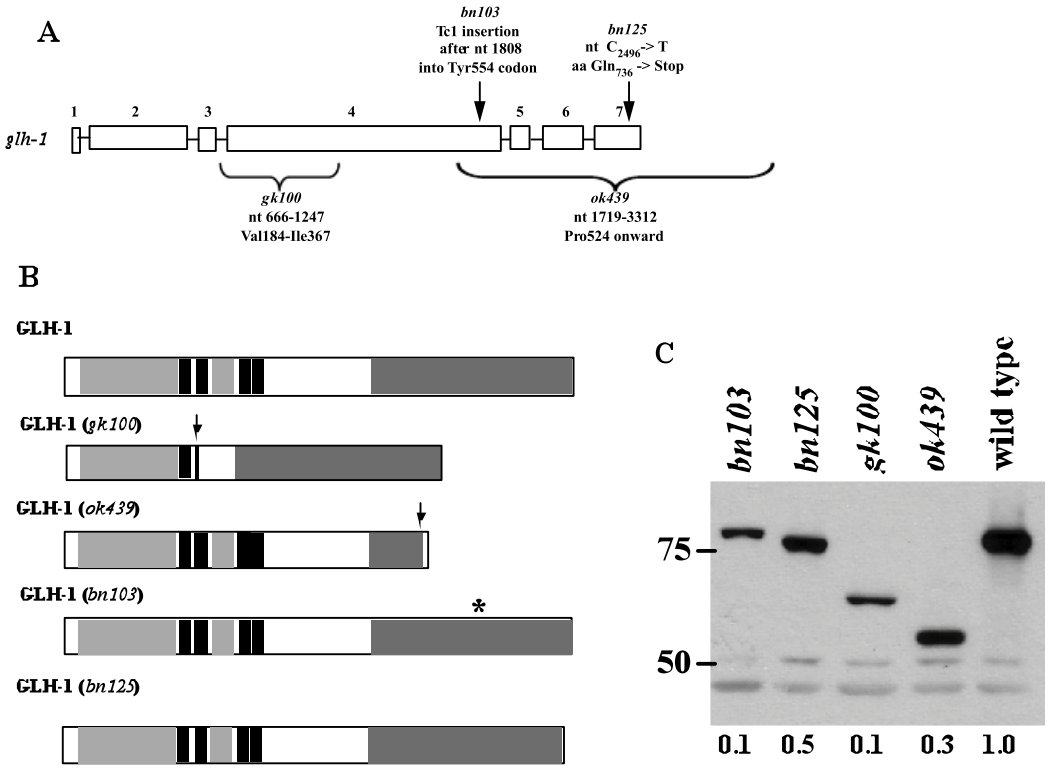

Figure 3.1. Mutant alleles of *glh-1*. (A) Schematic representation of the *glh-1* gene, showing the positions and molecular lesions of the four mutant alleles. Coding regions are shown as boxes, and introns as lines. (B) Cartoon of the GLH-1 polypeptide predicted to be produced by each mutant. Light gray box is Gly-rich region. Black box is a CCHC zinc finger. Dark gray is DEAD box helicase domain. The arrows in *gk100* and *ok439* indicate the positions of missing amino acids. The *ok439* lesion is predicted to fuse a novel 10 amino acid stretch to the carboxy terminus of GLH-1. The asterisk in *bn103* shows the position of the Tc1 insertion. *bn125* removes the last 28 amino acids. (C) Western blot analysis of the GLH-1 polypeptide produced by each mutant. The blot was reacted with affinity-purified rabbit anti-GLH-1 and mouse anti-actin as a

loading control. Values beneath the lanes are the levels of GLH-1, normalized to actin level and expressed relative to wild type.

Figure 3.2

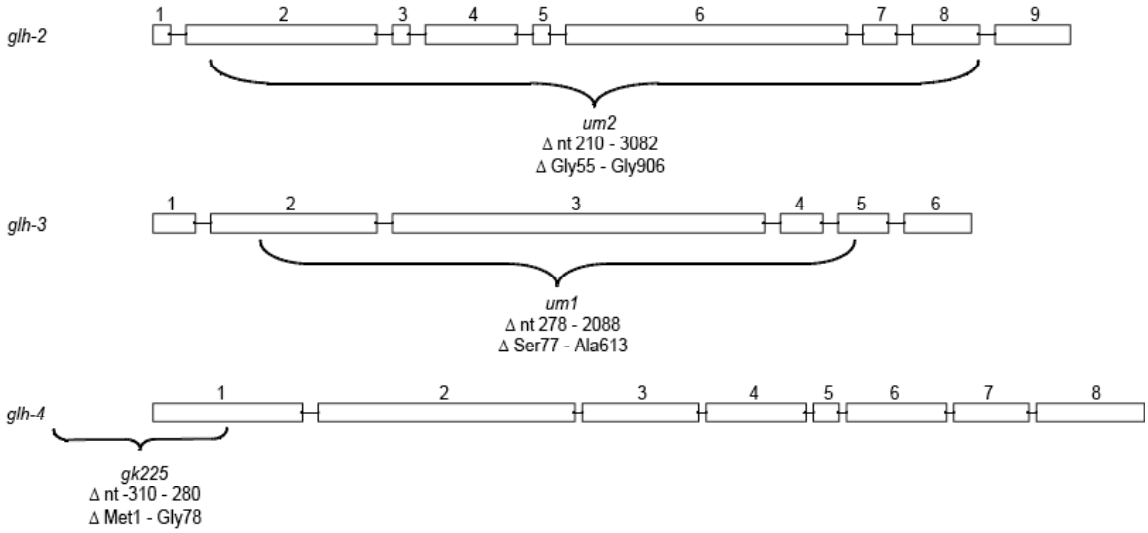

Figure 3.2. Mutant alleles of *glh-2*, *glh-3*, and *glh-4*. Schematic representation of each *glh* gene, showing the position and extent of each deletion allele. Coding regions are shown as boxes, and introns as lines.

2008 under the title, “Genetic analysis of the *Caenorhabditis elegans* GLH family of P-granule proteins” (Spike et al., 2008).

Methods

Strains

C. elegans strains were maintained as described in Brenner (1974). Strains used were wild-type variety Bristol strain N2, LGI *glh-1(bn103*, *bn125*, *gk100*, *ok439)*, *glh-2(um2)*, *glh-3(um1)*, *glh-4(gk225), dpy5(e61), unc-13(e1091), hDf8*, the GFP-tagged balancer *hT2[bli-4(e937) let-?(q782) qIs48]*, *unc-119(ed3),* and the *lag-2::GFP(jk2868)* marker strain. Strains were usually kept at 20°C at the permissive temperature unless otherwise noted.

Analysis of sterility

L4 stage *glh-1/hT2-GFP or glh-4 glh-1/hT2-GFP* hermaphrodites were picked to individual plates and incubated at 20 or 26°C. F1 M+Z- homozygous *glh* adult hermaphrodite progeny (non green worms) were scored for sterility at each temperature. Worms that lacked embryos in their uterus were visually scored as sterile. Worms that contained material in their uterus were transferred to individual plates, to assess whether they produced viable offspring. Fertile F1 M+Z- hermaphrodites were picked to new plates and placed back at each temperature to lay progeny. F2 M-Z- hermaphrodites were scored for sterility at each temperature as described for the F1 worms.

Germ cell counts

glh-1 M-Z- animals and *glh-4;glh-1* M+Z- animals were shifted to 26°C and their progeny fixed and stained with DNA dye Hoechst (Shim et al., 2002) as adults,

~24 hr after they were identified as midstage L4s. All germlines were scored for the presence of sperm and oocyte nuclei; animals used for precise germ cell counts are a subset of the total were selected at random. All identifiable germ cells other than sperm were counted. The germ cell counts were done by Strome laboratory member Dr. Caroline Spike.

DAPI staining dissected germ lines

glh/hT2-GFP mothers were shifted from 20°C to 26°C, their homozygous *glh/glh* offspring worms (M+Z-) picked to individual plates at 26°C, and their M-Z- hermaphrodite progeny analyzed as young adults, approximately one day beyond the L4 stage. Worms were picked into 10 μL of M9 containing 5 mM levamisole on a slide, cut, and their gonads extruded using a 15-gauge needle. Samples were overlaid with a coverslip, frozen on dry ice, fixed in formaldehyde fixation solution (3.73 mL 1M K_2HPO_4, 1.47 mL 1M KH_2PO_4, 10 mL 16% formaldehyde, 36.8 mL ddH_2O) for one hr at RT, rinsed, fixed in methanol at -20°C for 5 min, washed, stained with 0.01 μg/ml DAPI, mounted in Gelutol (Dupont), and observed with a Zeiss Axioplan microscope and a Spot CCD camera.

Gene Gun Bombardment

unc-119(ed3);glh-1(ok439) worms were initially grown and maintained on approximately forty 60mm NGM plates. Plates were maintained by picking a large number of worms and distributing them down the center of the plate. From

60mm plates, worms were transferred to 100mm plates, supplemented with 30% egg powder in OP50 *E. coli* for extra protein, every 5-7 days at 20ºC. The transfer ratio of worms was between 1:1 and 5:1 60mm plates to 100mm egg plates depending on the density of the 60mm plates. Once transferred, worms on the 100mm egg plates were ready for bombardment within 3-7 days. Between 10-20 large plates are required per bombardment (0.5-2ml of packed worms). Once worms on 100mm plates were ready (mostly adults) the worms were washed with 10-20mL of M9 salts, this wash was repeated to remove any contamination or extra food and to get any remaining worms off the plates. The worms were then collected in the wash liquid in a 50ml conical tube and allowed to settle for 5-10 minutes. To plate the cleaned worms, an unseeded 100mm plate was placed in the laminar flow hood with the lid off to air-dry for 30-60 minutes, and put on ice. Worms were then transferred to the dried/iced 100mm plate, spreading worms in a monolayer.

To prepare the gold beads 15mg of 1 μm sized micro gold beads were weighed into a siliconized Eppendorf tube. 1 ml of 70% EtOH was the added to the tube, the beads were vortexed for 5 minutes and then allowed to settle for 15 minutes. The tubes were then spun for 5 seconds at maximum speed in a bench top microfuge. The supernatant was aspirated carefully to reduce the loss of gold. We then added 1 mL of dH_2O, vortexed for 1 min, and allowed to settle for 1 min. Again the tubes were spun for 5 seconds and supernatant carefully aspirated. This wash was repeated 3 times. After the final wash, 250 μL of 50% glycerol

was added to the gold bead pellet. After this treatment, beads can then be stored at room temperature.

To load DNA onto the gold beads we measured quantities enough for seven bombardments at one time. Beads were first vortexed in the 50% glycerol for 5 minutes. We then aliquoted 10 μL/bombardment into a siliconized Eppendorf tube. We then added 4 μL/ bombardment of 0.1M spermidine (stored at -20°C), vortexed for 1 min, added 1 μL/ bombardment of the DNA construct with a concentration around 0.5 μg/μL, vortexed for 1 min, and finally added 10 μL/ bombardment of 2.5M $CaCl_2$. This mixture was then vortexed again for 3 min. The beads were then allowed to settle for 1 min and spun for 5 sec in a microfuge. The supernatant was removed using a pipetteman to avoid disturbing the gold bead pellet. The pellet was then resuspended in 30 μL/ bombardment with 70% EtOH. The tubes were then spun for 5 sec in a microfuge and the supernatant removed using a pipetteman. The pellet was again resuspended in 30 μL/ bombardment with 100% EtOH, followed by another spin and removal of the supernatant. Finally the beads were resuspended in 10 μL/ bombardment with 100% EtOH. The beads were then vortexed for at least 3 min, and continually resuspended until loaded onto the BioRad gene gun macrocarriers by scraping the bottom of the tube along the top of a tube rack.

The macrocarriers were first cleaned by dipping into iso-propanol and blotting with Kim-Wipes. The resuspended gold beads were then loaded, ~10 μL, onto

the center of the macrocarrier. They were then allowed to dry before loading into the PDS-1000 system (BioRad, www.biorad.com). We used 1350 psi rupture disks.

Following bombardment the worms were allowed to recover for 30-60 min. Worms were then washed with M9 salts (5 ml) and transferred to ten 100mm seeded (OP50) plates. Worms were then grown at 20°C for 1-2 days and then transferred to 26°C. After 7-10 days the plates were checked for early transformants, looking for rescue of the motility defect in *unc-119.*

PCR analysis

To test for the presence of the GFP::*glh-4* transgene in the *glh-1* mutant and potentially transgenic worms, primers specific to *gfp* (5' primer) and *glh-4* cDNA (3' primer) were used. The gfp 5' primer, 5'-CCA GAC AAC CAT TAC CTG TCG- 3', is 96 nucleotides upstream from the end of the *gfp* coding sequence. In the construct there are 81 nucleotides between the stop codon of *gfp* and the start of *glh-4*. The *glh-4* cDNA 3' primer, 5'- CAC CAC TCC TGT TCC- 3', is at the 3' most end of the cDNA. The total PCR product for GFP::*glh-4* transgene would be 4024 nucleotides in length.

Western Blot Analysis

To test for the presence of GFP::GLH-4 expression in the *glh-1(ok439);GFP::glh-4* transgenic strain versus wild type worms fifty worm of each were picked and

prepared for western blot analysis. Lysates were loaded onto 8% SDS-PAGE gels and run at 100V until all the dye had run off the bottom of the gel. The gels were then transferred to a nitrocellulose membrane for one hour at 100V. The membranes were blocked in 5% non-fat dry milk before developing with antibody. The membrane was incubated with rabbit anti-GFP antibody at 1:1000. After washing, the membrane was incubated with horseradish peroxidase-conjugated goat anti-rabbit at 1:20,000. After washing, signal was detected using Supersignal West Pico Chemiluminescence kit (Thermo Scientific).

Proteosome inhibitor experiments

Young *glh-1(gk100)* adults, 1 day beyond the L4 stage, were grown in liquid culture (7% χ1666), at 20°C with 1 μM MG132 (Calbiochem) or no inhibitor added. Inhibitor was added for the various times indicated and all worms were grown for a total of 5 hrs. Worms were collected and analyzed for DCR-1 by western blot analysis (50 worms/lane), using anti-actin (Abcam) as the loading control.

Results

Detailed Description of Strains

glh-1:

gk100: The *glh-1(gk100)* is a deletion mutant that removes 581 bp from intron 3 and exon 4 of the *glh-1* gene. RT-PCR analysis of mRNA products revealed that the remaining 15 nucleotides in intron 3 are not spliced out. The predicted protein product contains a 6 amino acid insertion and lacks 184 central amino acids (Val184-Ile367), which comprise 3 zinc fingers and a Gly-rich segment. The remaining sequence, which is in frame, does produce a truncated GLH-1 protein, at approximately 10% of wild-type levels. The mutant protein migrates at ~62 kD, consistent with its predicted size of 585 amino acids.

ok439: The *glh-1(ok439)* mutant deletes the last 1131 bp of the gene and extends well beyond the 3' UTR for a total of 1594-nucleotide deletion. By RT-PCR, the resulting mRNA would encode a protein product that lacks the last 240 amino acids of the protein (Pro524 onward) and thus lacks much of the DEAD box helicase domain, and contains a novel 10-amino acid C-terminal extension. Western blot analysis revealed that the *ok439* deletion does produce a truncated protein of approximately 57 kDa at 30% of wild-type levels.

bn103: *glh-1(bn103)* contains an insertion of a 1.6 kb Tc1 transposon in the fourth exon of *glh-1* at nucleotide 1808, resulting in a normal-sized GLH-1 protein that is produced at 10% of wild-type levels. Because the *bn125* mutants did not appear to have similar phenotypes as seen in the other *glh-1* mutants and also had a closely linked mutation in *mut-2/rde-3,* which on its own results in sterility at the non-permissive temperature of 26°C, its study was dropped from our experiments.

bn125: *glh-1(bn125)* is a point mutation in the seventh exon of *glh-1* resulting in a C to T change of nucleotide 2496. This nucleotide change produces a premature stop codon resulting in the deletion of 28 amino acids from the carboxyl terminus of the protein. By western blot analysis *bn125* does produce a protein that is slightly smaller than wild type GLH-1 and is expressed at 50% of wild type levels.

All four strains produce truncated, or in the case of *glh-1(bn103)* a normal-sized, GLH-1 protein as recognized by a rabbit N-terminal peptide antibody produced by the Bennett laboratory.

glh-2(um2): The deletion in this allele is 2873-nucleotides in length, deleting most of exon 2 and extending through exon 8. The sequence remains in frame and if translated would produce a small protein that is approximately 133 amino acids in length. While both the N and C terminal are left intact, the deletion does

remove all of the CCHC-zinc fingers and DEAD box helicase motifs, which are thought to be essential for protein function. A chicken antibody generated to an N terminal peptide does not recognize GLH-2 protein in the mutant strain by immunocytochemistry or western analysis. The peptide used for antibody production was CMSDDWDNNTAAAKTISFGSNPS.

glh-3(um1): This allele deletes 1811-nucleotides of the gene sequence, spanning from exon 2 through the end of exon 4. If translated the resultant protein would contain only the first 90 amino acids of sequence, lacking both the CCHC-zinc fingers and DEAD box helicase domains. The GLH-3 antibody was made against a C terminal peptide and therefore does not recognize any GLH-3 protein in the mutant background.

glh-4(gk225): This allele deletes the first 590-nucleotides of coding sequence in exon 1. The GLH-4 antibody was made against both an N terminal peptide and a fusion protein. Western analysis with this antibody results in no band of any size in the *glh-4(gk225)* strain, but does produce a band approximately 120-kDa in size in the wild type background.

glh-1(gk100), *glh-1(ok439)* and *glh-4(gk225)* were isolated by the *C. elegans* Genome Knock-out Consortium by performing gene-specific PCR on DNA from collections of UV-TMP mutagenized worms. The *glh-1(ok439) glh-4(gk255)* double mutant was generated in the Bennett laboratory by undergraduate Christopher Lee.

Brood Counts

All of the mutations in *glh-1* result in a temperature-sensitive embryonic lethality and sterility that display a strong maternal effect. From our analyses, the mutations in *glh-1* form an allelic hierarchy with *gk100* being the strongest, followed by *ok439*, and *bn103* as the weakest. To analyze the resultant phenotype from the *glh* mutations, brood counts of progeny from each strain were counted and assessed. Brood counts were done at 16ºC, 20ºC, 24.5ºC and 26ºC for both first and second generations. *glh-1* mutants and *glh-1;glh-4* double mutants are kept over a balancer chromosome making these strains heterozygous for the mutation in order to maintain the strain. The first generation of non-green worms produced from heterozygous green mothers inherits a maternal load of *glh-1* product but does not synthesize zygotic product. Therefore this first generation from balanced strains is considered maternal plus, zygotic minus (M+Z-), meaning that the progeny have some maternal rescue due to the fact that their mothers were heterozygous for the mutation. The second generation produced from homozygous (M+Z-) mothers is considered maternal minus, zygotic minus (M-Z-) because they have no maternal rescue (Fig. 3.3B). The second generation removed from the balancer is typically a more severe phenotype and more true to the RNAi phenotype. Therefore, the brood size of both generations was considered and analyzed.

At 16°C sterility was quite low. In the *glh-1(gk100)* mutants sterility ranged from 7-11% in the M+Z- to M-Z- generations respectively. Sterility at this temperature

increased slightly in the *glh-1(ok439)* mutant from 15-10%. And for both the *glh-1(bn125)* and *glh-4(gk225)* mutants sterility was at 6% in both generations. The biggest difference was seen with the *glh-1(ok439);glh-4(gk225)* double mutant strain which had sterility 38% sterility in the first generation and 100% sterility in the second. At 20°C *glh-1(gk100)* mutant sterility ranged from 10-14% sterility in the M+Z- to M-Z- generations respectively. Percent sterility in the *gk100* strain increased when raised at 26°C to 84-100% being sterile. The *glh-1(ok439)* strain showed 11% sterility at the permissive temperature in both generations and like the *gk100* strain sterility increased at the higher temperatures to 29-84%. Brood counts of the *glh-1(bn125)* revealed much similarity to the *ok439* strain. In the *bn125* mutant sterility at 20°C was 10-8%, but when raised at 26°C sterility increased to 38% in the first generation and 100% sterile in the second generation. The *glh-4(gk225)* mutant was also analyzed for sterility at both temperatures. The *glh-4* mutation appeared less deleterious and resulted in less sterility. When grown at 20°C the *glh-4* mutants were 6-5% sterile, which only increased slightly to 5-10% when grown at 26°C. Finally the brood sizes of the double mutant *glh-4(gk225);glh-1(ok439)* were evaluated to determine if there was an increased rate of sterility with the combination of both mutations. As expected from the RNAi work (Kuznicki et al., 2000), an increase in sterility was seen at both temperatures and most strongly in the second generation. For the double mutants grown at 20°C the rate of sterility was 25-97%, which increased to 40-100% at 26°C. Little difference in percent sterility was seen in the worms grown at 24.5°C as compared to the 20°C counts, with only a slight increase in

the second generation. Overall results from brood counts demonstrated that sterility increases dramatically when worms are grown at 26°C and worms are much less sterile at 16°C, 20°C, and 24.5°C. Percent sterility was increased in the second generation (M-Z-) at both temperatures but was most dramatic at the higher temperature (Fig. 3.3A and C). Additionally, the double mutant *glh-1(ok439);glh-4(gk225)* has a high percent of sterility at all temperatures indicating that the strain is not temperature-sensitive but does show more subtle temperature preferences. All of the sterility data is summarized in Figure 3.3.

The fertile M+Z- mothers from the 26°C brood counts were then analyzed for percent embryonic lethality. To do this, the number of dead embryos per plate that did not hatch were counted for all strains but *glh-1(gk100)*, which was 100% sterile in the M+Z- generation at 26°C. As seen in Figure 3.4, the differences in average percent embryonic lethality were not dramatic. The *glh-4(gk225)* strain demonstrated no embryonic lethality, while the two *glh-1* strains showed between 28-30% embryonic lethality. It is interesting to note that the *glh-1(ok439);glh-4(gk225)* double mutant strain had reduced embryonic lethality as compared to the *glh-1(ok439)* strain alone, this difference may be in part due to the fact that the double mutant has reduced numbers of germ cells as compared to the single mutant. Overall, the percent embryonic lethality for the individual mutant strains was low, however the range was very spread out, indicating a large variability in embryonic lethality among worms even of the same strain.

Figure 3.3

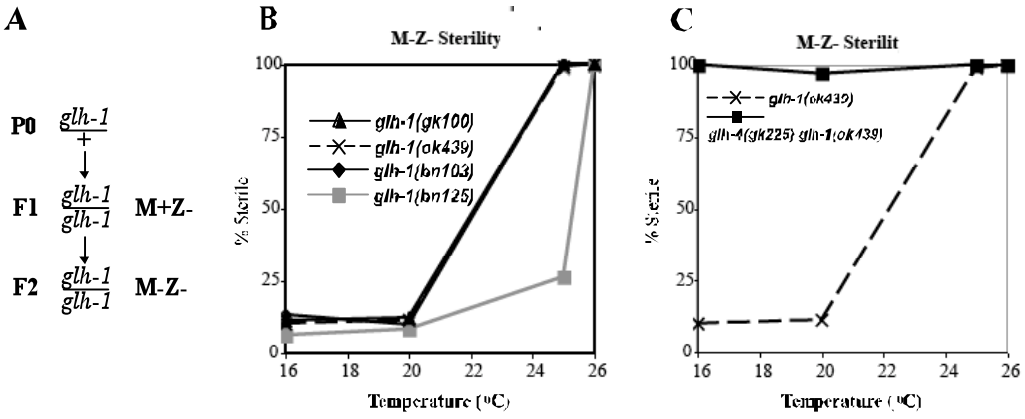

D

Genotype	16°C		20°C		24.5-25°C		26°C	
	% Ste F1	% Ste F2	% Ste F1	% Ste F2	% Ste F1	% Ste F2	% Ste F1	% Ste F2
N2	0	0	0	0	0	0	0	0
glh-1(gk100)	7	11	10	14	0	25	100	
glh-1(ok439)	15	10	11	11	15	19	41	100
glh-1(bn103) unc-13	12	13	12	10				
glh-1(bn125)	6	6	10	8	0	20	68	100
glh-4(gk225)	6	6	6	5	6	6	7	8
glh-4(gk225) glh1(ok439)	38	100	25	97	33	100	N. D.	N. D.

Figure 3.3. *glh-1* mutations result in sterility that is sensitive to maternal genotype and temperature and enhanced by a *glh-4* mutation. **A.** Cartoon showing the generation of M+Z- and M-Z- worms. **B.** Analysis of zygotic (M+Z-) and maternal-effect (M-Z-) sterility at different temperatures. **C.** Graphical display of sterility as a function of temperature for N2 (wild type) and M-Z- *glh-1*, *glh-4*, and *glh-4 glh-1* double mutants. *glh-1* sterility is relatively low at 16°C, 20°C, and 24.5°C, and high at 26°C. *glh-4 glh-1* sterility is high at all temperatures. **D.** Table summary of results from brood counts.

Figure 3.4

Genotype	Average % embryonic lethality [range]	Set #2	Average brood size [range]	Set #2
N2	0	0	169 [109-211]	167 [152-203]
glh-1(ok439)	28 [5-83]	9 [0-50]	47 [1-114]	49 [2-110]
glh-1(bn125)	30 [0-94]	2 [0-9]	53 [1-132]	45 [19-99]
*glh-4(gk225)**	0	16 [0-40]	46 [16-74]	45 [9-80]
glh-4(gk225) glh-1(ok439)	19 [0-95]	76 [45-93]	37 [3-93]	10 [1-37]

Figure 3.4. Embryonic lethality and brood size among fertile M+Z- *glh* hermaphrodites at 26ºC. *glh*/balancer mothers were shifted from 20ºC to 26ºC, and 10 of their *glh/glh* offspring worms (M+Z-) were picked for analysis. M+Z- worms that produced live progeny were analyzed for % of embryos laid that did not hatch (% embryonic lethality) and number of live progeny produced (brood size). *gk100* was not included, as M+Z- worms did not produce live progeny.

* *glh-4* worms are maintained as homozygotes. *glh-4/glh-4* mothers were shifted from 20ºC to 26ºC, and their *glh-4/glh-4* offspring worms (M-Z-) were analyzed as described above.

Analysis of Gonad Morphology

The morphology of the *glh-1(RNAi)* gonad differs dramatically from the wild type gonad. Wild type gonads are made up of two symmetrical arms consisting of hundreds, approximately 787 nuclei per gonad arm (Fig. 3.5), of germ cells that are undergoing mitosis and meiosis. When *glh-1* is knocked-down by RNAi and grown at the non-permissive temperature of 26°C the resultant gonad is much smaller in size, producing no oocytes and only non-functional sperm (Kuznicki et al., 2000). Similarly, the *glh-1* mutants have a smaller gonad when raised at non-permissive temperatures as compared to wild type. To analyze the effects of the mutations on gonad development and morphology *glh-1* mutants were fixed and stained with DAPI. Germ cells were then counted and compared to wild type (performed by April Orsborn Bauer, Ph.D. a former graduate student in the Bennett Laboratory). Additionally, images of the resultant gonads from second generation (M-Z-) raised at 26°C were taken to provide examples of these gonads. Figure 3.6 shows sample images of the homozygous *glh/glh* M-Z- hermaphrodite gonads that were stained with DAPI approximately 1 day past the L4 stage. The images represent a common phenotype for each strain. The *glh-1(bn125)* strain has a normal sized germline as compared to wild type worms (Fig. 3.6A vs. B). *glh-1(ok439)* has a variable phenotype with some germlines being close to wild type size and others being relatively small (Fig. 3.6C – D). Some of the *glh-1(ok439)* germlines were also observed to contain endo-mitotically replicating oocytes (EMO), which are the result of oocytes that continue to replicate their DNA without dividing (Fig. 3.6C, arrows). The *glh-*

Figure 3.5

Germline development in *glh-1* and *glh-4 glh-1* mutants

Maternal Genotype	Temp (°C)	Average no. of germ nuclei per gonad arm [range][a]	% Nearly empty gonad arms	% Gonad arms lacking oocytes[b]	% Gonad arms lacking sperm[b]
N2	26	787 [691-872]	0	0	0
glh-1(gk100)	26	193 [0-407][c]	38[c]	60	96
glh-1(ok439)	26	287 [0-525][c]	20[c]	41	64
glh-1(bn125)	26	nd[d]	14	27	27
glh-4(gk225)	26	nd[d]	0	0	3
glh-4(gk225) glh-1(ok439)	26	127 [0-667]*[c]	68*[c]	71*	74*
	20	nd[d]	39*	47*	39*

Figure 3.5. Germline development in *glh-1* and *glh-4; glh-1* mutants

L4-stage M-Z- worms from *glh-1*/balancer grandmothers were picked to individual plates and shifted from 20°C to 26°C. Their adult progeny were analyzed (24 hr after L4).

* L4-stage M+Z- progeny from *glh-4 glh-1*/balancer mothers were picked to individual plates and shifted from 20°C to 26°C. Their adult progeny were analyzed (24 hr after L4).

[a] Number of gonad arms examined was 8-30. Germ cells counts included oocytes.

[b] Number of gonad arms examined was 28-112.

[c] In *gk100* worms, 13% of gonad arms examined had 0 germ nuclei; 31% had >250 germ nuclei.

In *ok439* worms, 14% of gonad arms examined had 0 germ nuclei; 64% had >250 germ nuclei.

In *glh-4 glh-1* doubles, 63% of gonad arms examined had 0 germ nuclei; 27% had >250 germ nuclei.

[d] nd = not done.

Figure 3.6

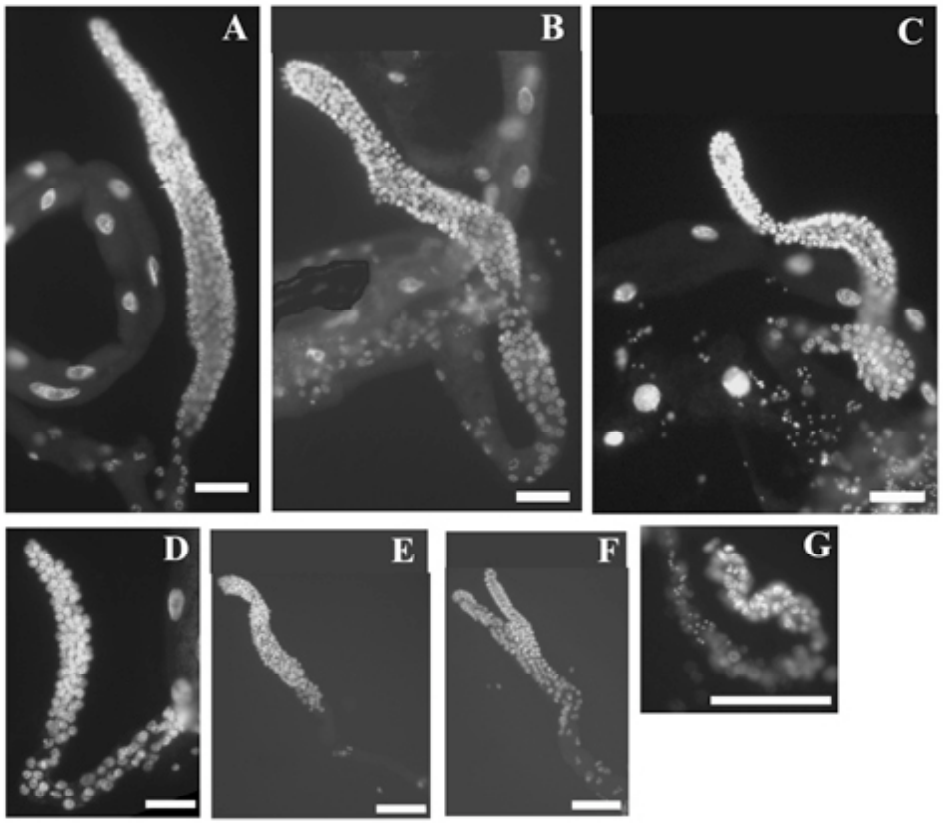

Figure 3.6. Gonad morphology of the *glh* mutants. Glh/balancer mothers were shifted from 20°C to 26°C, and their glh/glh offspring worms (M+Z-) were picked and replated at 26°C. The progeny from the M+Z- generation (M-Z-) were then selected for DAPI staining. Images are of the DAPI stained extruded gonad and are representatives of the most common phenotype found for each strain. **A.** Wild type (N2), **B.** *glh-1(ok439)* large gonad, **C.** *glh-1(ok439)* small gonad with EMO oocytes, **D.** *glh-1(gk100)* gonad, **E.** *glh-1(bn125)* gonad, **F.** *glh-4(gk225)*, "Y" shaped gonad seen in approximately 15% of gonads splayed, **G.** *glh-1(ok439); glh-4(gk225)* tiny gonad.

1(gk100) germline, the strongest of the *glh-1* alleles, typically results in a tiny germline, producing on average 193 germ cells per gonad arm (Fig. 3.6E and Fig. 3.4). The *glh-4(gk225)* strain has a relatively normal sized germline, and in a few rare cases (about 1-15% of the animals) one of the two gonad arms is bifurcated with two distal regions merging into a single gonad arm (Fig. 3.6F). Finally, the *glh-1(ok439);glh-4(gk225)* double mutant, which has 100% sterility at 26°C, results in the most dramatic phenotype. The majority of these double mutants have very small gonads (Fig. 3.6G) with on average only 127 germ nuclei per gonad arm (Fig. 3.4).

Analysis of the bifurcated *glh-4* gonad phenotype

While conducting the DAPI staining on the mutant *glh* gonads, Dr. Bennett observed something unusual in a *glh-4* gonad. One of the gonad arms appeared to have two distal regions merging into a single gonad. This phenotype had not previously been observed in our laboratory, which led us to pursue it further. We found when *glh-4* mutants were grown at 26°C for two generations there was a higher penetrance, approximately 15%, of the observed phenotype. Our laboratory was intrigued by this “bifurcated” phenotype and began to analyze the mutant strain more closely.

At the most distal region of the *C. elegans* gonad resides the somatic distal tip cell (DTC); this cell is important for signaling to the most distal germ cells to undergo mitosis. Because we saw two distal regions in the bifurcated gonad of the *glh-4(gk225)* mutant strain we asked if this were the result of the duplication of the DTC. To analyze this we crossed the *glh-4(gk225)* strain with a GFP tagged *lag-2* expressing strain, *jk2868* (Fig. 3.7) (cross performed by Ms. McEwen, current graduate student in the laboratory). LAG-2 is the ligand important for the signaling of mitosis that is secreted from the DTC. After crossing the two strains and obtaining the homozygous *glh-4(gk225);lag-2*::GFP strain worms were again grown for two generations at 26°C and screened by splaying for the bifurcated phenotype. Unexpectedly, the bifurcated *glh-4(gk225);lag-2*::GFP gonads were not the result of a duplication of the DTC. Figure 3.8 shows a representative gonad of this phenotype, where only on the lower distal region in the image is marked with a DTC expressing LAG-2::GFP.

Additionally, as mentioned previously, the most distal germ cells in the *C. elegans* gonad are undergoing mitosis. In the wild type germline there are on average 5-7 germ cells actively undergoing this process, as marked by the phospho-histone H3 (PPH-3) antibody. To determine if the bifurcation were due to a larger number of germ cells undergoing mitosis, we analyzed *glh-4(gk225)* worms grown for two generations at 26°C and reacted them with the anti-PPH-3 antibody. As seen in Fig. 3.9 an increased number of germ cells actively undergoing mitosis were observed in the *glh-4(gk225)* compared to wild type. In

the *glh-4* mutant animals exhibiting the bifurcated gonad phenoptype (Fig. 3.9B) only one of the distal arms had germ cells actively undergoing mitosis as marked

Figure 3.7

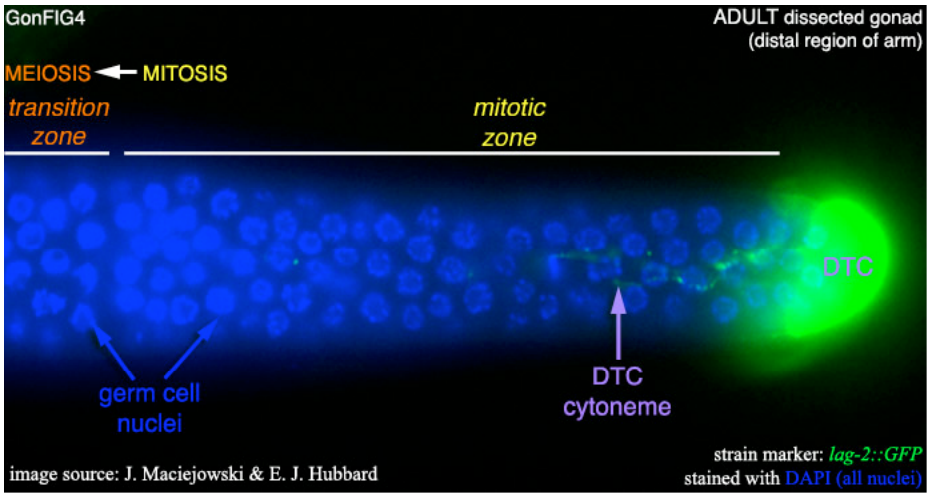

Figure 3.7. The *lag-2*::GFP strain, *jk2868*, with a green distal tip. Germ cell nuclei stained with DAPI (blue).

Figure 3.8

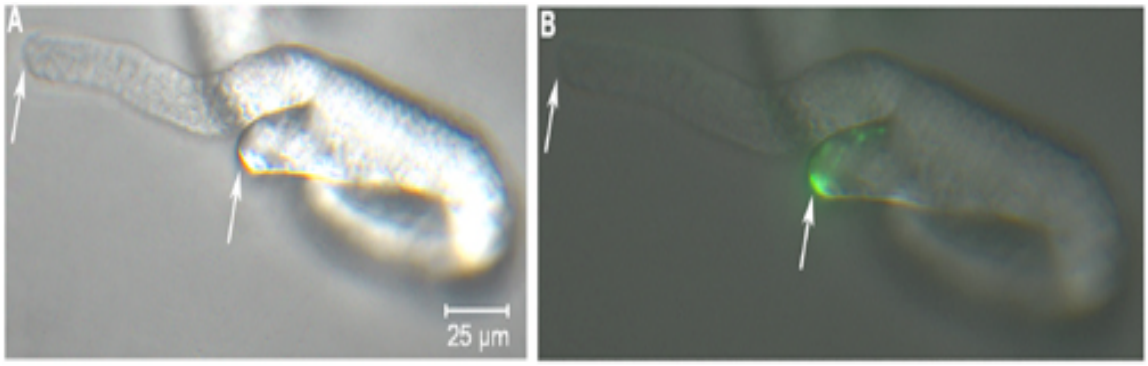

Figure 3.8. The *glh-4(gk225)* bifurcated gonad has a single distal tip cell. **A.** Nomarski optics of a *glh-4(gk225)* gonad extruded from the worm. **B.** Same gonad as A, with fluorescent filter showing a single distal tip cell, as marked by *lag-2*::GFP (green), on the lower distal tip. White arrows point to the two distal tips of the bifurcated gonad.

Figure 3.9

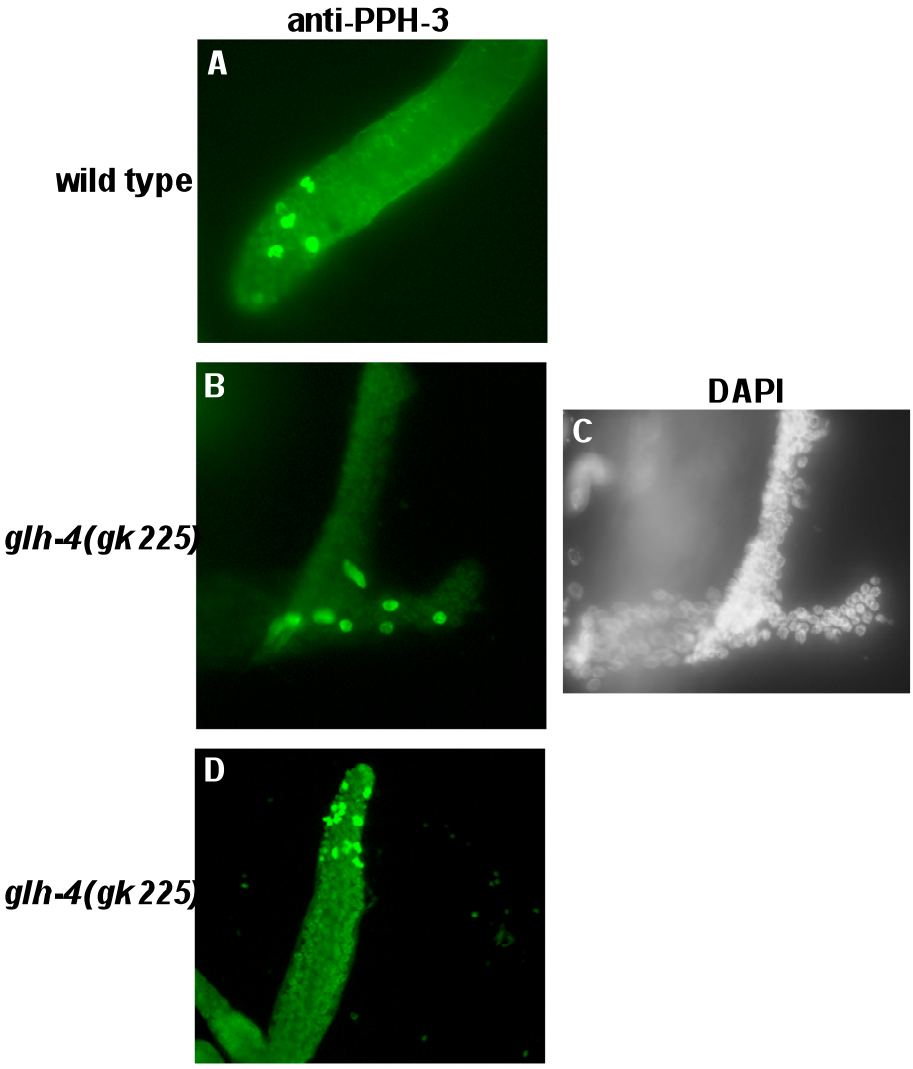

Figure 3.9. Phospho-histone H3 staining in wild type versus *glh-4(gk225)* gonads. **A.** Wild type gonad extruded from the worm and reacted with the anti-PPH-3 antibody (green). Approximately 6 nuclei are marked with the antibody. **B.** A *glh-4(gk225)* mutant gonad extruded from the worm and reacted with the anti-PPH-3 antibody (green). Approximately 7 nuclei are marked with the antibody, but only in a single arm of the bifurcated gonad. **C.** DAPI staining of the gonad seen in B. **D.** A *glh-4(gk225)* mutant gonad extruded from the worm

and reacted with the anti-PPH-3 antibody (green). Approximately 12-16 nuclei are marked with the antibody. All of the above worms were grown at 26°C for two generations before being analyzed.

with the anti-PPH-3 antibody. Overall, these results indicated that the bifurcation of the distal gonad may be due to an increase in mitotic germ cells but not due to a duplication in the DTC, which would signal germ cells in both distal regions to undergo mitosis.

A second mutation previously reported to result in the rare bifurcated gonad phenotype was the cell cycle gene *cye-1*. This gene is +1.32 map units away from *glh-4* (www.wormbase.org). To verify that the phenotype we saw in the glh-4 mutant was not due to a mutation in the closely linked *cye-1* gene Tamara McEwen performed PCR on the *glh-4* strain with *cye-1* specific primers. The *glh-4(gk225)* strain did not contain mutations in *cye-1*. We then hypothesized that crossing the double *glh-4(gk225)* strain with the *cye-1(eh10)* strain to make a double mutant would possibly result in a higher frequency of the bifurcated gonad. To accomplish this, I assisted my undergraduate researcher Jordan Marshall in crossing the two strains. This is not an easy task, especially for an undergraduate researcher to take on, as the genes are so closely linked and a rare crossover event between the two genes would have to occur. Jordan screened hundreds of worms by PCR checking for the presence of both mutations. In the end, Jordan was successful in identifying two groups of crosses that contained both the *glh-4(gk225)* and the *cye-1(eh10)* alleles. Unfortunately this strain was lost in the transition from Jordan to his understudy , Adrienne Brigham, and the project was later dropped primarily due to the low penetrance of the bifurcated gonad phenotype in the *glh-4(gk225)* strain.

GLH-4 can partially rescue the *glh-1(ok439)* strain

Based on the brood counts of the *glh* mutants and on RNAi results demonstrating that sterility is increased with loss, or decrease, of both GLH-1 and GLH-4 in combination, it was proposed that GLH-1 and GLH-4 might serve redundant and similar roles in germline development and maintenance. To test this we decided to produce a GFP::GLH-4 transgene expressing in the *glh-1(ok439)* mutant background to analyze if excess GLH-4 could rescue the sterility of the *glh-1(ok439)* strain at the restrictive temperature 26°C. To do this we used integrative gene bombardment, which utilizes a pressure chamber to blast DNA coated gold particles at the worms (Praitis et al., 2001). To first do this I crossed the *glh-1(ok439)* mutant with the *unc-119(ed3)* strain. The *unc-119* gene encodes for a novel protein that is required for the proper development of the nervous system (www.wormbase.org). The *unc-119(ed3)* mutation results in a strain of worms that can barely move and lie on the plate in a "C" shape. This serves as a useful screening tool as the plasmid containing your gene of interest also contains a rescuing *unc-119* gene fragment. Two weeks after the worms have been bombarded worms can be screened for rare transformants, which in the event of a successful transformation will be able to move around the plate and express GFP. The plasmid used for these experiments was previously made by April Orsborn. She had inserted *glh-4* cDNA into the *pie-1* vector generated by the Seydoux Lab containing the *pie-1* promoter and 3' UTR. The *pie-1* gene is a germline mRNA and therefore serves as a useful promoter for

germline expression (www.bs.jhmi.edu/MBG/SeydouxLab.htm). Using this construct, I was successful in obtaining a *glh-1(ok439);*GFP::*glh-4* transgenic strain. This strain was maintained at 26°C for six months, which demonstrated the ability of the extra copy of the GLH-4 to compensate for the *glh-1(ok439)* phenotype at 26°C, which is 94% sterile as a non-rescued (or non-balanced) homozygote.

To analyze the *glh-1(ok439);*GFP::*glh-4* strain for transformation, we used PCR analysis to amplify the GFP::*glh-4* transgene. Using a 5' GFP specific primer and a *glh-4* cDNA 3' specific primer we were able to obtain a product containing 4024 bp (Fig. 3.10A). Sequencing of the product revealed that it did match GFP and *glh-4* sequences. Western blot analysis of wild type worms versus the transgenic strain using an anti-GFP antibody to detect protein revealed that the transgene was expressed as protein. The GFP::GLH-4 product migrated at approximately 150 kDA, the predicted molecular weight for GLH-4 (120 kDa) with the addition of GFP (27 kDa) (Fig. 3.10B).

Overall, the above data indicates that GLH-4 can rescue the *glh-1(ok439)* temperature-sensitive phenotype. This suggests to us that GLH-1 and GLH-4, while they may have some separate functions, due serve redundant roles in germline development and maintenance.

Figure 3.10

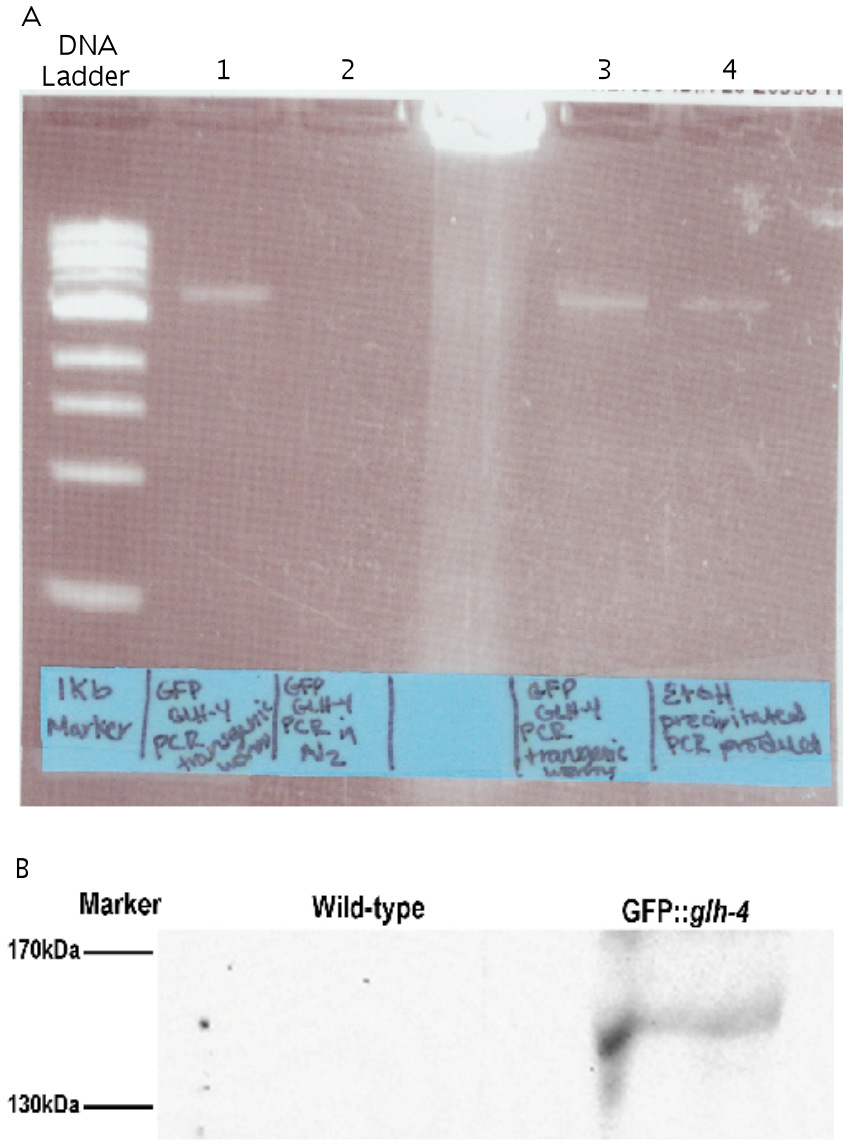

Figure 3.10 Presence and expression of GFP::*glh-4* in transgenic worms. **A.** PCR product using *gfp* and *glh-4* specific primers in transformed worm strain (lanes 1 and 3) and in wild type worms (lane 2). EtOH precipitated product used for sequencing (lane 4). **B.** Western blot analysis of wild type worms versus GFP::*glh-4* transgenic strain reacted with an anti-GFP antibody shows a band at approximately 150kDa in the transgenic strain but not in wild type.

We also tried multiple times to produce a GFP::*glh-1* transgenic strain by gene bombardment, but were unsuccessful. It is very difficult to produce germline transgenic strains as these genes are often silenced in the germline. This silencing also occurred in our *glh-1(ok439);*GFP::*glh-4* strain after being maintained for six months at the non-permissive temperature, as we lost both GFP expression and the ability to rescue sterility at this temperature.

DCR-1 does not accumulate in *glh-1(gk100)* worms after treatment with the proteosome inhibitor

Because DCR-1 levels in the *glh-1(gk100)* strain as compared to wild type (Chapter 2), but not the mRNA levels, we asked if the decreased levels might be due to DCR-1 degradation in the germline. To test this, I treated *glh-1(gk100)* worms, grown in liquid culture at 20ºC, for 0hr, 1hr, 2hr, 4hr, and 5hr with the proteosome inhibitor, MG132. At the end of the 5hr treatment I collected all the worms and analyzed them by western blot to determine the level of DCR-1 proteins. As seen in Fig. 3.11, DCR-1 levels started high in the 0hr untreated *glh-1(gk100)* worms and decreased dramatically starting with the 1hr treatment.

These results were unexpected for a number of reasons. First of all, we expected DCR-1 levels to be low in the *glh-1(gk100)* worms in the 0hr untreated control lane. The fact that they were not low may indicate that a different situation is occurring when the worms are grown in liquid culture versus when grown on standard NGM plates. Growing worms in liquid culture is generally thought as a

Figure 3.11

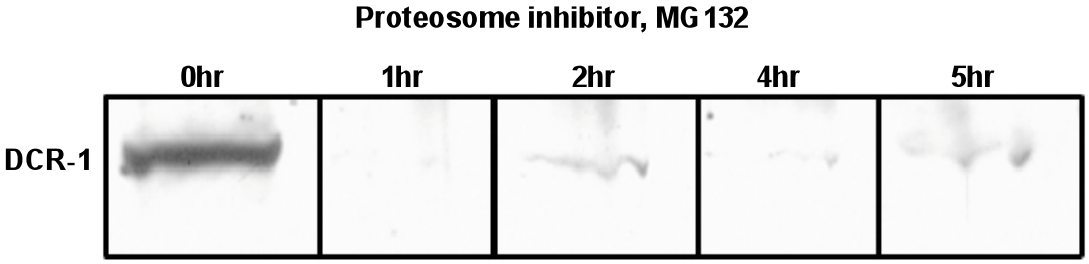

Figure 3.11. Treatment of *glh-1(gk100)* worms with the proteosome inhibitor, MG132, does not result in DCR-1 accumulation. Western blot analysis with anti-DCR-1 antibody of *glh-1(gk100)* worms, grown in liquid culture at 20ºC, treated with the proteosome inhibitor, MG132 for 0hr, 1hr, 2hr, 4hr, and 5hr time points.

stress situation, this stress may result in higher levels of DCR-1. Second, we expected DCR-1 levels to increase over time with the proteosome inhibited. This was not the case, DCR-1 levels were much reduced to absent in the treated versus untreated worms. Perhaps with the blocking of the proteosome in the stressed *glh-1(gk100)* worms we are activating another degradation pathway that is causing DCR-1 to become rapidly targeted for degradation. These results are opposite from what we see in wild type worms, grown in liquid culture, and treated with MG132. In fact, we see DCR-1 levels accumulate over time (Chapter 2). Perhaps with the reduction and mutation of GLH-1 in the mutant strain, DCR-1 is unstable and targeted for degradation, but via a different pathway.

Discussion

Through our genetic analyses we have uncovered a hierarchy of gene importance among the GLH family of genes. GLH-1 is the most critical for fertility in worms grown at higher temperatures (26°C). Loss of the zygotically transcribed GLH-1 results in a lower percentage of sterility, whereas loss of both maternal and zygotic GLH-1 results in sterility that is in some cases (as is for the *glh-1(gk100)* strain) complete. Loss of both GLH-1 and GLH-4 result in the higher precentages of sterility than the single *glh-1* mutants regardless of temperature (except of course for *glh-1(gk100)* at 26°C). Thus, in the absence of GLH-1 function, GLH-4 can promote germline development in worms grown at lower temperatures.

It is interesting to note that among the brood counts, percent sterility, and percent embryonic lethality there is a large range in phenotypes from worm to worm within the same strain. We have proposed that the differences seen may be due to the gradual loss of GLH-1 protein, and thus P-granule function, in the first and second generations. The first generation still has a maternal load of protein and therefore has a better chance for wild type germline development, but as GLH-1 protein is gradually depleted there may be some variability in the number of oocytes that mature to fertilization. Additionally, in the second generation this depletion is even greater but may vary from worm to worm. One example of this large variability is in the *glh-1(ok439)* M+Z- worms grown at 26°C that produce broods that range in embryonic lethality from 0% to 83%. The number of viable

offspring from these worms also ranges from 1 to 114, possibly demonstrating how different the effect of the maternal load of functional GLH-1 protein can have on the next generation of worms.

A second interesting finding from these studies is the temperature sensitivity of the *glh-1* mutant phenotypes. While these mutants do have a mild, less severe, phenotype at lower temperatures there is a marked increase in sterility when shifted to 26°C. Wild type worms are fertile at 26°C, but have significantly small broods and the temperature is thought to be enough to stress the worms and their ability to reproduce. With the loss of GLH-1 in combination with heat stress this appears enough to cause a higher percentage of sterility. Perhaps these findings come full circle back to our story of DCR-1 and GLH-1 in a heat stress situation. Although GLH-1 does not normally re-localize to stress-induced RNP granules under heat stress situations, it does appear necessary for DCR-1 localization (which does localize to RNPs under heat stress). Perhaps with the loss of GLH-1, what little DCR-1 protein that is present does not localize to RNP granules and therefore the maintenance of oocyte integrity is lost. We did not test for DCR-1 localization in heat stressed *glh-1* mutant animals, but this would be of interest in the future.

The temperature-sensitive phenotype observed in the single *glh-1* mutants was lost in the *glh-1(ok439);glh-4(gk225)* mutant, resulting in sterility at all temperatures, suggesting that GLH-4 can function in maintaining normal

germline development in the absence of GLH-1 at lower temperatures. In support of this hypothesis, the rescuing of the *glh-1(ok439)* temperature-sensitive sterility at 26°C with the GFP::*glh-4* transgene makes a strong case that the GLHs have similar and redundant roles in the germline.

Future Directions

Many unanswered questions remain regarding the function of the GLH proteins in germline development. Do they simply serve as structural components of P granules? Do they specifically regulate the translation of maternally transcribed mRNAs? What is their function in association with Dicer? Recent work by the Priess laboratory, described in Chapter 2, presented evidence that newly transcribed mRNAs are exported out of the nucleus, through the nuclear pores, and into P granules (Sheth et al., 2010). This raises the question, what mRNAs are regulated by P granules, and more specifically which are regulated by GLH-1? Future work by the Bennett laboratory will focus on identifying mRNA substrates bound by GLH-1 and then determining if the regulation of these transcripts is altered by the loss of GLH-1. We are also interested in identifying miRNAs associated with GLH-1 complex, to determine if miRNA-mediated regulation is occurring within this complex of proteins. Finally, we would like to identify other proteins bound in complex with GLH-1, specifically members of the RISC machinery including the Argonaute proteins ALG-1 and ALG-2.

Overall, much work is still required to determine the exact function of GLH-1 in germline maintenance and for determining the mechanism of GLH-1 function in regulating maternal mRNAs. The work presented here, combined with work by previous graduate students in the Bennett laboratory, laid the groundwork for understanding GLH-1 interactions with other protein components of known

function. It is of great interest to the Bennett Laboratory to take the GLH-1/DCR-1 story to the next step and determine how GLH-1 might be operating in the miRNA pathway.

References

Ambros, V. (2001). microRNAs: tiny regulators with great potential. *Cell* **107(7),** 823-826.

Anderson, P. and Kedersha, N. (2006). RNA granules. *J. Cell Biology: Mini-Review* **172(6)**, 803-808.

Balagopal, V. and Parker, R. (2009). Polysomes, P bodies and stress granules: states and fates of eukaryotic mRNAs. *Curr Opin Cell Biol.* **21(3)**, 403-408.

Bashkirov, V.I., Scherthan, H., Solinger, J.A., Buerstedde, J., and Heyer, W. (1997). A mouse cytoplasmic exoribonuclease (mXRN1p) with preference for G4 tetraplex substrates. *J. Cell Biology* **136(4)**. 761-773.

Bernstein, E., Caudy, A.A., Hammond, S.M. and Hannon, G.J. (2001). Role for a bidentate ribonuclease in the initiation step of RNA interference. *Nature* **409(6828)**, 295-6.

Bhattacharyya, S.N., Habermacher, R., Martine, U., Closs, E.I., and Filipowicz, W. (2006). Relief of microRNA-mediated translational repression in human cells subjected to stress. *Cell* **125**, 1111-1124.

Boag, P.R., Nakamura, A., and Blackwell, T.K. (2005). A conserved RNA-protein complex component involved in physiological germline apoptosis regulation in *C. elegans*. *Development* **132(22)**, 4975-4986.

Brengues, M., Teixeira, D., and Parker, R. (2005). Movement of eukaryotic mRNAs between polysomes and cytoplasmic processing bodies. *Science* **310**, 486-489.

Brenner, S. (1974). The genetics of *Caenorhabditis elegans*. *Genetics* **77**, 71-94.

Brohawn, S.G., Partridge, J.R., Whittle, J.R.R., and Schwartz, T.U. (2009). The nuclear pore complex has entered the atomic age. Structure **17**, 1156-1167.

D'Angelo, M.A., and Hetzer, M.W. (2008). Structure, dynamics and function of nuclear pore complexes. Trends in Cell Biology **18(10)**, 456-466.

Davis, L.I. and Blobel, G. (1986). Identification and characterization of a nuclear pore complex protein. *Cell* **45(5)**, 699-709.

Ding, L., Spencer, A., Morita, K., and Han, M. (2005). The developmental timing regulator AIN-1 interacts with miRISCs and may target the Argonaute protein ALG-1 to cytoplasmic P bodies in *C. elegans*. *Molecular Cell* **19**, 437-447.

Draper, B.W., Mello, C.C., Bowerman, B., Hardin, J., and Priess, J.R. (1996). MEX-3 is a KH domain protein that regulates blastomere identity in early *C. elegans* embryos. *Cell* **87(2)**, 205-216.

Duchaine, T.F., Wohlschlegel, J.A., Kennedy, S., Bei, Y., Conte Jr., D., Pang, K., Brownell, D.R., Harding, S., Mitani, S., Ruvkun, G., Yates III, J.R., and Mello, C.C. (2006). Functional proteomics reveals the biochemical niche of *C. elegans* DCR-1 in multiple small-RNA-mediated pathways. *Cell* **124**, 343-354.

Eddy, E.M. (1975). Germ plasm and differentiation of the germ cell line. *Int. Rev. Cytol.* **43:** 229280.

Emmerth, S., Schober, H., Gaidatzis, D., Roloff, T., Jacobeit, K., and Bühler, M. (2010). Nuclear retention of fission yeast Dicer is a prerequisite for RNAi-mediated heterochromatin assembly. *Developmental Cell* **18**, 102-113.

Epstein, H.F. and Shakes, D.C. (1995). *Caenorhabditis elegans*: Modern biological analysis of an organism. *(Methods in Cell Biology) San Diego: Academic Press*.

Etemad-Moghadam, B., Guo, S., and Kemphues, K.J. (1995). Asymmetrically distributed PAR-3 protein contributes to cell polarity and spindle alignment in early *C. elegans* embryos. *Cell* **83(5)**, 743-752.

Eiring, A.M., Harb, J.G., Neviani, P.,Garton, C., Oaks, J.J., Spizzo, R., Liu, S., Schwind, S., Santhanam, R., Hickey, C.J. et al. (2010). miR-328 functions as an RNA decoy to modulate hnRNP E2 regulation of mRNA translation in leukemic blasts. *Cell* **140,** 652-665.

Findley, S. D., Tamanaha, M., Clegg, N.J., and Ruohola-Baker, H. (2003). Maelstrom, a *Drosophila* spindle-class gene, encodes a protein that colocalizes with Vasa and RDE1/AGO1 homolog, Aubergine, in nuage. *Development* **130(5)**, 859-871.

Fougerolles, A., Vornlocher, H., Maraganore, J., and Lieberman, J. (2007). Interfering with disease: a progress report on siRNA-based therapeutics. *Nature Reviews Drug Discovery* **6**, 443-453.

Gallo, C.M., Munro, E., Rasoloson, D., Merritt, C., and Seydoux, G. (2008). Processing bodies and germ granules are distinct RNA granules that interact in *C. elegans* embryos. *Developmental Biology* **323**, 76-87.

Gavis, E.R., Lunsford, L., Bergsten, S.E., Lehmann, R. (1996). A conserved 90 nucleotide element mediates translational repression of nanos RNA. *Development* **122(9)**, 2791-2800.

Gruidl, M.E., Smith, P.A., Kuznicki, K.A., McCrone, J.S., Kirchner, J., Strome, S. and Bennett, K. L. (1996). Multiple potential germline helicases are components of the germline-specific P granules of *Caenorhabditis elegans*. *Proc. Natl. Acad. Sci.* **USA93**, 13837-13842.

Guedes, S., and Priess, J.R. (1997). The *C. elegans* MEX-1 protein is present in germline blastomeres and is a P granule component. *Development* **124(3)**, 731-739.

Guo, S., and Kemphues, K.J. (1995). *par-1*, a gene required for establishing polarity in *C. elegans* embryos, encodes a putative Ser/Thr kinase that is asymmetrically distributed. *Cell* **81(4)**, 611-620.

Hammell, C.M., Lubin, I., Boag, P.R., Blackwell, T.K., and Ambros, V. (2009). *nhl-2* modulates microRNA activity in *Caenorhabditis elegans. Cell* **136**, 926-938.

Hay, B., Jan, L.Y., and Jan, Y.N. (1988). A protein component of *Drosophila* polar granules is encoded by Vasa and has extensive sequence similarity to ATP-dependent helicases. *Cell* **55(4)**, 577-578.

Herman, R.K., Albertson, D.G., and Brenner, S. (1976). Chromsome rearrangements in *Caenorhabditis elegans*. *Genetics* **83(1)**, 91-105.

Jacobs, D., Glossip, D., Xing, H., Muslin, A. J. and Kornfeld, K. (1999). Multiple docking sites on substrate proteins form a modular system that mediates recognition by ERK MAP kinase. *Genes Dev.* **13**, 163-175.

Jakymiw, A., Lian, S., Eystathioy, T., Songqing, L., Satoh, M., Hamel, J.C., Fritzler, M.J., and Chan, E.K.L. (2005). Disruption of GW bodies impairs mammalian RNA interference. *Nature Cell Biology* **7(12)**, 1267-1273.

Jin, Z. and Xie, T. (2007). Dcr-1 maintains *Drosophila* ovarian stem cells. *Current Biology* **17**, 539-544.

Johnstone, O. and Lasko, P. (2004). Interaction with eIF5B is essential for Vasa function during development. *Development* **131(17)**, 4167-4178.

Jones, A. R., Francis, R. and Schedl, T. (1996). GLD-1, a cytoplasmic protein essential for oocyte differentiation, shows stage- and sex-specific expression during *Caenorhabditis elegans* germline development. *Dev. Biol.* **180**, 165-183.

Jud, M., Razelun, J., Bickel, J., Czerwinski, M., and Schisa, J.A. (2007). Conservation of large foci formation in arrested oocytes of *Caenorhabditis* nematodes. *Dev Genes Evol*. **217(3)**, 221-226.

Jud, M.C., Czerwinski, M.J., Wood, M.P., Young, R.A., Gallo, C.M., Bickel, J.S., Petty, E.L., Mason, J.M., Little, B.A., Padilla, P.A., and Schisa, J.A. (2008). Large P body-like RNPs form in *C. elegans* oocytes in response to arrested ovulation, heat shock, osmotic stress, and anoxia and are regulated by the major sperm protein pathway. *Developmental Biology* **318**, 38-51.

Kamath, R.S. and Ahringer, J. (2003). Genome-wide RNAi screening in *Caenorhabditis elegans*. *Methods* **30(4)**, 313-321.

Kawasaki, I., Shim, Y.H., Kirchner, J., Kaminker, J., Wood, W.B. and Strome, S. (1998). PGL-1, a predicted RNA-binding component of germ granules, is essential for fertility in *C. elegans*. *Cell* **94**, 635-645.

Kedde, M., Strasser, M.J., Boldjipour, B., Oude Vrielink, J.A.F., Slanchev, K., leSage, C., Nagel, R., Voorhoeve, P.M., van Duijse, J., Orom, U.A., Lund, A.H., Perrakis, A., Raz., E., and Agami, R. (2007). RNA-binding protein Dnd1 inhibits microRNA access to target mRNA. *Cell* **131**, 1273-1286.

Kedersha, N., Stoecklin G., Ayodele, M., Yacono, P., Lykke-Andersen, J., Fritzler, M.J., Scheuner, D., Kaufman, R.J., Golan, D.E., and Anderson, P. (2005). Stress granules and processing bodies are dynamically linked sites of mRNP remodeling. *J. Cell Biology* **169(6)**, 871-884.

Knight, S.W., Bass, B.L. (2001). A role for the RNase III enzyme DCR-1 in RNA interference and germ line development in *Caenorhabditis elegans*. *Science* **293(5538)**, 2269-2271.

Kotaja, N., Bhattacharyya, S. N., Jaskiewicz, L., Kimmins, S., Parvinen, M., Filipowicz, W., Sassone-Corsi, P. (2006). The chromatoid body of male germ cells: similarity with processing bodies and presence of Dicer and mircroRNA pathway components. *Proc. Natl. Acad. Sci. USA* **103**, 2647-2652.

Kuznicki, K.A., Smith, P.A., Leung-Chiu, W.M., Estevez, A.O., Scott, H.C., Bennett, K.L. (2000). Combinatorial RNA interference indicates GLH-4 can compensate for GLH-1; these two P-granule components are critical for fertility in *C. elegans*. *Development* **13**, 2907-2916.

LaMunyon, C.W., and Ward, S. (1998). Larger sperm outcompete smaller sperm in the nematode *Caenorhabditis elegans*. *PNAS* **265(1409)**, 1997-2002.

Lasko, P.F. and Ashburner, M. (1988). The product of the *Drosophila* gene *vasa* is very similar to eukaryotic initiation factor-4A. *Nature* **335(6191)**, 611-617.

Lee, R., Feinbaum, R., and Ambrow, V. (1993). The C. elegans heterochronic gene lin-4 encodes small RNAs with antisense complementarity to lin-14. *Cell* **75**, 843-854.

Lian, S., Jakymiw, A., Eystathioy, T., Hamel, J.C., Fritzler, M.J., and Chan, E.K.L. (2006). GW Bodies, micro RNAs, and the cell cycle. *Cell Cycle* **5(3)**, e1-e3.

Liang, L. Diehl-Jones, W., and Lasko, P. (1994). Localization of vasa protein to the *Drosophila* pole plasm is independent of its RNA-binding and helicase activities. *Development* **120(5)**, 1201-1211.

Liu, J.L., and Gall, J.G. (2007). U bodies are cytoplasmic structures that contain uridine-rich small nuclear ribonucleoproteins and associate with P bodies. *Proc. Natl. Acad. Sci. USA.* **104(28)**, 11655-11659.

Liu, J., Rivas, F.V., Wohlsclegel, J., Yates, J.R., Parker, R., and Hannon, G. (2005). A role for the P-body component GW182 in microRNA function. *Nature Cell Biology* **7(12)**, 1261-1266.

Liu, J., Valencia-Sanchez, M.A., Hannon, G., and Parker, R. (2005). MicroRNA-dependent localization of targeted mRNAs to mammalian P-bodies. *Nature Cell Biology* **7(7)**, 719-723.

Liu, N., Han, H., and Lasko, P. (2009). Vasa promotes *Drosophila* germline stem cell differentiation by activating Mei-P26 translation by directly interacting with a (U)-rich motif in its 3' UTR. *Genes Dev.* **23(23)**, 2742-2752.

Luense, L.J, Carletti, M.Z., and Christenson, L.K. (2009). Role of Dicer in female fertility. *Trends in Endocrinology and Metabolism* **20(6)**, 265-272.

Megosh, H. B., Cox, D. N., Campbell, C., and Lin, H. (2006). The Role of PIWI and the miRNA machinery in *Drosophila* germline determination. *Current Biology* **16**, 1884-1894.

Minasaki, R., Puoti, A., and Streit, A. (2009). The DEAD-box protein MEL-46 is required in the germ line of the nematode *Caenorhabditis elegans*. *BMC Dev Biol.* **9:35**.

Murchison, E. P., Stein, P., Xuan, Z., Pan, H., Zhang, M.Q., Schultz, R.M., and Hannon, G.J. (2007). Critical roles for Dicer in the female germline. *Genes Dev.* **21**, 682-683.

Nagamori, I. and Sassone-Corsi, P. (2008). The chromatoid body of male germ cells. *Cell Cycle* **7:22**, 3503-3508.

Navarro, R.E., Shim, E.Y., Kohara, Y. Singson, A. and Blackwell, T.K. (2001). *cgh-1*, a conserved predicted RNA helicases required for gametogenesis and protection from physiological germline apoptosis in *C. elegans*. *Development* **128:** 3221-3232.

Navarro, R.E. and Blackwell, T.K. (2005). Requirement for P Granules and meiosis for accumulation of the germline RNA helicase CGH-1. *Genesis* **42**, 172-180.

Noble, S.L., Allen, B.L., Goh, L.K., Nordick, K., Evans, T.C. (2008). Maternal mRNAs are regulated by diverse P body-related mRNP granules during early *Caenorhabditis elegans* development. *J Cell Biol.* **182(3)**, 559-572.

Olsen, P.H. and Ambros, V. (1999). The lin-4 regulatory RNA controls developmental timing in Caenorhabditis elegans by blocking LIN-14 protein synthesis after the initiation of translation. *Dev. Biology* **216(2)**, 671-680.

Orlicky, S., Tang, X., Willems, A., Tyers, M. and Sicheri, F. (2003). Structural basis for phosphodependent substrate selection and orientation by the SCF Cdc4 ubiquitin ligase. *Cell* **112**, 243-256.

Orsborn, A.M, Li, W., McEwen, T.J., Mizuno, T., Kuzmin, E., Matsumoto, K.,

Bennett, K.L. (2007). GLH-1, the *C. elegans* P granule protein, is controlled by the JNK KGB-1 and by the COP9 subunit CSN-5. *Development* **18**, 3383-3392.

Pfaffl, M.W. (2001). A new mathematical model for relative quantification in real-time RT-PCR. *Nucl. Acids Res.* **29(9 *00*),** 2002 – 2007.

Roussell, D.L. and Bennett, K.L. (1993). GLH-1: a germline putative RNA helicase from *Caenorhabditis* has four zinc fingers. *Proc. Natl. Acad. Sci. USA* **90**, 9300-9304.

Schisa, J.A., Pitt, J.N., and Priess, J.R. (2001). Analysis of RNA associated with P granules in germ cells of *C. elegans* adults. *Development* **128(8)**, 1287-1298.

Schedl, T. and Kimble J. (1988). *fog-2*, a germ-line-specific sex determination gene required for hermaphrodite spermatogenesis in *Caenorhabditis elegans*. *Genetics* **119(1)**, 43-61.

Sen, G.L., and Blau, H.M. (2005). Argonaute 2/RISC resides in sites of mammalian mRNA decay known as cytoplasmic bodies. *Nat Cell Biol.* **7(6)**, 633-636.

Sharrocks, A. D., Yang, S.H. and Galanis, A. (2000). Docking domains and substrate specificity determination for MAP kinases. *Trends Biochem. Sci.* **25**, 448-453.

Sheth, U., Pitt, J., Dennis, S., and Priess, J.R. (2010). Perinuclear P granules are the principal sites of mRNA export in adult *C. elegans* germ cells. *Development* **137**, 1305-1314.

Slanchev, K., Stebler, J., Goudarzi, M., Cojocaru, V., Weidinger, G., and Raz, E. (2009). Control of Dead end localization and activity – implications for the function of the protein in antagonizing miRNA function. *Mech. Dev.* **126**, 270-277.

Smith, P. A., Leung-Chiu, W.M., Montgomery, R., Orsborn, A., Kuznicki, K.A., Gressman-Coberly, E., Mutapcic L. and Bennett, K. L. (2002). The GLH proteins, *Caenorhabditis elegans* P-granule components, associate with CSN-5 and KGB-1, proteins necessary for fertility, and with ZYX-1 a predicted cytoskeletal protein. *Dev. Biol.* **251**, 333-347.

Spike, C., Meyer, N., Racen, E., Orsborn, A., Kirchner, J., Kuznicki, K., Yee, C., Bennett, K., Strome, S. (2008). Genetic analysis of the *Caenorhabditis elegans* GLH family of P-granule proteins. *Genetics* **178(4)**, 1973-1987.

Strome, S, and Lehmann, R. (2007). Germ versus soma decisions: lessons from flies and worms. *Science* **316(5823)**, 392-393.

Strome, S. and Wood, W. B. (1982). Immunofluorescence visualization of germ-line-specific cytoplasmic granules in embryos, larvae, and adults of *Caenorhabditis elegans*. *Proc. Natl. Acad. Sci. USA* **79**, 1558-1562.

Strome, S. and Wood, W. B. (1983). Generation of asymmetry and segregation of germ-line granule in early *C. elegans* embryos. *Cell* **35**, 15-25.

Styhler S., Nakamura, A., Swan, A., Suter, B., and Lasko, P. (1998). Vasa is required for GURKEN accumulation in the oocyte, and is involved in oocyte differentiation and germline cyst development. *Development* **125(9)**, 1569-1578.

Sulston, J. E., and Brenner, S. (1974). The DNA of *Caenorhabditis elegans*. *Genetics* **77(1)**, 95-104.

The *C. elegans* Sequencing Consortium (1998). Genome Sequence of the Nematode *C. elegans*: A platform for investigating biology. Science **282(5396)**, 2012-2018.

Teixeira, D., Sheth, U., Valencia-Sanchez, M.A., Brengues, M., and Parker, R. (2005). Processing bodies require RNA for assembly and contain nontranslating mRNAs. *RNA* **11**, 371-382.

Tomancak, P., Guichet, A., Zavorszky, P., and Ephrussi, A. (1998). Oocyte polarity depends on regulation of *gurken* by Vasa. *Development* **125(9)**, 1723-1732.

Updike, D.L. and Strome, S. (2009). A genomewide RNAi screen for genes that affect the stability, distribution and function of P granules in *Caenorhabditis elegans*. *Genetics*. **183**, 1397-1419.

Villanueva, A., Lozano, J., Morales, A., Lin, X., Deng, X., Hengartner, M.O., and Kolesnick, R.N. (2001). *jkk-1* and *mek-1* regulate body movement coordination and response to heavy metals through *jnk-1* in *Caenorhabditis elegans*. *EMBO J.* **20(18)**, 5114-5128.

Voronina, E., and Seydoux, G. (2010). The nucleoporin Nup98 is required for the integrity and function of germline P granules in *C. elegans. Development* (In press)

Welker, N. C., Habig, J.W. and Bass, B.L. (2007). Genes mis-regulated in *C. elegans* deficient in Dicer, RDE-4, or RDE-1 are enriched for innate immunity

genes. *RNA* **13(7)**, 1090-1102.

Wickens, M and Goldstrohm, A. (2003). A place to die, a place to sleep. *Science* **300**, 753-755.

Wolf, N., Priess, J., and Hirsh, D. (1983). Segregation of germline granules in early embryos in *Caenorhabditis elegans*: an electron microscopic analysis. *J. Embryol. Exp. Morphol.* **73**, 297-306.

Wolpert, L., Beddington, R., Jessell, T., Lawrence, P., Meyerowitz, E., and Smith, J. "Principles of Development". *Oxford University Press*. Second Edition. (2001): 3-9. Print.

Ye, X., Nalepa, G., Welcker, M., Kessler, B.M., Spooner, E., Qin, J., Elledge, S. J., Clurman, B.E. and Harper, J.W. (2004). Recognition of phosphodegron motifs in human cyclin E by the SCF Fbw7 ubiquitin ligase. *J. Biol. Chem.* **279**, 50110-50119.

Zhao, S. and Liu, M.F. (2009). Mechanisms of microRNA-mediated gene regulation. *Sci China C Life Sci.* **52(12)**, 1111-1116.

VITA

Erica Leigh (Racen) Beshore was born on March 13, 1982 in St. Louis, Missouri to the parents of Peter and Linda Racen. She attended both elementary and secondary education in the county of St. Louis, Missouri. Erica graduated from Parkway South High School in 2000. Following High School she then attended Covenant College in Lookout Mountain, Georgia earning a B.A. in Biology Pre-Med. Erica then moved back to Missouri to pursue her Ph.D. in the Department of Molecular Microbiology and Immunology. She married Brent Cornell Beshore on October 18, 2008.